

Gravitino LSP scenario at the LHC
Gravitino LSP Szenario am LHC

Diploma Thesis
Jan Heisig

May 2010

II. Institut für Theoretische Physik
UNIVERSITÄT HAMBURG

Abstract

In this thesis we discuss the phenomenology of the gravitino LSP scenario at the large hadron collider (LHC) experiment. We concentrate on a long-lived stau NLSP which gives rise to a prominent signature in the LHC detector as a ‘slow muon’. We discuss the production channels and compute the cross sections for direct production via the Drell-Yan process. On this basis we claim a conservative estimation of the discovery potential for this scenario at the LHC.

Zusammenfassung

In dieser Arbeit diskutieren wir die phänomenologischen Perspektiven eines Gravitino LSP Szenarios am Large Hadron Collider (LHC). Wir konzentrieren unsere Betrachtungen auf ein meta-stabiles Stau als das NLSP. Letzteres wird eine deutliche Signatur als „langsames Myon“ aufweisen. Wir diskutieren die Produktionskanäle und berechnen die Wirkungsquerschnitte für direkte Stau Produktion via Drell-Yan. Auf der Basis dieser Berechnungen schätzen wir das Potential des LHC für eine 5σ -Entdeckung des Staus ab.

Contents

1	Introduction	7
2	The supersymmetry Lagrangian	9
3	Choice of scenarios	19
4	Elemental stau production processes	29
5	Physics at hadron colliders	40
6	Predictions for the LHC	52
7	Conclusion and Outlook	66
A	Conventions	68
B	Supersymmetry interactions	69
C	Transformation of velocities and angles	73
D	The corrections to the Drell-Yan process in α_s	74

1 Introduction

The history of developing supersymmetry theories has over time gone through different stages with different aspects becoming the focus of the research. The original motivation of adopting the supersymmetry algebra to physics [42, 58, 69] might be primarily supported by the pure esthetic aspect that it is the only external symmetry extension of the Poincaré algebra with a non-trivial S-matrix [43]. That is of course a strong motivation for observing quantities of such a theory in general. But since it is clear that supersymmetry is a candidate to cure the hierarchy problem, phenomenological research is almost completely concentrated on the TeV scale supersymmetry, which is constrained to provide this feature. This means that the superpartner masses in such a theory (since supersymmetry obviously has to be a broken symmetry at accessible energy scales) are somehow constrained to be roughly of order a few hundred GeV, but not much higher than 1 TeV.

Anyway, within this thesis our viewpoint is that of a TeV scale supersymmetry. So we will take the hierarchy problem as a boundary condition. Nevertheless it is still a purely theoretical condition, since the Higgs has not been discovered yet. On the other hand, if we would assume the superpartner masses to be at a much higher scale, then the LHC would be no experiment to discover supersymmetry anymore. So, in that sense the theoretical condition has some overlap with the technical one.

Besides curing the hierarchy problem a second theoretically desired feature of supersymmetry is the unification of the gauge coupling at a high scale through quantum corrections of the extended particle content [11]. Another motivation comes from cosmological concerns. The lightest supersymmetric particle (LSP) makes a natural dark matter candidate [48, 39, 57]. Neutralino LSP scenarios have already been studied widely over the past decade, whereas gravitino LSP scenarios have only recently moved into the center of interest. So, it is natural to ask what signatures such a scenario would lead to in the ongoing LHC experiment.

It is clear that the gravitino itself will not be detected directly nor will the gravitino play a dominant role (if at all) in the production and decay processes of supersymmetric particles at a collider. Thus, the signature of a gravitino LSP scenario is to be found in the behavior of the other supersymmetric particles, especially the next-to-lightest supersymmetric particle (NLSP). Within this thesis we concentrate on a stau NLSP that is furthermore assumed to be long-lived. Such a particle will give rise to a prominent collider signature. As a massive charged particle it will pass the detector and will be recognized as a ‘slow muon’. Such scenarios have occasionally been discussed in the literature [13, 35, 36, 47, 49]. The best current collider bounds on staus come from the OPAL experiment at LEP which excludes masses below 98.0 GeV and 98.5 GeV for right- and left-handed staus and smuons, respectively [64].

We will restrict ourselves to the direct production of staus via the Drell-Yan process and give a detailed analysis of the quantities that are crucial for the discrimination of staus from muons. Finally we will show how to claim a 5σ -discovery.

This thesis is organized as follows. In section 2 we will give a brief introduction to

the supersymmetric Lagrangian and soft breaking terms. Although this work is about a gravitino LSP scenario, we will not go into a detailed discussion of supergravity, since this is not relevant for the collider signatures. Once we have assembled all the relevant expressions, in section 3 we will frame our choice of scenario against the breaking models and motivate our further considerations.

A diploma thesis marks the transition a student passes through when entering into the business of current research. Hence, we present some main arguments that are specific to this work in a rather detailed manner, such that it is comprehensible for other students working on their diploma in the field of particle physics. Therefore in section 4 we give a detailed derivation of the stau cross section via photon and Z at parton level from the Lagrangian terms onwards. In section 5 we will then introduce the effects that take place at hadron level, which are crucial ingredients when discussing the LHC. In section 6, finally, we will display and discuss the results obtained by Monte Carlo generators.

2 The supersymmetry Lagrangian

What is Supersymmetry? The SM and its Lagrangian are based on a few powerful principles. These are renormalizability, invariance under the $SU(3)_C \times SU(2)_L \times U(1)_Y$ gauge transformations as well as invariance under the Poincaré transformations. The latter is an external symmetry, that is it concerns spacetime. Its generators are of bosonic nature, they are vector- and tensor-like.

Now, supersymmetry is a (unique) extension of the symmetries under which the Lagrangian should be invariant. And its generators are of fermionic nature. Thus a supersymmetry transformation turns a bosonic field into a fermionic field and vice versa. Within the SM one cannot identify any of those boson-fermion-pairs. Hence, this symmetry requires us to double the particle content of the SM, giving each SM particles its so called superpartner.

In this section we will motivate and write down the supersymmetric Lagrangian. Our intention is not to give a reasonably complete derivation and discussion. Those are already published in a variety of works [44, 4, 30, 45, 31, 60] including the much referred to introduction by Martin [55] which we are following in this section. Our task here is to assemble all the relevant expressions for later discussion.

As conventional in the business of supersymmetry we will employ the two-component Weyl spinor notation for fermions. (Later on, for the calculation of cross sections we will also use four-component Dirac spinors, but the fermions there will be just the SM fermions in the initial state of collider experiments.) We will use the following short-hand notation, in which the SM fermions are denoted as

$$\begin{aligned}
 Q_i &= \begin{pmatrix} u \\ d \end{pmatrix}, \begin{pmatrix} c \\ s \end{pmatrix}, \begin{pmatrix} t \\ b \end{pmatrix} \\
 \bar{u}_i &= \bar{u}, \bar{s}, \bar{t} \\
 \bar{d}_i &= \bar{d}, \bar{c}, \bar{b} \\
 L_i &= \begin{pmatrix} \nu_e \\ e \end{pmatrix}, \begin{pmatrix} \nu_\mu \\ \mu \end{pmatrix}, \begin{pmatrix} \nu_\tau \\ \tau \end{pmatrix} \\
 \bar{e}_i &= \bar{e}, \bar{\mu}, \bar{\tau}
 \end{aligned} \tag{1}$$

where a fermion \bar{f} is defined to fulfill

$$\begin{pmatrix} f \\ \bar{f}^\dagger \end{pmatrix} = \begin{pmatrix} f_L \\ f_R \end{pmatrix} \tag{2}$$

which is again the well known four-component Dirac spinor. In this notation, for instance, the kinetic and gauge terms for the leptons of the SM read

$$\mathcal{L} = i\bar{L}_i^\dagger \bar{\sigma}^\mu D_\mu L^i + i\bar{e}_i^\dagger \bar{\sigma}^\mu D_\mu e^i, \tag{3}$$

with the family index summed over and D_μ the covariant derivative for the SM gauge interactions.

The same structure is to be doubled in order to describe the superpartners of the fermions, applying a tilde on all these fields, $\tilde{Q}_i, \tilde{u}_i, \tilde{d}_i, \tilde{L}_i, \tilde{e}_i$. These sfermions are scalars. We will refer to the superpartner of the left-(right-)handed fermion as the left-(right-)handed sfermion, although they obviously do not carry spin. The superpartners of the gauge bosons g, W^0, W^\pm, B^0 are the spin-1/2 fermions $\tilde{g}, \tilde{W}^0, \tilde{W}^\pm, \tilde{B}^0$, called the gauginos. The Higgs sector is a bit more complicated. In contrast to the SM, supersymmetry requires two complex Higgs isodoublets, one with hypercharge $Y = +1/2$, $H_u = (H_u^+, H_u^0)$, giving masses to the up-type quarks and one with hypercharge $Y = -1/2$, $H_d = (H_d^0, H_d^-)$, giving masses to the down-type quarks and charged leptons.¹ The superpartners of the Higgs bosons are also spin-1/2 fermions, the higgsinos \tilde{H}_u, \tilde{H}_d .

These fields build up the particle content of the Minimal Supersymmetric Standard Model (MSSM). Now, let's sketch some of the steps on the way to a MSSM Lagrangian.

As long as we discuss unbroken supersymmetry, the Lagrangian is required to build a renormalizable gauge-theory that is invariant under supersymmetry transformation. The latter means that fermion and boson fields (and their interaction terms) transform in such a way into each other under a supersymmetry transformation, that the Lagrangian stays invariant at least up to a total derivative.

We are starting with the chiral supermultiplets. These contain a left-handed two-component Weyl fermion ψ , its superpartner a complex scalar field ϕ (together building the matter fields of the theory) and a complex auxiliary field F (that doesn't propagate) which is required in order to let the supersymmetry algebra close off-shell as well. The free supersymmetric Lagrangian is

$$\mathcal{L}_{\text{free}}^{\text{chiral}} = -\partial^\mu \phi^{*i} \partial_\mu \phi_i + i\psi^\dagger \bar{\sigma}^\mu \partial_\mu \psi_i + F^{*i} F_i, \quad (4)$$

where the index i is to run over the different chiral supermultiplets, that are all gauge and flavor degrees of freedom; spinor indices are suppressed.

The non-gauge interactions between the fields within a supermultiplet are again restricted by the requirement that the corresponding Lagrangian terms are invariant under supersymmetry transformation. These interactions are usually expressed by the superpotential

$$W = \frac{1}{2} M^{ij} \phi_i \phi_j + \frac{1}{6} y^{ijk} \phi_i \phi_j \phi_k, \quad (5)$$

in which the parameters M^{ij} and y^{ijk} are restricted to be symmetric under the interchange of i, j, k (forthwith, we have dropped a supersymmetry-possible term linear in ϕ that can only occur if ϕ is a gauge singlet, which will not appear in the MSSM with minimal field content). The interacting Lagrangian then reads

$$\mathcal{L}_{\text{int}}^{\text{chiral}} = \left(-\frac{1}{2} W^{ij} \psi_i \psi_j + W^i F_i \right) + \text{c.c.} \quad (6)$$

¹Due to the structure of supersymmetry one Higgs doublet does not suffice to give masses to both types. Another distinct requirement is due to the fact, that if there were only one Higgs field, its superpartner would cause a gauge anomaly. But the existence of two isodoublets with $Y = \pm 1$ maintain the anomaly cancelation, that takes place in the SM.

in which W^i and W^{ij} denote the first and second derivative of W with respect to ϕ_i , respectively. Putting together (4) and (6) one obtains purely algebraic equations of motion for the auxiliary fields F :

$$F_i = -W_i^*, \quad F^{*i} = -W^i, \quad (7)$$

so that one can eliminate them in favor of expressions in the scalar fields. The chiral supermultiplet Lagrangian thus reads

$$\begin{aligned} \mathcal{L}^{\text{chiral}} = & -\partial^\mu \phi^{*i} \partial_\mu \phi_i + i\psi^\dagger{}^i \bar{\sigma}^\mu \partial_\mu \psi_i \\ & - M_{ik}^* M^{kj} \phi^{*i} \phi_j - \frac{1}{2} M^{in} y_{jkn}^* \phi_i \phi^{*j} \phi^{*k} - \frac{1}{2} M_{in}^* y^{jkn} \phi^{*i} \phi_j \phi_k - \frac{1}{4} y^{ijn} y_{kln}^* \phi_i \phi_j \phi^{*k} \phi^{*l} \\ & - \frac{1}{2} M^{ij} \psi_i \psi_j - \frac{1}{2} M_{ij}^* \psi^\dagger{}^i \psi^\dagger{}^j - \frac{1}{2} y^{ijk} \phi_i \psi_j \psi_k - \frac{1}{2} y_{ijk}^* \phi^{*i} \psi^\dagger{}^j \psi^\dagger{}^k, \end{aligned} \quad (8)$$

where we have organized the kinetic terms, the scalar potential and the fermion mass plus Yukawa couplings to appear in the first, second and third line, respectively.

Since we are on the way to describe the possible Lagrangian terms for the MSSM we also have to include the gauge interactions introducing the gauge supermultiplets and all possible gauge interactions that couple gauge bosons and gauginos to the matter fields. The gauge supermultiplet Lagrangian reads

$$\mathcal{L}_{\text{gauge}} = -\frac{1}{4} F_{\mu\nu}^a F^{\mu\nu a} + i\lambda^\dagger{}^a \bar{\sigma}^\mu D_\mu \lambda^a + \frac{1}{2} D^a D^a, \quad (9)$$

where $F_{\mu\nu}^a$ is the appropriate Yang-Mills field strength (the kinetic term of the vector fields and their self interactions) and

$$D_\mu \lambda^a = \partial_\mu \lambda^a + g f^{abc} A_\mu^b \lambda^c \quad (10)$$

is the covariant derivative, giving rise to the couplings within the gauge supermultiplets. Again an auxiliary field is required to let the supersymmetry algebra close off-shell. D^a is a non-propagating real scalar field.

Now let's look at the possible gauge couplings. To achieve gauge invariance one has to replace the ordinary derivatives in the kinetic terms of the chiral supermultiplet Lagrangian by the covariant derivatives

$$\begin{aligned} D_\mu \phi_i &= \partial_\mu \phi_i - ig A_\mu^a (T^a \phi)_i \\ D_\mu \phi^{*i} &= \partial_\mu \phi^{*i} + ig A_\mu^a (\phi^* T^a)^i \\ D_\mu \psi_i &= \partial_\mu \psi_i - ig A_\mu^a (T^a \psi)_i \end{aligned} \quad (11)$$

(where T^a are the hermitian gauge group generators) causing the vector field A_μ^a to couple to the matter fields.

Now, further gauge invariant Lagrangian terms are possible, which couple gauginos and the auxiliary field to the matter fields:

$$-\sqrt{2}g(\phi^*T^a\psi)\lambda^a, \quad (12)$$

$$-\sqrt{2}g\lambda^{\dagger a}(\psi^\dagger T^a\phi), \quad (13)$$

$$g(\phi^*T^a\phi)D^a, \quad (14)$$

where the coefficients are fixed by the requirement of supersymmetry (as one could imagine, the supersymmetry transformation laws for the matter fields—which we don't want to display here—had to be modified when introducing these extra terms).

Considering the gauge supermultiplet Lagrangian plus (14) one observes that the auxiliary field is again—as it was in the case of chiral supermultiplets—expressible purely algebraically in terms of the scalar field, since it provides the equation of motion

$$D^a = -g(\phi^*T^a\phi), \quad (15)$$

and so, this term gives another contribution to the scalar potential. Thus the full supersymmetry Lagrangian reads

$$\begin{aligned} \mathcal{L}^{\text{susy}} = & \ i\psi^\dagger\bar{\sigma}^\mu D_\mu\psi_i - \frac{1}{2}M^{ij}\psi_i\psi_j - \frac{1}{2}M_{ij}^*\psi^\dagger_i\psi^\dagger_j \\ & + i\lambda^{\dagger a}\bar{\sigma}^\mu D_\mu\lambda^a \\ & - D^\mu\phi^{*i}D_\mu\phi_i - V(\phi, \phi^*) \\ & - \frac{1}{4}F_{\mu\nu}^a F^{\mu\nu a} \\ & - \frac{1}{2}y^{ijk}\phi_i\psi_j\psi_k - \frac{1}{2}y_{ijk}^*\phi^{*i}\psi^\dagger_j\psi^\dagger_k - \sqrt{2}g(\phi^{*i}T^a\psi_i)\lambda^a - \sqrt{2}g\lambda^{\dagger a}(\psi^\dagger_i T^a\phi_i), \end{aligned} \quad (16)$$

where we have summarized the scalar potential terms in

$$\begin{aligned} -V(\phi, \phi^*) = & \\ & - M_{ik}^*M^{kj}\phi^{*i}\phi_j - \frac{1}{2}M_{in}^*y^{jkn}\phi^{*i}\phi_j\phi_k - \frac{1}{2}M^{in}y_{jkn}^*\phi_i\phi^{*j}\phi^{*k} - \frac{1}{4}y^{ijn}y_{klm}^*\phi_i\phi_j\phi^{*k}\phi^{*l} \\ & - \frac{1}{2}g_a^2(\phi^{*i}T^a\phi_i)^2. \end{aligned} \quad (17)$$

It is common to refer to the scalar potential terms coming from the superpotential as the F -terms, we have arranged them to appear in the first line of the right hand side of (17). Similarly, the term in the last line is called D -term. Appendix B displays all the interaction vertices (16) gives rise to.

We want to emphasize that almost all of the couplings within the Lagrangian (16) are determined by the already known SM parameters. These are the SM gauge coupling constants g in (10), (11) and (12)-(14) that determine the interactions $A \leftrightarrow \lambda$, $A \leftrightarrow \phi$, ψ and $\lambda \leftrightarrow \phi, \psi$.

Furthermore one observes that the Yukawa couplings in (16) coming from the superpotential are restricted by gauge invariance

$$W^i(T^a\phi)_i = 0, \quad (18)$$

causing the coupling y^{ijk} to vanish for supermultiplet fields that transform in representations that can combine to form a gauge singlet (a similar argument holds for the mass matrix M_{ij}). An additional restriction comes from R -parity [37] conservation. In contrast to the SM, in the MSSM the mere demand of renormalizability does not automatically preserve baryon number (B) and lepton number (L) and therefore does not prevent a disastrous proton decay. The conservation of the multiplicative quantum number

$$P_R = (-1)^{3(B-L)+2s} \quad (19)$$

fixes this problem (s is the spin).² All SM particles (including fermions, gauge bosons and the Higgs scalars) have even R -parity while all the others have odd R -parity. As a consequence the SM particles only couple to an even number of supersymmetric particles³.

After all—returning to the argument—it turns out that each allowed Yukawa coupling term in (16) includes exactly one Higgs supermultiplet field, that is a Higgs or higgsino. Thus, due to the symmetry of y^{ijk} under the interchange of any of the three indices one concludes that all the Yukawa couplings y^{ijk} are determined by the SM Yukawa couplings that give masses to the fermions. If one writes down the corresponding superpotential, applying the short hand notation (1), it reads

$$W_{\text{MSSM}} = \tilde{u}\mathbf{y}_u\tilde{Q}H_u - \tilde{d}\mathbf{y}_d\tilde{Q}H_d - \tilde{e}\mathbf{y}_e\tilde{L}H_d + \mu H_u H_d \quad (20)$$

where the Yukawa couplings are expressed by the three 3×3 matrices in family space \mathbf{y}_u , \mathbf{y}_d and \mathbf{y}_e . (A reasonable approximation is that only the third family component of each matrix is important,

$$\mathbf{y}_f = \text{diag}(0, 0, y_f), \quad \text{for } \mathbf{f} = \mathbf{u}, \mathbf{d}, \mathbf{e}, \quad (21)$$

due to the fact that the top quark, bottom quark and tau lepton are the heaviest fermions compared to the others with equal gauge quantum numbers.) The only remaining new parameter of the unbroken supersymmetry Lagrangian is the so called μ -term $\mu = M^{H_u H_d} = M^{H_d H_u}$.

²There are indeed interesting R -parity violating theories that are currently being discussed. In these theories the amount of R -parity violation is strongly restricted by experiment, especially by the proton lifetime. Although a small amount of R -parity violation would change the decay branching ratios of the stau (and therefore provided different cosmological scenarios), it wouldn't spoil our later results concerning the direct stau production at colliders, anyway. Introductory reviews in the subject of R -parity violation can be found in [17, 32].

³Within this thesis we will use the term *supersymmetric particles* interchangeably for particles with odd R -parity. Similarly, we will refer to *SM particles* as those with even R -parity, despite the fact that the second Higgs doublet is properly not included in the SM.

This esthetical feature seems to switch completely if one introduces the necessary breaking of supersymmetry. But this might only be true as long as we are not able to determine the breaking mechanism. Verily there are several elaborated proposals of breaking mechanisms available at the present state of research. And most of them successfully reduce the 105 new parameters that a general supersymmetry breaking extension (without any assumptions) brings along to the number of five parameters or so.

But let's step back and get in touch with the supersymmetry breaking Lagrangian. The unbroken supersymmetric Lagrangian naturally provides the feature that the quadratic divergencies that appear in the quantum corrections to the Higgs squared mass (the hierarchy problem) vanish in such a way that the fermion and boson contributions (within a supermultiplet) cancel each other. (Therefore it is crucial that the (scalar)⁴-coupling is the square of the corresponding Yukawa coupling, which is confirmed when looking at (16) and (17).) We want to maintain this feature when introducing supersymmetry breaking. The simplest way to achieve this without assuming any breaking mechanism is just to add an appropriate effective supersymmetry breaking Lagrangian. In order not to spoil the cancelation of quadratic divergencies it has to contain only dimensionful couplings (of positive mass dimension) of order m_{soft} which corresponds to the mass scale of the supersymmetry particles. In such a Lagrangian loop corrections to the Higgs squared mass are proportional to m_{soft}^2 and thus can only be logarithmically divergent (there is no (scalar)⁴-coupling or Yukawa coupling in such an effective Lagrangian). The most general Lagrangian of this form, that is compatible with gauge invariance and R -parity, is

$$\begin{aligned}
\mathcal{L}_{\text{soft}}^{\text{MSSM}} = & -\frac{1}{2} \left(M_3 \widetilde{g}\widetilde{g} + M_2 \widetilde{W}\widetilde{W} + M_1 \widetilde{B}\widetilde{B} + \text{c.c.} \right) \\
& - \left(\widetilde{u} \mathbf{a}_u \widetilde{Q} H_u - \widetilde{d} \mathbf{a}_d \widetilde{Q} H_d - \widetilde{e} \mathbf{a}_e \widetilde{L} H_d + \text{c.c.} \right) \\
& - \widetilde{Q}^\dagger \mathbf{m}_Q^2 \widetilde{Q} - \widetilde{L}^\dagger \mathbf{m}_L^2 \widetilde{L} - \widetilde{u} \mathbf{m}_u^2 \widetilde{u}^\dagger - \widetilde{d} \mathbf{m}_d^2 \widetilde{d}^\dagger - \widetilde{e} \mathbf{m}_e^2 \widetilde{e}^\dagger \\
& - m_{H_u}^2 H_u^* H_u - m_{H_d}^2 H_d^* H_d - (b H_u H_d + \text{c.c.}) ,
\end{aligned} \tag{22}$$

where the couplings M_1 , M_2 , M_3 , \mathbf{a}_u , \mathbf{a}_d , \mathbf{a}_e and \mathbf{m}_Q^2 , \mathbf{m}_L^2 , \mathbf{m}_u^2 , \mathbf{m}_d^2 , \mathbf{m}_e^2 , $m_{H_u}^2$, $m_{H_d}^2$, b each are a priori independent parameters of order m_{soft} and m_{soft}^2 , respectively. The bold characters denote that the respective quantities are 3-matrices in family space (they have to be hermitian in order to keep the Lagrangian real). We don't put tildes on the subscripts. Counting all introduced parameters of the broken MSSM, that are masses, mixing angles and phases, the said number of 105 remains after absorbing trivial parameters that could be rotated away by redefining the fields. Together with the 19 SM parameters it yields 124 parameters for the MSSM.

Anyway, even without assuming any dynamic principle as a breaking mechanism, it would be sensible to make restrictions on the parameter space. Many of the entries of the mass matrices can in principle give rise to large flavor-changing and CP-violating effects, those effects have in experiment been found to be very small. Hence, one doesn't want to introduce additional flavor-changing and CP-violating contributions from the MSSM

(at least those should be relatively small). Therefore one usually makes the following assumption, sometimes called *universality relations*:

First, the sfermion mass matrices are flavor blind,

$$\mathbf{m}_{\mathbf{F}}^2 = m_{\mathbf{F}}^2 \mathbf{1}, \quad \text{for } \mathbf{F} = \mathbf{Q}, \mathbf{L}, \bar{\mathbf{u}}, \bar{\mathbf{d}}, \bar{\mathbf{e}}. \quad (23)$$

Second, only the (3, 3)-component of the trilinear couplings \mathbf{a} should be non zero, and thus proportional to the Yukawa couplings in the approximation (21),

$$\mathbf{a}_{\mathbf{f}} = A_0 \mathbf{f} \mathbf{y}_{\mathbf{f}}, \quad \text{for } \mathbf{f} = \mathbf{u}, \mathbf{d}, \mathbf{e} \quad (24)$$

(that's just a common notation, nevertheless the numerical value of a_{33}^i has a priori nothing to do with the one of the SM parameter y_{33}^i , since A_{i0} is the free parameter). Third, the A_{f0} and the M_i (bilinear gaugino terms in (22)) are assumed to be real.

With these assumptions one is able to reduce the parameters the broken MSSM additionally introduces to 14.

Although these assumptions are sufficient they are not necessary. However, one can find breaking-mechanisms that provide such restrictions 'naturally'.

Sparticle masses and mixings

Like the mixing of the coupling and mass eigenstates of the gauge bosons in the SM, in supersymmetry the higgsinos and electroweak gauginos mix with each other within the same charge through electroweak symmetry breaking. The neutral higgsinos, \tilde{H}_u^0 and \tilde{H}_d^0 , and the bino \tilde{B} and wino \tilde{W}^0 mix to form the neutral mass eigenstates $\tilde{\chi}_i^0$, $i = 1, \dots, 4$, the neutralinos. The charged higgsinos, \tilde{H}_u^\pm and \tilde{H}_d^\pm , and winos \tilde{W}^\pm mix to form two sets of charged mass eigenstates $\tilde{\chi}_i^\pm$, $i = 1, 2$.⁴ For the dominating contents in this sector, one can formulate a rule of thumb [56]: If $|\mu| > M_2$ the lighter neutralinos and charginos $\tilde{\chi}_1^0, \tilde{\chi}_2^0, \tilde{\chi}_1^\pm$ will be predominantly gaugino-like while the heavier ones $\tilde{\chi}_3^0, \tilde{\chi}_4^0, \tilde{\chi}_2^\pm$ will be more higgsino-like. If $|\mu| < M_2$ it will be the other way around.

Similarly, in the case of scalars, in principle any scalars with same electric charge, color charge and R -parity can mix with each other. First, let's briefly treat the case of Higgs scalars. The MSSM contains two complex $SU(2)_L$ -doublets, that are eight (real) degrees of freedom. After electroweak symmetry breaking three of them are the massless Nambu-Goldstone modes G^0 and G^\pm , which become the longitudinal modes of Z^0 and W^\pm , when they have mass. After electroweak symmetry breaking there remain five Higgs mass eigenstate fields. These are the neutral CP-even scalars h^0 and H^0 (where the latter is defined to be the heavier one), the neutral CP-odd scalar A^0 and the charged scalars H^+ and H^- . H_u and H_d mix up in the following pairs: (h^0, H^0) , (G^0, A^0) and (G^\pm, H^\pm) . This reads

$$\begin{pmatrix} H_u^0 \\ H_d^0 \end{pmatrix} = \begin{pmatrix} \langle H_u^0 \rangle \\ \langle H_d^0 \rangle \end{pmatrix} + \frac{1}{\sqrt{2}} \mathcal{R}_\alpha \begin{pmatrix} h^0 \\ H^0 \end{pmatrix} + \frac{i}{\sqrt{2}} \mathcal{R}_{\beta_0} \begin{pmatrix} G^0 \\ A^0 \end{pmatrix}, \quad (25)$$

⁴In the case of mass eigenstates the numeration is always defined to be increasing with increasing masses.

$$\begin{pmatrix} H_u^\pm \\ H_d^{\mp*} \end{pmatrix} = \mathcal{R}_{\beta_\pm} \begin{pmatrix} G^\pm \\ H^\pm \end{pmatrix}, \quad (26)$$

where \mathcal{R} are four orthogonal rotation matrices, each characterized by one angle (displayed in the subscript). $\langle H_u^0 \rangle$ and $\langle H_d^0 \rangle$ are the Higgs vacuum expectation values (VEVs) that give masses to the up- and down-type fermions, respectively. The ratio of the VEVs is traditionally called

$$\tan \beta = \langle H_u^0 \rangle / \langle H_d^0 \rangle. \quad (27)$$

Now, let's have a closer look at the sfermion mixings and masses. The situation of the squarks and sleptons is quite similar. Therefore, we will restrict ourselves exemplarily (and since this case is of importance for this work) to the latter case. The terms of the full soft broken Lagrangian that give rise to sfermion masses are

$$\begin{aligned} \mathcal{L}_{\mathbf{L}}^{\text{mass}} = & \mu^* \left(\tilde{e} \mathbf{y}_e \tilde{L} H_u^* + \text{c.c.} \right) - \left| \mathbf{y}_e \tilde{L} H_d \right|^2 - \tilde{e} \mathbf{y}_e \tilde{e}^\dagger |H_d^0|^2 \\ & - \frac{1}{2} g_Y^2 (|H_d^2| + |H_u^2|) \left(|\tilde{e}|^2 - \frac{1}{2} |\tilde{L}|^2 \right) - g_L^2 \sum_a \left(H_d^\dagger T^a H_d + H_u^\dagger T^a H_u \right) \tilde{L}^\dagger T^a \tilde{L} \\ & - \tilde{e} \mathbf{a}_e \tilde{L} H_d - \tilde{L}^\dagger \mathbf{m}_{\mathbf{L}}^2 \tilde{L} - \tilde{e} \mathbf{m}_{\tilde{e}}^2 \tilde{e}^\dagger, \end{aligned} \quad (28)$$

where we have arranged the F -term contributions, D -term contributions and soft terms to appear in the first, second and third line, respectively.

Now we can relate the parameters in the Lagrangian (that we have introduced and discussed above) to the mixings and masses that appear in the mass matrix $\mathbf{M}_{\mathbf{L}}^2$, storing all the contributions to the mass:

$$\mathcal{L}_{\mathbf{L}}^{\text{mass}} = (\tilde{e}_L^*, \tilde{e}_R^*) \mathbf{M}_{\mathbf{L}}^2 \begin{pmatrix} \tilde{e}_L \\ \tilde{e}_R \end{pmatrix}, \quad (29)$$

where \tilde{e} stands for $\tilde{e}, \tilde{\mu}, \tilde{\tau}$. In the sneutrino case only the LL -component of $\mathbf{M}_{\mathbf{L}}^2$ survives, that's why in what follows won't grapple to find a notation that takes the sneutrino case along explicitly.⁵ After the Higgs acquires a VEV the mass matrix takes the form

$$\mathbf{M}_{\mathbf{L}}^2 = \begin{pmatrix} M_{\mathbf{e}LL}^2 & M_{\mathbf{e}LR}^2 \\ M_{\mathbf{e}LR}^2 & M_{\mathbf{e}RR}^2 \end{pmatrix}, \quad (30)$$

with

$$\begin{aligned} M_{\mathbf{e}LL}^2 &= \mathbf{m}_{\mathbf{L}}^2 + (T_e^3 - Q_e \sin^2 \theta_W) \cos 2\beta m_Z^2 \mathbf{1} + m_\tau^2 \text{diag}(0, 0, 1) \\ M_{\mathbf{e}RR}^2 &= \mathbf{m}_{\tilde{e}}^2 + Q_e \sin^2 \theta_W \cos 2\beta m_Z^2 \mathbf{1} + m_\tau^2 \text{diag}(0, 0, 1) \\ M_{\mathbf{e}LR}^2 &= m_\tau^2 (A_{0e} - \mu^* \cot \beta) \text{diag}(0, 0, 1) \end{aligned} \quad (31)$$

⁵Thus in (31) $\mathbf{m}_{\mathbf{L}}^2$ is consistently meant to denote only the $T^3 = -1/2$ -components of the Isodoublets. Nevertheless, the first line in (31) is also true for sneutrinos applying the respective $T^3 = +1/2$ entries of $\mathbf{m}_{\mathbf{L}}^2$ and without the last term.

where the entries of $\mathbf{M}_{\mathbf{L}}^2$ are matrices in 3×3 family space, that is what the bold characters on the right hand side of (31) refer to (not to be confused with the bold character of $\mathbf{M}_{\mathbf{L}}^2$ itself). m_τ is the mass of the τ -lepton. In (31) we have already adopted (21) and (24), that's the reason for the appearance of $m_\tau \text{diag}(0, 0, 1)$. The last term in each line comes from the F -term. The second term in the first two lines comes from the D -term. Finally, the first term in each line comes from the soft terms. Since $M_{\mathbf{e}LR}^2$ is responsible for the mixing between interaction and mass eigenstates, such a mixing depends strongly on $\tan\beta$ as well as on the trilinear coupling A_0 .

We said above that in principle all sleptons can mix with each other. True, formally another choice of $\mathbf{a}_{\mathbf{e}}$ and $\mathbf{y}_{\mathbf{e}}$ could of course lead to substantial cross-family mass mixings. But since the trilinear terms $\mathbf{a}_{\mathbf{e}}$ are constrained by experiment—as we stated above—it is most likely that we have very small off-diagonal contributions for the first two families.

To obtain the mass eigenstates we have to perform a rotation via a unitary matrix \mathcal{R} that diagonalizes (30):

$$\mathcal{R} \mathbf{M}_{\mathbf{L}}^2 \mathcal{R}^\dagger = \begin{pmatrix} m_{\mathbf{e}2} & 0 \\ 0 & m_{\mathbf{e}1} \end{pmatrix}. \quad (32)$$

A unitary 2×2 matrix is determined by one angle and one phase and thus can be written in the form

$$\mathcal{R} = \begin{pmatrix} e^{i\varphi} \cos \theta_{\mathbf{e}} & \sin \theta_{\mathbf{e}} \\ -\sin \theta_{\mathbf{e}} & e^{i\varphi} \cos \theta_{\mathbf{e}} \end{pmatrix}. \quad (33)$$

The eigenvalues $m_{\mathbf{e}1,2}$ then read

$$m_{\mathbf{e}1,2} = \frac{1}{2} \left\{ (M_{\mathbf{e}LL}^2 + M_{\mathbf{e}RR}^2) \mp \sqrt{(M_{\mathbf{e}LL}^2 - M_{\mathbf{e}RR}^2)^2 + 4|M_{\mathbf{e}LR}^2|^2} \right\}. \quad (34)$$

And the mixing angle is

$$\begin{aligned} \cos \theta_{\mathbf{e}} &= \frac{-|M_{\mathbf{e}LR}^2|^2}{\sqrt{|M_{\mathbf{e}LR}^2|^2 + (m_{\mathbf{e}2}^2 - M_{\mathbf{e}LL}^2)^2}}, \\ \sin \theta_{\mathbf{e}} &= \frac{M_{\mathbf{e}LL}^2 - m_{\mathbf{e}2}^2}{\sqrt{|M_{\mathbf{e}LR}^2|^2 + (m_{\mathbf{e}2}^2 - M_{\mathbf{e}LL}^2)^2}}. \end{aligned} \quad (35)$$

We want to emphasize that if one allows to choose the appearing parameters in (31) independently, $m_{\mathbf{e}1,2}$ and $\theta_{\mathbf{e}}$ are in principle three independent parameters.

The transformation of the stau eigenstates reads explicitly

$$\begin{aligned} \tilde{\tau}_1 &= \cos \theta_{\tilde{\tau}} \tilde{\tau}_R + \sin \theta_{\tilde{\tau}} \tilde{\tau}_L, \\ \tilde{\tau}_2 &= \cos \theta_{\tilde{\tau}} \tilde{\tau}_L - \sin \theta_{\tilde{\tau}} \tilde{\tau}_R. \end{aligned} \quad (36)$$

For a vanishing mixing $\cos \theta_{\tilde{\tau}}$ goes to 1 and $\tilde{\tau}_1 = \tilde{\tau}_R$.

Let us review what we have done so far. We have built up a supersymmetry preserving Lagrangian that is furthermore renormalizable, gauge invariant under the SM gauge

group, R-parity preserving and it serves to describe the particle content of the SM (and especially its gauge multiplet structure) under the premise of minimality (and thereby introduces the superpartners). Furthermore we met the obvious experimental requirement of supersymmetry breaking under the theoretical restrictions from the hierarchy problem by adding up soft mass terms for the superpartners. And we showed that further experimental conditions could be met by applying the universality relations. Now, as we said there still (after applying the latter) remain 14 new free parameters. So, as long as there are no further experimental exclusions on the parameter space considering supersymmetry means to consider a large variety of models. There are many possibilities for the mass spectrum and thus for the decay channels and production rates of these particles. So, in the present state of research it is sensible to restrict oneself to a more or less specific choice of scenario.

There are basically two approaches to restrict oneself to a certain scenario. The first is to classify a scenario on the basis of its signature in a specific experiment like the LHC, these are experiment motivated scenarios. The second is to classify a scenario by its underlying theoretical model. While in the first approach one has in principle to scan the whole parameter space to cover all possible sources of a certain signature, in the second approach one has a certain model in mind and tries to look for the different incarnations in phenomenology it may lead us to. In most cases it is more or less a mixture of both approaches, and we are no exception here. Therefore, in the next section we will introduce some supersymmetry-breaking models, that lead to more or less specific predictions. Although each model still allows a certain parameter space, there are some basic features provided, for example what the LSP and the NLSP would most likely be.

3 Choice of scenarios

In the last section we have followed a low-energy approach in just parameterizing the desired breaking effects without worrying how such terms can be generated by a dynamic mechanism. Let's go one step back in our progression in building a viable supersymmetric model and consider a generic supersymmetric Lagrangian of the form (16). It is easy to show [55] that supersymmetry is spontaneously broken if the expectation value of at least one of the auxiliary fields F and D does not vanish in the vacuum state (or some higher energy metastable state which we live in). The corresponding mechanisms that fulfill these conditions are called F -term and D -term breaking, respectively. But if one tries to acquire these mechanisms solely within the particle content and interactions of the MSSM, one gets into trouble. So it seems to be clear that one has to extend the MSSM somehow.

We will concentrate our further considerations for the case of F -term breaking, since it offers broader phenomenological prospects. The general ansatz in extending the MSSM is to state that there is a breaking source sector that is distinct from the fields that make up the MSSM. In most models the fields that reside in the breaking source sector are assumed to be neutral under the SM gauge group, why it is usually called the 'hidden sector' (in contrast to the 'visible sector' that hosts the MSSM). The scope of breaking scenarios is to describe how supersymmetry breaking is communicated from the source to the MSSM. A phenomenologically valid model could not be achieved only with renormalizable interactions at tree level. The tree-level squared mass sum rules would not allow the required overall mass-shift of the superpartners nor would there be any (gaugino)²(scalar)-coupling (that is required to give masses to the gauginos at tree-level) in a supersymmetric Lagrangian with the restrictions of section 2. Therefore we have to contemplate scenarios in which the mediation between the two sectors arise radiatively or by some effective field theory that describes the low-energy limit of a fundamental theory, which we are not able to describe fundamentally yet. If the mediating interactions are flavor-blind, we will furthermore fulfill the universality relations 'naturally'.

No matter what the hidden sector might be, as long as it contains an auxiliary field F that obtains a VEV to break supersymmetry, there is a massless Nambu-Goldstone mode that belongs to the supermultiplet according to F . Due to the Goldstone-Theorem it is characterized by the same quantum numbers as the generator of the (broken) symmetry. Thus, the Nambu-Goldstone particle is a Weyl fermion (spin 1/2) that is neutral under the SM gauge group. It is called the goldstino \tilde{G} . In principle the goldstino interacts with all the particles in the visible sector but its interactions are suppressed by $1/\langle F \rangle$. We will see below of which order of magnitude $\langle F \rangle$ can be for the different breaking models. The interactions of the goldstino with all the other supermultiplets can be described by the supersymmetric Goldberger-Treiman relation [38, 25, 53]

$$\mathcal{L}_{\text{int}}^{\tilde{G}} = -\frac{1}{\langle F \rangle} j^{\mu\alpha} \partial_\mu \tilde{G}_\alpha + \text{c.c.}, \quad (37)$$

where j_α^μ is the supercurrent that depends on all fermion-boson pairs

$$j_\alpha^\mu = (\sigma^\nu \bar{\sigma}^\mu \psi_i)_\alpha \partial_\nu \phi^{*i} - \frac{1}{2\sqrt{2}} (\sigma^\nu \bar{\sigma}^\rho \sigma^\mu \lambda^{\dagger a})_\alpha F_{\nu\rho}^a + \dots \quad (38)$$

($F_{\nu\rho}^a$ is the Yang-Mills field strength of the gauge group a).

The gravitino

Whatever the mediating interaction between the hidden and the visible sector may be, there is one interaction that always couples to both sectors, since all particles carry energy⁶: gravity. The question is if this interaction is the dominant part in the mediation between the two sectors or not. In case it is, one speaks of gravity-mediation (or sometimes Plack-scale-mediation) and we will give some characteristic features of it below, when listing a few further breaking-models.

If dominant or not, to introduce gravity in the context of supersymmetry models means to add another supermultiplet to the scene. And that might lead to phenomenological signatures. So, although gravity by itself is irrelevant for collider experiments, the so called supergravity [59, 20] can principally provide very interesting aspects to our predictions.

The new supermultiplet contains the graviton $g_{\mu\nu}$ (the spin 2 tensor field) and its fermionic superpartner, the gravitino Ψ_α^μ , a Majorana vector field with spin 3/2 (therefore it carries both indices, a vector index μ and the spinor index α). As long as supersymmetry is unbroken both fields are massless, but when there is an auxiliary field that obtains a VEV to break supersymmetry, the gravitino gets a mass. This mechanism is called the super-Higgs mechanism [26] for it is similar to the Higgs mechanism that take place in the case of electroweak symmetry breaking. Let us explain this.

The only ingredient to the step from (ordinary) supersymmetry to supergravity is to make the supersymmetry transformation local. In this sense supergravity appears as a gauge theory of global supersymmetry, whose gauge field is the gravitino. Just as in the case of electroweak symmetry breaking, the gauge field absorbs the Nambu-Goldstone mode of the broken symmetry, which afterwards formally disappeared, but leave its degrees of freedom to the gauge field. Hence, by absorbing the goldstino, the gravitino gets its mass and inherits the spin 1/2 components. The gravitino now has 4 spin states. The interactions of the spin 1/2 components can be approximately described by (37), thus from the perspective of interaction with other particles we can interchangeably speak of a gravitino or a goldstino since the spin 1/2- or goldstino-couplings are relatively enhanced by a factor of $M_{\text{P}}^2/\langle F \rangle$ with respect to the couplings of the spin 3/2-components that are of gravitational strength. At tree-level the gravitino mass can be estimated to give [52]

$$m_{3/2} = \frac{\langle F \rangle}{\sqrt{3}M_{\text{P}}} . \quad (39)$$

⁶This simply is our notion of particles.

Supersymmetry scenarios from the model-building perspective

In the phenomenology of supersymmetry breaking models the lightest supersymmetric particle (LSP) plays a key role. This is due to the fact that all supersymmetric particles—once they are produced—will directly or indirectly (through cascades) decay into the LSP. But since one considers models that provide an LSP that is neutral with respect to electric and color charge or even to the whole SM gauge group (as is the case with the gravitino) the direct decay from heavy supersymmetric particles into the LSP is usually suppressed. Because of this—at least in the latter case of a gravitino LSP—the next-to-lightest supersymmetric particle (NLSP) is of special interest, too.

We will now sketch some of the scenarios the different supersymmetry breaking models will provide. All breaking mechanisms successfully reduce the parameter space of 105 supersymmetry parameters to a few parameters. These parameters fix the particles' masses at the entrance scale (the scale of the supersymmetry breaking source). The soft masses at the electroweak scale can then be omitted by evolving the particle masses via the renormalization group (RG) equations.

In *gauge-mediated supersymmetry breaking* models [27, 29, 28] (see also [40, 51]) one extends the MSSM by a messenger sector containing new chiral multiplets that take part in the $SU(3)_C \times SU(2)_L \times U(1)_Y$ gauge group interactions of the MSSM and a hidden sector that provides the supersymmetry breaking VEV $\langle F \rangle$. The direct coupling of the messenger particles to the hidden sector leads to a supersymmetry breaking mass spectrum in the messenger sector. The messenger particles appear in the loop corrections to the MSSM particle masses and so the messenger particles transmit supersymmetry breaking to the visible sector by virtue of these virtual corrections.

Taken a characteristic scale M_{mess} for the masses of the messenger particles one can estimate the order of magnitude of the induced soft masses by dimensional analysis. The soft masses must vanish in the unbroken limit $\langle F \rangle \rightarrow 0$ as well as in the limit $M_{\text{mess}} \rightarrow \infty$ where the messenger particles are too heavy to give reasonable contributions to virtual corrections. One obtains

$$m_{\text{soft}} \sim \frac{\alpha_a}{4\pi} \frac{\langle F \rangle}{M_{\text{mess}}} . \quad (40)$$

Here, $\alpha_a/(4\pi)$ is the one-loop factor for the gauge interaction a . If we take M_{mess} and $\langle F \rangle$ to be of the same order of magnitude, the desired soft masses of a few hundred GeV can be obtained by setting the supersymmetry breaking scale to $\sqrt{\langle F \rangle} \sim 10^5$ GeV. Applying (39), this leads to a gravitino mass that is typically in the eV to keV range. But, depending on the chosen parameters the gravitino mass can in principle also be much higher. Nevertheless, in this scenario, the gravitino would reasonably be the LSP. As the NLSP the lightest neutralino $\tilde{\chi}_1^0$ or the lighter stau $\tilde{\tau}_1$ are a possibility. From (40) you can also see that gauge-mediation tends to separate the mass spectrum in strongly coupled and electroweak coupled particles due to the larger value of α_s . Figure 1 shows a gauge-mediation spectrum with a $\tilde{\tau}$ NLSP, the benchmark point SPS 7 [7]. The high-scale parameters in gauge-mediation are $\Lambda = \langle F \rangle / \langle S \rangle$ (S is the corresponding scalar field to F), M_{mess} , $\tan \beta$, $\text{sgn}(\mu)$ and N_{mess} , the messenger index that parameterizes the

structure of the messenger sector.

In *gravity-mediated supersymmetry breaking* models [22, 46] Planck-scale physics is the source of supersymmetry breaking. Formally the mediation between the hidden sector and the MSSM is applied by introducing non-renormalizable terms in the Lagrangian where the couplings of negative mass dimension are of the order of powers of $1/M_P$. In gravity-mediated breaking models the soft masses are of order

$$m_{\text{soft}} \sim \frac{\langle F \rangle}{M_P}, \quad (41)$$

which can again be obtained by dimensional analysis. In contrast to gauge-mediation one yields a much higher breaking scale to cover the desired order of m_{soft} , roughly $\sqrt{\langle F \rangle} \sim 10^{11}$ GeV and the gravitino mass is comparable to m_{soft} . So, the gravitino may or may not be the LSP. Another candidate is the lightest neutralino. With some further assumptions, at the Planck-scale the soft parameters take a particularly simple form:

$$\mathbf{m}_{\mathbf{Q}}^2(M_P) = \mathbf{m}_{\mathbf{L}}^2(M_P) = \mathbf{m}_{\mathbf{u}}^2(M_P) = \mathbf{m}_{\mathbf{d}}^2(M_P) = \mathbf{m}_{\mathbf{e}}^2(M_P) = m_0 \mathbf{1} \quad (42)$$

$$m_{H_u}^2(M_P) = m_{H_d}^2(M_P) = m_0^2 \quad (43)$$

$$\mathbf{a}_{\mathbf{f}} = A_0 \mathbf{y}_{\mathbf{f}}, \quad \mathbf{f} = \mathbf{u}, \mathbf{d}, \mathbf{e}, \quad (44)$$

as well as

$$M_1(M_U) = M_2(M_U) = M_3(M_U) = m_{1/2} \quad (45)$$

for the bilinear gaugino terms, where M_U is the unification scale. With this the high-scale parameters in gravity-mediation are m_0 , $m_{1/2}$, A_0 , $\tan \beta$ and $\text{sgn}(\mu)$.

As we stated above gravitational phenomena are always present, and supergravity effects will give a contribution to the supersymmetry-breaking. Speaking of gauge-mediation for instance only means that the virtual exchange of the messenger particles dominates over the gravitational interaction between the hidden and visible sector. Anyway, in principle there could be a mixture of both competing mechanisms and thus one can achieve any gravitino mass in between the keV range and m_{soft} . But of course, it is fair to ask why the two distinct mechanisms should be roughly of the same order.

These are the most studied breaking models. Anyway, there are further very interesting proposals.

In *gaugino-mediation* [50, 21] the supersymmetry breaking source is hidden by extra dimensions. The matter fields of the MSSM live on a 3-brane that is spatially separated (in the extra dimensions) from the brane that contains the breaking source. Whereas, the gauge supermultiplet fields propagate in the bulk and therefore receive mass through direct interaction with the source brane. The sfermion masses are absent at the input scale but they are generated via loop corrections (thanks to the appearance of the gaugino masses in the RG equation) at lower scales. In a large domain of parameter space a gravitino LSP is favored. Its mass can be estimated to be $m_{3/2} \gtrsim 10$ GeV and it is naturally accompanied by a stau NLSP [19]. Figure 1 shows a spectrum for the gaugino-mediation model with $m_{1/2} = 500$ GeV, $\tan \beta = 10$, $\mu > 0$, $m_0 = A_0 = 0$.

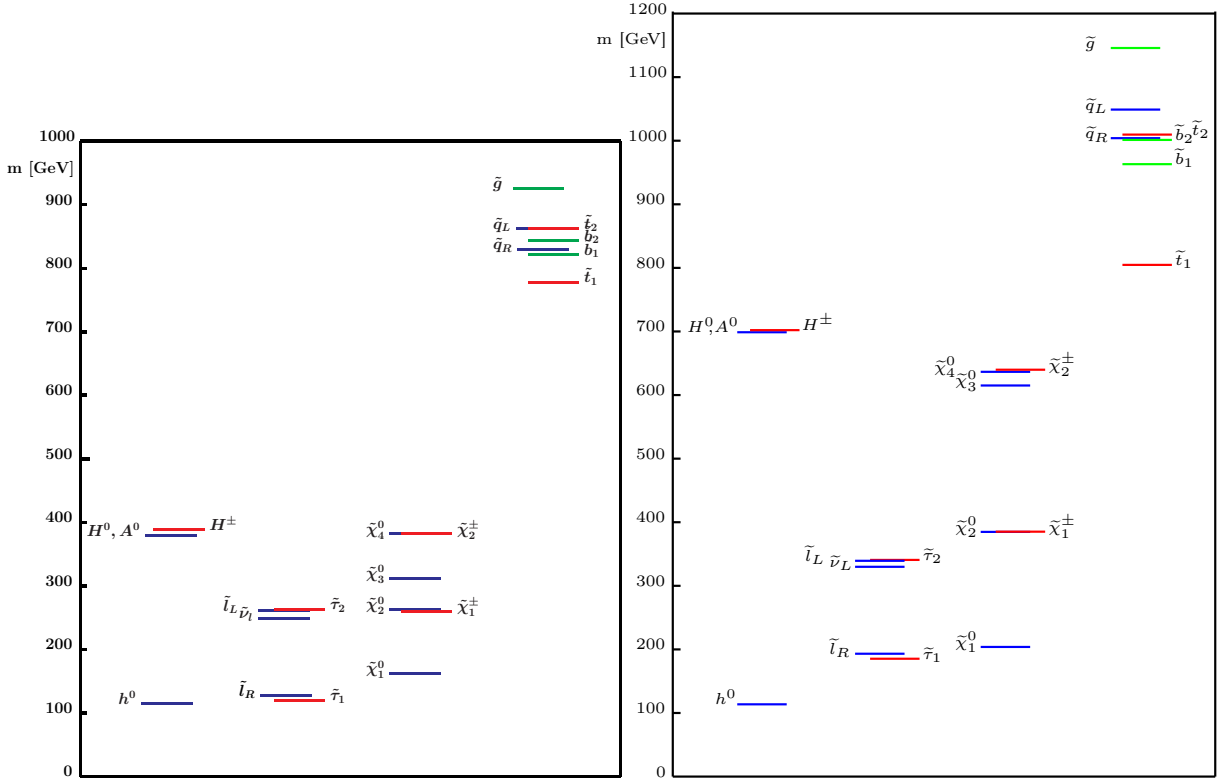


Figure 1: Left: Spectrum of a gauge-mediation scenario with $\Lambda = 40$ TeV, $M_{\text{mess}} = 80$ TeV, $\tan \beta = 15$, $\mu > 0$ and $N_{\text{mess}} = 3$, this is the benchmark point SPS 7, taken from [7]. Right: Spectrum of a gaugino-mediation scenario with $m_{1/2} = 500$ GeV, $\tan \beta = 10$, $\mu > 0$, $m_0 = A_0 = 0$, calculated with SOFTSUSY [6]. Both scenarios provide a gravitino LSP and a stau NLSP. The stau mass mixing angle is $\cos^2 \theta_{\tilde{\tau}} = 0.977$ and 0.980 in the case of gauge- and gaugino mediation, respectively.

Another model is the *anomaly-mediated supersymmetry breaking* [41, 65], where scalar and gaugino masses arise at the quantum level from the superconformal anomaly. These models predict very high gravitino masses (typically above m_{soft}) and therefore cannot provide for a gravitino LSP.

The gravitino-stau scenario from a collider experiment perspective

We have seen that different supersymmetry breaking models exist that provide for a gravitino LSP. The possible gravitino masses cover the whole range from eV up to the soft masses. A stau NLSP is possible in all these models. We will now investigate in the collider signature of a gravitino-stau scenario.

In a collider like the LHC scattering of SM particles is the origin of all further processes. Hence, due to R -parity (or else due to the relative suppression of R -parity-violating interactions) supersymmetric particles will (almost) always be produced in pairs. Once they are produced they will almost certainly decay promptly into the stau NLSP. This is because all supersymmetric particles, except the gravitino, share the SM gauge interactions. And furthermore the masses of the SM particles that are involved in the three-body decay of one supersymmetric particle into a lighter one, like $\tilde{e}_L^- \rightarrow e_r^- \tau_L^+ \tilde{\tau}_R^-$, are typically very light with respect to the involved supersymmetric particles. Hence, those decays are usually kinematically not suppressed. There might be exceptions. If, for instance, the slepton mass eigenstates \tilde{e}_R , $\tilde{\mu}_R$ and $\tilde{\tau}_1$ are degenerate to within less than m_τ , the three body decay (such of the form from above) are kinematically not allowed. In such a case \tilde{e}_R , $\tilde{\mu}_R$ and $\tilde{\tau}_1$ act as co-NLSPs. Such a situation could be evoked by small values of $\tan\beta$. Another (exotic) exception would be a relatively light stop \tilde{t}_R , whose mass is less than $m_{\tilde{\tau}_1} + m_t$. But we don't know breaking models that favor such situations.

Anyway, we will not discuss such scenarios, although in a co-NLSP scenario the co-NLSP(s) would behave much like the NLSP and therefore such a scenario is qualitatively similar to the one-NLSP case. To a first approximation the additional co-NLSPs just give another degree of freedom to sum over when calculating the production cross section.

Now, once the sparticles have decayed into the NLSP, the NLSP by itself will decay into the LSP, the gravitino. Of course as we showed above, the gravitino does not share the SM gauge interactions and therefore this decay is suppressed according to the strength of the goldstino coupling. Depending on the gravitino mass this decay can be prompt, delayed or quasi-stable (that is, the stau is long-lived and will escape the detector). Ok, if the decay is prompt the above argument that *all* heavy sparticles decay initially into the NLSP may not be right anymore. Anyway, from (37) one can derive the decay width of a sparticle \tilde{X} decaying into its SM partner X and the gravitino (respectively its goldstino components \tilde{G}).

$$\Gamma(\tilde{X} \rightarrow X\tilde{G}) = \frac{m_{\tilde{X}}^5}{16\pi\langle F \rangle^2} \left(1 - m_X^2/m_{\tilde{X}}^2\right)^4. \quad (46)$$

By applying (39) to this formula and neglecting m_X one obtains the decay length

$$\frac{d}{\text{cm}} \simeq 1.7 \times 10^{13} v\gamma_v \left(\frac{m_{3/2}}{\text{keV}}\right)^2 \left(\frac{m_{\tilde{\tau}}}{\text{GeV}}\right)^{-5}, \quad (47)$$

where v and γ_v (the relativistic gamma-factor according to v) are expressed in the laboratory frame. In figure 2 this expression is plotted for $v = 0.6$ ($v\gamma_v = 3/4$). It shows the curves of equal decay length d in cm in the $m_{\tilde{G}}-m_{\tilde{\tau}_1}$ -plane. The characteristic dimension of a LHC detector is roughly 10^3 cm.⁷ Thus, in the case the decay length is well below

⁷Since the staus will be detected in the muon chambers that are positioned cylindrically around the inner detector, their way of flight through the detector depends on the scattering angle (the angle of their motion with respect to the beam axis). The minimal distance from the interaction point to the muon

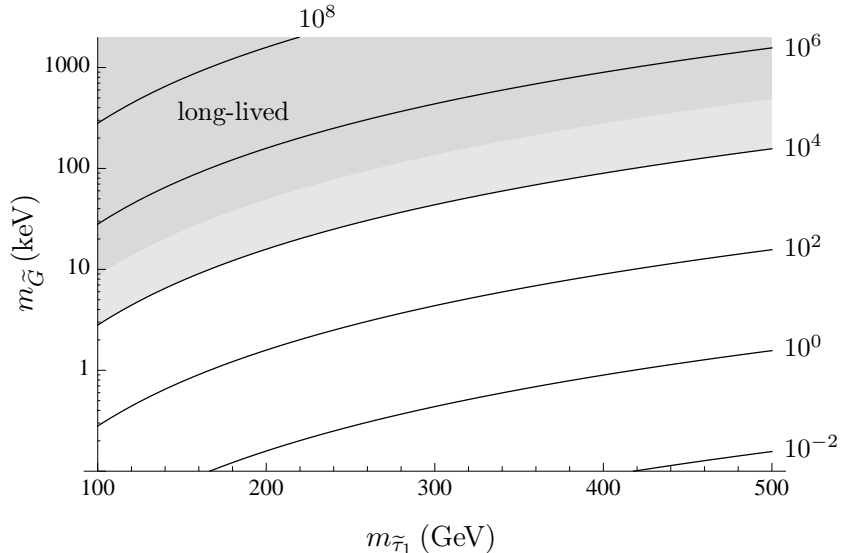


Figure 2: Curves of equal decay length d in cm in the $m_{\tilde{G}}-m_{\tilde{\tau}_1}$ -plane, obtained from the formula (47). v is set to the low velocity detection-limit of 0.6. Thus, since the velocity distribution of staus typically increases with increasing velocity—as we will already see in the next section—these values give a conservative estimation of $m_{\tilde{G}}-m_{\tilde{\tau}_1}$ -regions that provide a long-lived stau. If the velocity is higher the curves have to be pulled down with respect to the factor $(v\gamma_v)^{-1/2}$.

10^3 cm the decay would most likely take place inside the detector. This will lead to interesting phenomenology. The signature of such an event would be a high- p_{\perp} τ -lepton plus missing energy.

In the region $d \gtrsim 10^4$ cm roughly 90% (and in the region $d \gtrsim 10^5$ cm roughly 99%) of the staus would escape the detector. These staus are accessible to direct detection. As a charged massive particle, the staus will be registered as ‘heavy muons’ in the detector. In contrast to the muons, the staus will not be throughout ultrarelativistic at LHC-energies and therefore will cause high ionization tracks and anomalously long time-of-flight measurements. Moreover, the number of long-lived NLSP staus in an event will always be even (although this doesn’t mean that one is always able to identify both tracks, be it because of failing discrimination from the muons or insensitive detector

chambers (in the transverse direction) is 7.5 m and 11 m for the CMS and ATLAS detector, respectively. The maximal distance (to the outermost corner where the barrel and end-caps come together) is ~ 12 m and ~ 16 m, respectively [3, 1].

regions—around the beam axis—or even that the staus are too slow, to match them with the right bunch crossing). These are indeed very attractive phenomenological features.

Let’s have a closer look at the production channels of staus. We discuss electroweak and strong production. First we consider the electroweak production. At a pp-collider like the LHC quark-antiquark annihilation allows scalar-pair production via s-channel Z and A (photon) or W^\pm at lowest order (α^2).

In the case of Z, A direct stau NLSP production is accessible. This is a unique feature, since this production is independent of all the supersymmetry parameters but the stau mass (and its mixing angle). Furthermore the two staus within one event always come with opposite charge and their momenta will be strongly correlated (to the extent of the smallness of higher order corrections when one adds up parton radiation, but we will still see this feature in higher orders, as our later calculation will show up). This is a very prominent collider signature, that gives us a (relatively) simple experimental access. Of course, Z, A can also produce heavier particles that will afterwards decay into the $\tilde{\tau}_1$, but these will surely not give much contribution. The production at hadron colliders via Z, A in the s-channel is traditionally called Drell-Yan process.

In the production via W^\pm it is unlikely to directly produce a $\tilde{\tau}_1$. This is because the W^\pm only couples to the $\tilde{\tau}_L^\pm$ and not to the $\tilde{\tau}_R^\pm$.⁸ So, the production is suppressed by $\sin^2 \theta_{\tilde{\tau}}$, which is typically $\lesssim 0.1$ (in our exemplary scenarios whose spectra are shown in figure 1 $\sin^2 \theta_{\tilde{\tau}}$ is even as small as ~ 0.02). Furthermore the sneutrino will obviously be heavier than the stau NLSP (in many models the ratio $m_{\tilde{\nu}_\tau}/m_{\tilde{\tau}_1}$ is typically around $1.8 \sim 2.0$). So, these two facts will overcompensate the factor of ~ 10 to which the W^\pm -coupling is typically larger than the Z -coupling. The processes $W^+ \rightarrow \tilde{\tau}_2^+ \tilde{\nu}_\tau$ and $W^- \rightarrow \tilde{\tau}_2^- \tilde{\nu}_\tau$ by contrast could be roughly of the same order as the direct production of $\tilde{\tau}_1$ via Z, A . The $\tilde{\tau}_2$ and $\tilde{\nu}_\tau$ each decays in a three-body decay into the $\tilde{\tau}_1$ and a τ . Due to the charge asymmetry of the initial state particles (that are two protons), the production via W^+ is favored by a factor of roughly $3/2$ with respect to the one via W^- . This could cause a small amount of charge asymmetry in the final state staus in the case that $\sin^2 \theta_{\tilde{\tau}}$ is not too small (and therefore the intermediate state in the three-body decay is allowed to be wino-like). However, in contrast to the case of Z, A the two staus in a single event do not necessarily have opposite charge.

Let’s consider the strong production. Since the LHC is a proton-proton collider it is clear that strong production processes are in principle favored. At leading order (α_s^2) squark-and gluon-pair production each allows a variety of diagrams that already includes gg -annihilation, which is a dominant hadronic channel at the LHC.⁹ The squark-pair could either be a squark-antisquark-pair of the same flavor (from a gluon in the s-channel, a squark in the t- or u-channel or from the four-vertex $gg \rightarrow \tilde{q}^+ \tilde{q}^-$, see (146)) or a squark-antisquark pair of different flavor coming from a gluino in the t- or u-channel or even a squark-pair of the same charge also coming from a gluino in the t- or u-channel.

⁸Remember, the supersymmetric counterpart of the allowed SM vertex $W^+ \rightarrow \tau_R^+ \nu_\tau$ is $W^+ \rightarrow \tilde{\tau}_L^+ \tilde{\nu}_\tau$.

⁹Section 5 will show that the hadronic channel gg is about one to even two orders of magnitude larger in the region of interest than $q\bar{q}$, that is the only hadronic channel accessible for electroweak production at lowest order.

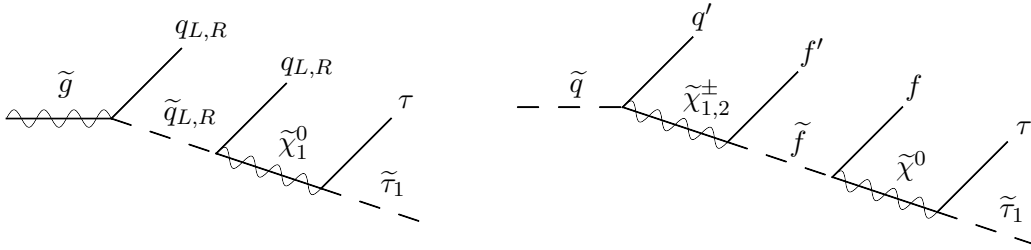


Figure 3: Exemplary cascade decay chains of strongly produced sparticles down to the stau NLSP. Each vertex in these decay chains is of the form (147, 148). The chargino changes the flavor, this is denoted with a prime. The last decay within these chains is suggestively displayed as transmitted by the lightest neutralino. Here is the reason: A chargino is either higgsino- or wino-like. While the higgsino-coupling is suppressed by the relatively lightness of the SM partners of the involved sparticles, the wino coupling to the $\tilde{\tau}_1$ is suppressed by $\sin^2 \theta_{\tilde{\tau}}$. Thus, it is most likely to have a bino-like neutralino in the last link of the decay chain. Now, in a stronger version of the rules of thumb, that we formulated in the last section, one can state that in supergravity models the lightest neutralino is most likely to be bino-like.

Additionally there are s-, t- and u-channel diagrams for squark-gluino production from the hadronic channel qg . Figure 3 shows two exemplary decay chains starting from one gluino and one squark. The production rate of staus via these cascade decays is only suppressed by the largeness of the masses of the produced strongly interacting sparticles.

Just for completeness we want to mention that there is one more direct production channel of $\tilde{\tau}_1$ -pairs, the production via Higgs bosons. Of course, production via h would be negligible, but the resonance of H could in principle appear in the invariant mass spectrum of the staus. If $\sin^2 \theta_{\tilde{\tau}}$ is not so small this might possibly be measurable. Since H only couples to left-right-handed stau-pairs, the direct production of a NLSP stau pair is highly sensitive to $\sin^2 \theta_{\tilde{\tau}}$. But we will not discuss this further, since the contribution to the total cross section will be negligible, too.

Now, the strong production of staus via cascade decays is most likely to be the dominant production channel. Nevertheless within a sensible range for the masses of the sparticles a dominant electroweak production is not ruled out. (We will briefly discuss this subject again in section 6.) The problem with cascade decays is, that if one makes predictions for the stau cross sections, nearly all soft parameters enter this calculation. Thus, to do such a calculation one either has to restrict oneself to a specific choice of parameters or one has to scan the whole parameter space, which is truly not a trivial task. Anyway, within this thesis we won't specify on a certain choice of parameters, but consider only the direct production of staus via the Drell-Yan process. Therefore our predictions are fully independent of the parameter space concerning the particles that are heavier than the NLSP. The only remaining parameters are $m_{\tilde{\tau}_1}$ and $\theta_{\tilde{\tau}}$. We know

that the direct production via Drell-Yan is always present. So in that sense our estimation of the discovery potential of staus at the LHC gives a strict prediction, at worst a very conservative one.

In the next section we will thoroughly derive the cross section formulas for the Drell-Yan process, starting from the Lagrangian terms we've introduced in the last section. We'll do this first on the elementary level (that is as a scattering process of quarks). In the then following section we will stick to the hadron level.

4 Elemental stau production processes

In order to calculate the stau-pair production via the Drell-Yan process, in this section we will derive the cross section for the elemental process $q\bar{q} \rightarrow Z, A \rightarrow \tilde{\tau}^-\tilde{\tau}^+$ from the supersymmetry Lagrangian of section 2 at tree-level.

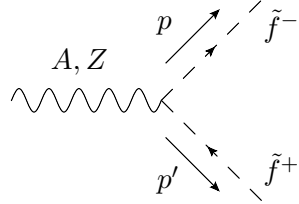
Thus, we need to have the Vertex function for $Z, A \rightarrow \tilde{\tau}^-\tilde{\tau}^+$. Such a term is only obtained from the scalar gauge coupling term that appears in the first term in the third line of (16), see also (145). The relevant $SU(2)_L \times U(1)_Y$ covariant derivative reads in terms of the mass eigenstate fields Z_μ and A_μ

$$D_\mu = \partial_\mu - i\frac{g}{\cos\theta_w}Z_\mu(T^3 - Q\sin^2\theta_w) - ieQA_\mu \quad (48)$$

where $g = e/\sin\theta_w$ (and we have left out the W_μ^\pm -contributions). For the corresponding Lagrangian term we obtain

$$\begin{aligned} & -D^\mu\phi^{*i}D_\mu\phi_i \Big|_{A,Z \rightarrow \tilde{f}_R\tilde{f}_R, \tilde{f}_L\tilde{f}_L} \\ &= -i(\phi^{*i}\partial^\mu\phi_i - \phi_i\partial^\mu\phi^{*i}) \left(\frac{g}{\cos\theta_w}Z_\mu(I_3 - Q\sin^2\theta_w) + ieQA_\mu \right) \end{aligned} \quad (49)$$

yielding the Vertex function

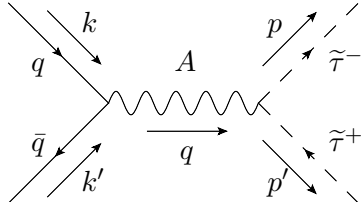


$$= -i \left(\frac{g}{\cos\theta_w}(T^3 - Q\sin^2\theta_w) + eQ \right) (p - p')^\mu. \quad (50)$$

In (49) and (50) T^3 and $Q = T^3 + Y$ are meant to be the respective eigenvalues of the corresponding $SU(2)_L \times U(1)_Y$ generators. The formulas hold for all sfermions \tilde{f} . We obtain $Q = -1$ and $T^3 = -1/2$ (0) for charged left-handed (right-handed) sleptons.

QED interaction

In a first step we consider the photon exchange, using the A_μ contribution of (50). This contribution is independent of T^3 . Hence, it holds either for left- or for right-handed staus. Multiplied by the SM photon propagator, $q\bar{q} \rightarrow A$ -vertex and Dirac-spinors of the incoming quarks, the matrix element reads



$$= ie(p - p')^\mu \frac{-ig_{\mu\nu}}{(k + k')^2} \bar{v}(k')(-iee_q\gamma^\nu)u(k). \quad (51)$$

Since in the end we will use the formulas in the context of the Drell-Yan process we assume the spin orientation of the incoming quark-antiquark pair to be arbitrarily distributed. Therefore we have to average over the quark spins by applying $1/4 \sum_{\text{spins}}$ to the squared matrix of the process:

$$\begin{aligned}
\frac{1}{4} \sum_{\text{spins}} |\mathcal{M}|^2 &= \frac{e^4 e_q^2 (p-p')_\mu (p-p')_\nu}{(k+k')^4} \frac{1}{4} \sum_{\text{spins}} \bar{v}(k') \gamma^\mu u(k) \bar{u}(k) \gamma^\nu v(k') \\
&= \frac{e^4 e_q^2}{(k+k')^4} (p-p')_\mu (p-p')_\nu \frac{1}{4} \text{tr}[(\not{k}' - m_q) \gamma^\mu (\not{k} + m_q) \gamma^\nu] \\
&= \frac{e^4 e_q^2}{(k+k')^4} (p-p')_\mu (p-p')_\nu \{k'^\mu k^\nu + k^\mu k'^\nu - g^{\mu\nu} (k' \cdot k + m_q^2)\}.
\end{aligned} \tag{52}$$

$(p-p')_\mu (p-p')_\nu$ is symmetric under the exchange of $\mu\nu$. Thus we can combine the first two terms of the sum in curly brackets. Together with $(p-p')^2 = 2(m_\tau^2 - p' \cdot p)$ concerning the last term in the curly brackets we arrive at

$$\frac{1}{4} \sum_{\text{spins}} |\mathcal{M}|^2 = \frac{e^4 e_q^2}{(k+k')^4} 2\{ (p-p') \cdot k' (p-p') \cdot k + (p' \cdot p - m_\tau^2)(k' \cdot k + m_q^2) \} \tag{53}$$

This is the general expression, although it is not very handy. But before we express the occurring quantities in a Lorentz-invariant way (which will be very useful later on), let's first step into the cm-frame of this process where we can already observe some central quantities. In the cm-frame one can find ($\sqrt{\hat{s}}$ is the cm-energy of this process):

$$k^0 = k'^0, \quad \mathbf{k} = -\mathbf{k}' \tag{54}$$

$$p^0 = p'^0, \quad \mathbf{p} = -\mathbf{p}' \tag{55}$$

$$k+k' = \begin{pmatrix} \sqrt{\hat{s}} \\ \mathbf{0} \end{pmatrix} \tag{56}$$

$$p-p' = \begin{pmatrix} 0 \\ 2\mathbf{p} \end{pmatrix} \tag{57}$$

$$p \cdot p' = p^{02} + \mathbf{p}^2 = m_\tau^2 + 2\mathbf{p}^2 \tag{58}$$

$$k \cdot k' = k^{02} + \mathbf{k}^2 = m_q^2 + 2\mathbf{k}^2 \tag{59}$$

And so, with $\mathbf{p} \cdot \mathbf{k} = |\mathbf{p}||\mathbf{k}| \cos \theta$ the curly bracket in (53) turn into

$$-4\mathbf{p}^2 \mathbf{k}^2 \cos^2 \theta + 4\mathbf{p}^2 (m_q^2 + \mathbf{k}^2). \tag{60}$$

We shall neglect the quark mass, $m_q = 0$, $\mathbf{k}^2 = \hat{s}/4$, and so the squared matrix element is

$$\frac{1}{4} \sum_{\text{spins}} |\mathcal{M}|^2 = \frac{2e^4 e_q^2}{\hat{s}} \mathbf{p}^2 (1 - \cos^2 \theta). \tag{61}$$

Therewith the cross section is

$$\begin{aligned}
\frac{d\hat{\sigma}}{d\Omega} &= \frac{|\mathbf{p}|}{32\pi^2 \hat{s}^{3/2}} \frac{1}{4} \sum_{\text{spins}} |\mathcal{M}|^2 \\
&= \frac{e^4 e_q^2}{16\pi^2} \frac{|\mathbf{p}|^3}{\hat{s}^{5/2}} (1 - \cos^2 \theta) \\
&= \frac{\alpha^2 e_q^2}{8\hat{s}} \left(1 - \frac{(2m_{\tilde{\tau}})^2}{\hat{s}} \right)^{\frac{3}{2}} (1 - \cos^2 \theta).
\end{aligned} \tag{62}$$

In the last line we have applied $|\mathbf{p}|^2 = \hat{s}/4 - m_{\tilde{\tau}}^2$ as well as $e^4 = (4\pi\alpha)^2$ (since we work in Heaviside-Lorentz units).

The angle dependency is that of a spherical harmonic with $\ell = 1$, $m_\ell = -1, 1$. This is not surprising since the exchanged photon has spin 1 and furthermore the incoming particles are assumed to be massless, thus the spin orientation has to be parallel to the beam axis ($m_\ell = -1, 1$). (In this ultrarelativistic limit there is no overlap with the $\ell = 1$, $m_\ell = 0$ wave function.) Thus, the staus carry an angular momentum $L = 1$.

Integrating over the angles replaces the angle dependency by the factor of $\int d\Omega (1 - \cos^2 \theta) = 8\pi/3$, obtaining the total cross section¹⁰

$$\hat{\sigma}_{\text{tot}} = \frac{\pi\alpha^2 e_q^2}{3\hat{s}} \left(1 - \frac{(2m_{\tilde{\tau}})^2}{\hat{s}} \right)^{\frac{3}{2}}. \tag{63}$$

We would like to compare these results to the case of the SM muon pair production, since this is our SM background. The respective tree-level cross section (in the limit of relativistic muons) reads [61]

$$\left(\frac{d\hat{\sigma}}{d\Omega} \right) (q\bar{q} \rightarrow \mu^- \mu^+) = \frac{\alpha^2 e_q^2}{4\hat{s}} (1 + \cos^2 \theta) \tag{64}$$

and since $\int d\Omega (1 + \cos^2 \theta) = 16\pi/3$,

$$\hat{\sigma}_{\text{tot}}(q\bar{q} \rightarrow \mu^- \mu^+) = \frac{4\pi\alpha^2 e_q^2}{3\hat{s}}. \tag{65}$$

The muons have a completely different angle distribution. That is because the spins of the outgoing muons are favored to be parallel to the spins of the incoming quarks that is parallel to the beam axis. But since the muons are ultrarelativistic the direction of their momentum is correlated similarly. By contrast, the angle distribution of the staus vanishes in the direction of the beam axis.

Let's consider the total cross sections. Their ratio (as a function of \hat{s}) behaves like

$$\frac{\hat{\sigma}_{\text{tot}}^{\tilde{\tau}^- \tilde{\tau}^+}}{\hat{\sigma}_{\text{tot}}^{\mu^- \mu^+}} \sim \left(1 - \frac{(2m_{\tilde{\tau}})^2}{\hat{s}} \right)^{\frac{3}{2}} \Theta \left(1 - \frac{(2m_{\tilde{\tau}})^2}{\hat{s}} \right) \tag{66}$$

¹⁰Let's plug in some numerical values to see in which order of magnitude the cross section turns out to be. Applying $\alpha(M_Z)^{-1} \simeq 128$ and choosing $\sqrt{\hat{s}} = 1$ TeV and $e_q = +2/3$ for an up-quark (-anti-quark) pair the stau mass-independent factor of (63) is $\hat{\sigma}_{\text{tot}}|_{(4m_{\tilde{\tau}}^2/\hat{s}) \rightarrow 0} \simeq 11$ fbarn.

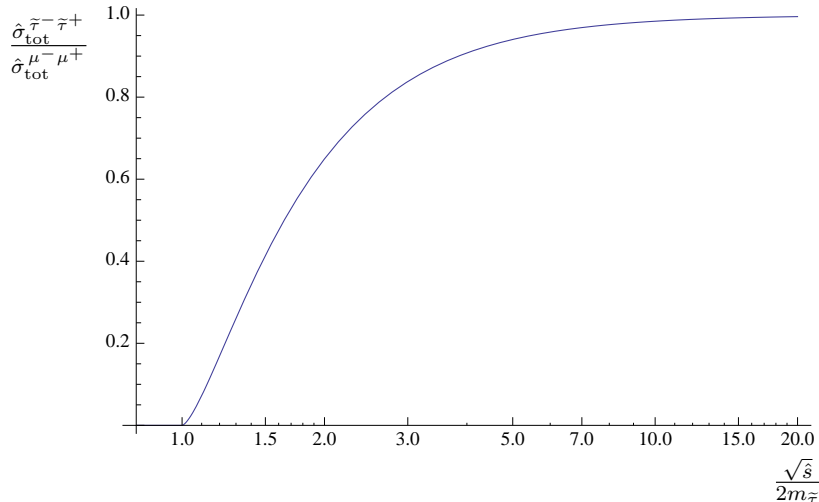


Figure 4: Ratio (66) of muon and stau pair production at tree-level QED as a function of the cm-energy normalized to the stau production threshold. The ordinate is arbitrarily normalized. (By the way, of course, above the threshold $\sqrt{\hat{s}}/(2m_{\tilde{\tau}})$ is just γ —the Lorentz factor regarding the stau velocity v —and the function itself is equal to v^3 .)

where the Θ -function expresses the stau threshold (and therefore ensures the ratio to be real). So, (66) says that as a function of \hat{s} the ratio of stau production and muon production is simply zero below the threshold $(2m_{\tilde{\tau}})^2$ and increases relatively rapid over a region of a few times the threshold energy to converge asymptotically against a constant value¹¹ for high \hat{s} (figure 4).

If the incoming quarks don't come with a defined cm-energy, but come with a certain distribution $L_{q\bar{q}}(\hat{s})$ of cm-energies (like it is the case in a hadron collider experiment) it would be sensible to compare a quantity like this:

$$\int d\hat{s} L_{q\bar{q}}(\hat{s}) \hat{\sigma}_{\text{tot}}(\hat{s}). \quad (67)$$

If we consider the ratio of this quantity for staus and muons, the situation will be quite different than in the case of (66). There might be a huge amount of offset muons that come from the contribution below the threshold, where the stau production is kinematically forbidden. Thus, depending on $L_{q\bar{q}}(\hat{s})$ and the stau mass this—latter—ratio might be very small. That's a simple fact, but it is the one that makes the detection difficult—the amount of background muons can be very large.

¹¹When comparing (63) with (65) the constant is 1/4. (Of course, this holds in general for the ratio $\hat{\sigma}_{\text{tot}}^{\tilde{f}^- \tilde{f}^+} / \hat{\sigma}_{\text{tot}}^{f^- f^+}$ in the high energy limit, where f and \tilde{f} denotes some kind of fermion and its superpartner). But, in (65) we consider left- and right handed muons (due to the spin sums that are applied in the derivation) whereas in (63) we consider only one scalar (that could either be the superpartner of the left- or the right-handed stau).

For simplicity let's assume $L_{q\bar{q}}(\hat{s})$ to be constant in the region above the threshold and let's assume to have some detector in the cm-frame that could measure the velocity of the particles with a statistical uncertainty. Then one possibility to distinguish the staus from the muons would be to set a cut on the velocity (that is considering events with $v \leq v_{\text{cut}}$). The muons could be assumed to have $v = 1$, thus to have a velocity distribution that is a delta-function. Since

$$\hat{s} = \frac{(2m_{\tilde{\tau}})^2}{1 - v^2} \quad (68)$$

and thus $d\hat{s} v^3 / \hat{s} = dv 2v^4 / (1 - v^2)$, the velocity distribution of the staus behave like

$$\frac{d\hat{\sigma}}{dv} \sim \frac{v^4}{1 - v^2}, \quad (69)$$

which is plotted in figure 5. This distribution is universal for sfermion production via a massless vector boson, at tree level, as long as the initial state particles are assumed to be relativistic, that is it doesn't depend on the mass nor on species.¹² It peaks sharply at $v = 1$ due to the broad range of \hat{s} that causes relativistic staus. Such a feature would be of course absent when multiplying a non-trivial $L_{q\bar{q}}(\hat{s})$ that in particular should have a compact support, since in a hadron collider experiment the maximum quark energy is set by the beam energy. According to (68) a maximum \hat{s} will cause a maximum velocity. (We will see in the next section how $d\hat{\sigma}/dv$ changes in the case of a non-trivial $L_{q\bar{q}}(\hat{s})$.)

Thus the number of staus that are accessible to detection $\int^{v_{\text{cut}}} (d\hat{\sigma}/dv) dv$ increases rapidly if one raises v_{cut} . On the other hand the statistical uncertainty of the measurement could have us consider lowering v_{cut} away from 1, since depending on how big the amount of muons under the threshold is, even a small statistical uncertainty could cause a lot of mis-identified muons.¹³

We already see a central challenge in the detection of massive charge particles here. Depending on the statistical error of the velocity measurement and the distribution $L_{q\bar{q}}(\hat{s})$ below (and above) the threshold one might prefer a certain value of v_{cut} to obtain an optimal signal-to-background ratio. (We will return to this subject in section 6.)

Please keep in mind that the appearing quantities are expressed explicitly in the cm-frame of the $q\bar{q}$ -process. At a hadron collider it is not possible to build up a detector in the cm-frame of the $q\bar{q}$ -process. The cm-frame changes according to the fact that the momenta of the incoming quarks are in general not distributed symmetrically in

¹²Of course the running couplings that we assumed to be constant when writing down the proportionality (69) would somewhat spoil this argument. This becomes obvious when considering the QCD case (the s-channel process differs only by the coupling and a color factor), since there is no self consistent way to treat tree-level calculations, due to the lack of an α_0 that gives us an asymptote for the coupling in the tree-level regime, like it is the case in QED. For the weak coupling the Z propagator would alter this expression, although it gives a good approximation, for the case that the sfermion mass is sufficiently larger than M_Z .

¹³A contribution from slow muons (from respective low energies) would spoil our consideration. But that's no problem at collider experiments, since a simple p_{\perp} -cut ($p_{\perp} \geq p_{\text{cut}}$) would ensure the desired assumption of $v = 1$ for the muons.

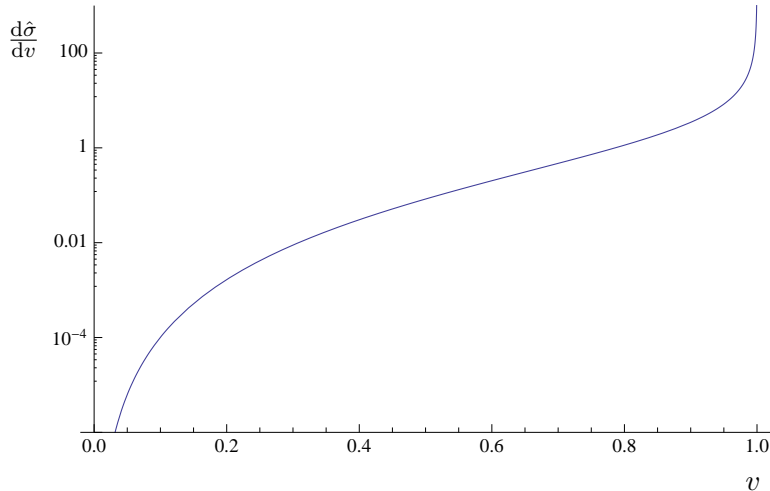


Figure 5: Velocity distribution of the QED stau-pair production in the cm-frame for a flat distribution of cm-energies, at tree-level. The normalization is arbitrarily chosen. (The result holds for all sfermions.)

the laboratory frame. In the next section we will therefore formulate the appropriate framework for such a situation. But first we will express the stau cross section in a Lorentz invariant way, since (62) is not easy to handle when boosting the cm-frame along the beam axis. The appearing polar angle θ behaves quite unpleasantly under a Lorentz transformation, which we will briefly demonstrate in appendix C.

To set up our formula (53) for the case that the cm-frame and our laboratory frame don't coincide we use Mandelstam variables:

$$\begin{aligned}
 \hat{s} &= (p + p')^2 = (k + k')^2 \\
 \hat{t} &= (k - p)^2 = (k' - p')^2 \\
 \hat{u} &= (k' - p)^2 = (k - p')^2.
 \end{aligned}
 \tag{70}$$

Again, we assume the quark mass to be negligible, $m_q = k^2 = k'^2 = 0$. Then we could express all occurring scalar products in (53) in terms of \hat{s} , \hat{t} , \hat{u} and $m_{\tilde{\tau}}$. (70) gives us

$$\begin{aligned}
 2pp' &= \hat{s} - 2m_{\tilde{\tau}}^2, & 2kk' &= \hat{s} \\
 2kp &= 2k'p' = -\hat{t} + m_{\tilde{\tau}}^2 \\
 2k'p &= 2kp' = -\hat{u} + m_{\tilde{\tau}}^2
 \end{aligned}
 \tag{71}$$

And so (53) turns into

$$\frac{1}{4} \sum_{\text{spins}} |\mathcal{M}|^2 = \frac{e^4 e_q^2}{\hat{s}^2} \frac{1}{2} \{ (-\hat{u} + \hat{t})(-\hat{t} + \hat{u}) + \hat{s}(\hat{s} - 4m_{\tilde{\tau}}^2) \}
 \tag{72}$$

Let's recall that \hat{s} , \hat{t} , \hat{u} and $m_{\tilde{\tau}}$ are restricted through momentum conservation, leading to the requirement

$$\hat{s} + \hat{t} + \hat{u} = \sum_{\text{particles}} m_i^2 = 2m_{\tilde{\tau}}^2, \quad (73)$$

where the last equal sign holds for our case. With this condition we could make further simplifications on the squared matrix element. Just write the curly brackets as

$$\begin{aligned} & 2\hat{u}\hat{t} - (\hat{u}^2 + \hat{t}^2 + \hat{s}^2) + 2\hat{s}^2 - 4\hat{s}m_{\tilde{\tau}}^2 \\ &= 2\hat{u}\hat{t} - (\hat{u} + \hat{t} + \hat{s})^2 + 2\hat{u}\hat{t} + 2\hat{u}\hat{s} + 2\hat{t}\hat{s} + 2\hat{s}^2 - 4\hat{s}m_{\tilde{\tau}}^2 \end{aligned} \quad (74)$$

and apply (73) on the second and on the last term. Then the squared matrix element shrinks down to the very handy expression

$$\frac{1}{4} \sum_{\text{spins}} |\mathcal{M}|^2 = \frac{2e^4 e_q^2}{\hat{s}^2} (\hat{u}\hat{t} - m_{\tilde{\tau}}^4). \quad (75)$$

Therewith the cross section becomes¹⁴

$$\begin{aligned} \frac{d\hat{\sigma}}{d\hat{t}} &= \frac{1}{16\pi\hat{s}^2} \frac{1}{4} \sum_{\text{spins}} |\mathcal{M}|^2 \\ &= \frac{e^4 e_q^2}{8\pi\hat{s}^4} (\hat{u}\hat{t} - m_{\tilde{\tau}}^4). \end{aligned} \quad (76)$$

Electroweak interaction

In the same way we derived the QED cross section formula we now want to complete the expression involving the amplitude for the weak coupling via neutral current.

Since the weak coupling distinguishes between left- and right-handed particles, we now have to care about the handedness of the involved particles. Let's first stick to the 'handedness' of the staus. We expect $\tilde{\tau}_L$ and $\tilde{\tau}_R$ to mix to the mass eigenstates $\tilde{\tau}_1$ and $\tilde{\tau}_2$ ($m_1 < m_2$) according to (33):

$$\begin{pmatrix} \tilde{\tau}_1 \\ \tilde{\tau}_2 \end{pmatrix} = \mathcal{R}^{\tilde{\tau}} \begin{pmatrix} \tilde{\tau}_R \\ \tilde{\tau}_L \end{pmatrix} = \begin{pmatrix} \cos \theta_{\tilde{\tau}} & \sin \theta_{\tilde{\tau}} \\ -\sin \theta_{\tilde{\tau}} & \cos \theta_{\tilde{\tau}} \end{pmatrix} \begin{pmatrix} \tilde{\tau}_R \\ \tilde{\tau}_L \end{pmatrix}. \quad (77)$$

¹⁴Comparing (62) with (76) one finds the relation

$$\frac{\hat{u}\hat{t} - m_{\tilde{\tau}}^4}{\hat{s}^{3/2}} d\hat{t} = \frac{|\mathbf{p}|^3}{2\pi} \sin^2 \theta d\Omega.$$

The Z -contribution of (60) then becomes

$$\begin{aligned}
&= -ie \frac{1}{c_W s_W} \left\{ \left(-\frac{1}{2} + s_W^2 \right) \mathcal{R}_{iL}^{\tilde{\tau}} \mathcal{R}_{jL}^{\tilde{\tau}} + s_W^2 \mathcal{R}_{iR}^{\tilde{\tau}} \mathcal{R}_{jR}^{\tilde{\tau}} \right\} (p - p')^\mu \\
&= -ie g_{\tilde{\tau}_i \tilde{\tau}_j} (p - p')^\mu,
\end{aligned} \tag{78}$$

where we define $g_{\tilde{\tau}_i \tilde{\tau}_j}$ and use the abbreviations $s_W = \sin \theta_W$, $c_W = \cos \theta_W$. Next we display the SM $q\bar{q} \rightarrow Z$ -vertex

$$\begin{aligned}
&= -ie \frac{1}{c_W s_W} \gamma^\mu \left\{ (T_q^3 - e_q s_W^2) \frac{1 - \gamma^5}{2} - e_q s_W^2 \frac{1 + \gamma^5}{2} \right\} \\
&= -ie \gamma^\mu \{ g_V^q - g_A^q \gamma^5 \},
\end{aligned} \tag{79}$$

where we introduce $g_V^q = (T_q^3 - 2e_q s_W^2)/(2c_W s_W)$ and $g_A^q = T_q^3/(2c_W s_W)$. The first line of (79) displays the left- and right-handed parts of the weak coupling, whereas the notation in the second line corresponds to the vector current and axial vector current. Since we are not specifying the spin of the initial state particles, we will use the second description.

Let's throw everything together, yielding the amplitude for the Z -coupling:

$$i\mathcal{M}_{ij}^q = (-ie)^2 g_{\tilde{\tau}_i \tilde{\tau}_j} (p - p')^\mu \frac{-i(g_{\mu\nu} - q_\mu q_\nu / M_Z^2)}{q^2 - M_Z^2} \bar{v}(k') \gamma^\nu \{ g_V^q - g_A^q \gamma^5 \} u(k). \tag{80}$$

The propagator term in this formula simplifies to $-ig_{\mu\nu}/(q^2 - M_Z^2)$, since $(p - p')^\mu q_\mu = (p - p')^\mu (k + k')_\mu = 0$.

In contrast to the Z -coupling the A -coupling doesn't allow a final state of two different staus, since there is no mixing between the coupling eigenstates and the mass eigenstates. Thus for each stau with mass m_i we can apply the amplitude (51). So the tree-level amplitude for the process $q\bar{q} \rightarrow \tilde{\tau}_i^- \tilde{\tau}_j^+$ via s-channel photon and Z boson exchange is

$$\mathcal{M}_{ij}^q = -e^2 (p - p')^\mu \left\{ \left(\frac{e_q \delta_{ij}}{\hat{s}} - g_V^q \frac{g_{\tilde{\tau}_i \tilde{\tau}_j}}{\hat{s} - M_Z^2} \right) \bar{v}(k') \gamma_\mu u(k) + g_A^q \frac{g_{\tilde{\tau}_i \tilde{\tau}_j}}{\hat{s} - M_Z^2} \bar{v}(k') \gamma_\mu \gamma^5 u(k) \right\}. \tag{81}$$

Let's display some steps of the computation of the averaged squared matrix element.

The first thing to bring up is that there is no interference term between the vector and axial vector part. To show this let's drop everything but the vector and spinor structure

of the interference term:

$$\begin{aligned}
& (p-p')^\mu (p-p')^\nu \sum_{\text{spins}} (\bar{v}(k') \gamma_\mu u(k) \bar{u}(k) \gamma_\nu \gamma^5 v(k') + \bar{v}(k') \gamma_\mu \gamma^5 u(k) \bar{u}(k) \gamma_\nu v(k')) \\
&= (p-p')^\mu (p-p')^\nu (\text{tr}[(\not{k}' - m_q) \gamma_\mu (\not{k} + m_q) \gamma_\nu \gamma^5] + \text{tr}[(\not{k}' - m_q) \gamma_\mu \gamma^5 (\not{k} + m_q) \gamma_\nu]) .
\end{aligned} \tag{82}$$

Since $\text{tr}[\gamma_\mu \gamma_\nu \gamma^5] = \text{tr}[\gamma_\mu \gamma_\nu \gamma_\rho \gamma^5] = 0$ and $\{\gamma^5, \gamma^\mu\} = 0$, the two traces are equal and further more proportional to $\epsilon^{\rho\mu\sigma\nu}$, thus antisymmetric in the exchange of μ and ν , whereas $(p-p')^\mu (p-p')^\nu$ is symmetric. So it vanishes.

Henceforth we will now directly drop the quark mass wherever it appears ($m_q = 0$).

$$\begin{aligned}
\frac{1}{4} \sum_{\text{spins}} |\mathcal{M}_{ij}^q|^2 &= \frac{1}{4} e^4 (p-p')^\mu (p-p')^\nu \left\{ \left(\frac{e_q \delta_{ij}}{\hat{s}} - g_V^q \frac{g_{\tilde{\tau}_i \tilde{\tau}_j}}{\hat{s} - M_Z^2} \right)^2 \text{tr}[\not{k}' \gamma_\mu \not{k} \gamma_\nu] \right. \\
&\quad \left. + \left(g_A^q \frac{g_{\tilde{\tau}_i \tilde{\tau}_j}}{\hat{s} - M_Z^2} \right)^2 \text{tr}[\not{k}' \gamma_\mu \gamma^5 \not{k} \gamma_\nu \gamma^5] \right\} \\
&= e^4 \left\{ \frac{e_q^2 \delta_{ij}}{\hat{s}^2} - \frac{2e_q g_V^q \delta_{ij} g_{\tilde{\tau}_i \tilde{\tau}_j}}{\hat{s}(\hat{s} - M_Z^2)} + (g_V^{q2} + g_A^{q2}) \frac{g_{\tilde{\tau}_i \tilde{\tau}_j}^2}{(\hat{s} - M_Z^2)^2} \right\} \\
&\quad \times \{ 2(p-p') \cdot k (p-p') \cdot k' - (p-p')^2 k \cdot k' \}
\end{aligned} \tag{83}$$

The momentum dependency is equal to the case of QED, yielding the same dependency on the Mandelstam variables \hat{t} and \hat{u} and therefore the same angle dependency, but with one exception: The case of $i \neq j$. In this case the mass belonging to p is not equal to the one belonging to p' . Thus to cover the general case we now write

$$\begin{aligned}
(p-p')^2 &= m_{\tilde{\tau}}^2 + m_{\tilde{\tau}}'^2 - 2p \cdot p' \\
2pp' &= \hat{s} - m_{\tilde{\tau}}^2 - m_{\tilde{\tau}}'^2 \\
2kk' &= \hat{s} \\
2kp &= -\hat{t} + m_{\tilde{\tau}}^2 \\
2k'p' &= -\hat{t} + m_{\tilde{\tau}}'^2 \\
2k'p &= -\hat{u} + m_{\tilde{\tau}}^2 \\
2kp' &= -\hat{u} + m_{\tilde{\tau}}'^2 .
\end{aligned} \tag{84}$$

In a similar way to the above case of QED these equations lead us to

$$2(p-p') \cdot k (p-p') \cdot k' - (p-p')^2 k \cdot k' = 2 \left[\hat{u} \hat{t} - m_{\tilde{\tau}}^2 m_{\tilde{\tau}}'^2 \right] , \tag{85}$$

yielding the final result

$$\left(\frac{d\hat{\sigma}}{d\hat{t}} \right)_{ij}^q = \frac{e^4}{8\pi \hat{s}^2} \left[\hat{u} \hat{t} - m_{\tilde{\tau}_i}^2 m_{\tilde{\tau}_j}^2 \right] \left\{ \frac{e_q^2 \delta_{ij}}{\hat{s}^2} - \frac{2e_q g_V^q \delta_{ij} g_{\tilde{\tau}_i \tilde{\tau}_j}}{\hat{s}(\hat{s} - M_Z^2)} + (g_V^{q2} + g_A^{q2}) \frac{g_{\tilde{\tau}_i \tilde{\tau}_j}^2}{(\hat{s} - M_Z^2)^2} \right\} . \tag{86}$$

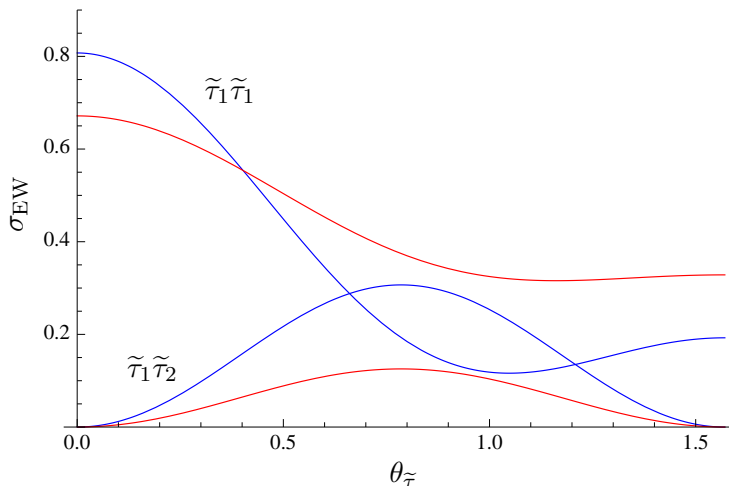


Figure 6: Dependence of the stau cross section (86) on the stau mixing angle $\theta_{\tilde{\tau}}$ for the production of $\tilde{\tau}_1\tilde{\tau}_1$ and $\tilde{\tau}_1\tilde{\tau}_2$ from an up-type quark-pair (red) and a down-type quark-pair (blue). We have not displayed the $\tilde{\tau}_2\tilde{\tau}_2$ -curve, since it is just the same as the $\tilde{\tau}_1\tilde{\tau}_1$ -curve but mirrored around the point $\pi/4$. The curves are normalized such that the sum over all final state contributions is 1. We have set $\sqrt{\hat{s}} = 5M_Z$ and taken $\sin^2 \theta_W = 0.231$.

Figure 6 shows the dependence of (86) on the mixing angle $\theta_{\tilde{\tau}}$ for the case of the final states $\tilde{\tau}_1\tilde{\tau}_1$ and $\tilde{\tau}_1\tilde{\tau}_2$ for an up-type and down-type quark-pair in the initial state. If $\theta_{\tilde{\tau}}$ differs slightly from zero the cross section for a $\tilde{\tau}_1$ -pair decreases. The exact shape of the curve differs with the cm-energy. We have plotted it for $\sqrt{\hat{s}} = 5M_Z$. Figure 7 shows the ratio of the photon-coupling cross section (76) to the whole electroweak cross section (86). The amount of change of the curves in figure 6 with $\sqrt{\hat{s}}$ is precisely of the same behavior as the change of the ratio (76)/(86) with $\sqrt{\hat{s}}$. It is just the effect of the Z -mass in the denominator of the Z propagator. Figure 7 shows that the ratio (76)/(86) is approximately constant from a few times M_Z on. This encourages us to consider only the case of $\theta_{\tilde{\tau}} = 0$ ($\tilde{\tau}_1 = \tilde{\tau}_R$) in the further discussion and keep in mind that another $\theta_{\tilde{\tau}}$ just decreases the cross section according to figure 6. Since we will consider stau at masses above 100 GeV (and we additionally will require a minimum velocity and minimum transverse momentum) it will be quite a good approximation to state that $\sigma_{\tilde{\tau}}(\theta_{\tilde{\tau}})$ doesn't depend on the kinematics.

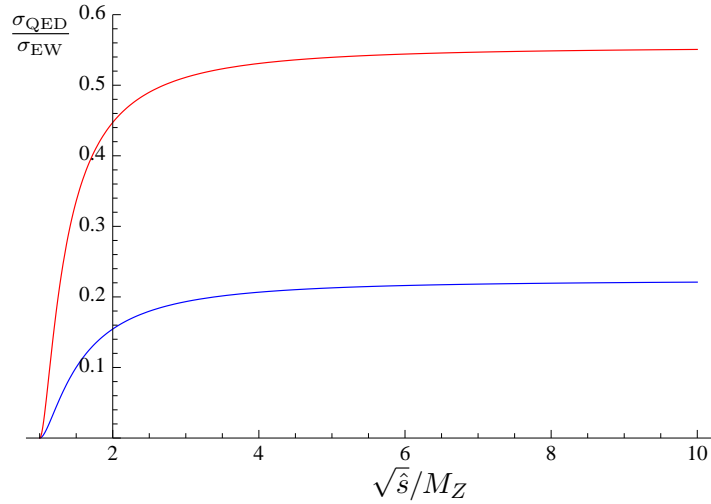


Figure 7: Ratio between the QED cross section (76) and the full electroweak cross section (86) as a function of the cm-energy $\sqrt{\hat{s}}$ for an up-type quark-pair (red) and a down-type quark-pair (blue) in the initial state. We have chosen $\sin^2 \theta_W = 0.231$.

This fact also motivates a posteriori to spend some time in the above discussion after equation (62), since applying the whole electroweak coupling would just cause another constant factor, approximately.

In all these formulas we haven't paid attention to the colors of the quark-antiquark pair yet. To do this, we have to apply a factor of $1/3$ to the cross section, that takes into account that there are three possible color states for the incoming quark-antiquark pair, but for each quark a possibility of $1/3$ to be in that color state. And so a resulting factor of $3 \times 1/3 \times 1/3 = 1/3$.

5 Physics at hadron colliders

In the last section we have considered the stau-pair production at the most elementary level. But since the LHC is a pp-collider and protons are built out of quarks, antiquarks and gluons (collectively called the partons) that are strongly coupled, we have to know how to treat such a complex process. Therefore in this section we will discuss (at least very briefly) some topics of QCD. Since for a hadron-hadron collision the laboratory frame and the center-of-momentum frame no longer coincide, we will also introduce appropriate variables that are common in the business of collider physics.

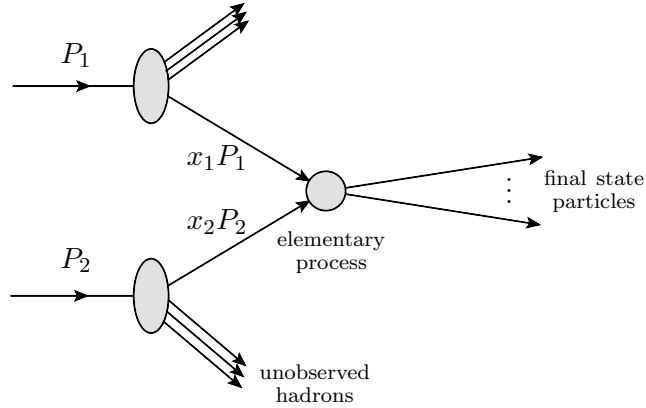


Figure 8: The situation at a hadron collider, schematically.

Schematically the situation at the hadron collider looks as shown in figure 8, where the grey circles indicate the interaction points at first without further specifications. The 'elementary process'-circle containing the hard scattering of the process is calculable perturbatively while the proton-circles containing QCD binding states are in principle not accessible to perturbative QCD (and since respective ab initio lattice QCD calculations are not applicable at the present state they have to be of empirical nature). This is due to the asymptotic freedom of the strong interaction. Thus, the desired formulation of such a problem would be to separate the two regimes from each other. This is provided by the factorization theorem [24, 23] which allows to formulate process independent parton distribution functions (PDF)s. Those factorize from the cross section $\hat{\sigma}$ of the hard scattering process performed in the matrix-element description. This leads to the convolution integral

$$\sigma_{pp} = \sum_{k,l} \int_0^1 \int_0^1 dx_1 dx_2 f_k(x_1, \mu) f_l(x_2, \mu) \times \hat{\sigma}^{kl}(x_1, x_2) \Theta(\text{mass cut}), \quad (87)$$

where (k, l) runs over all possible combinations of partons, called the hadronic channels (for instance (u, \bar{u}) , (\bar{u}, u) , (d, \bar{d}) , ... for the elementary process of the last section). The PDFs $f_k(x_1, \mu)$ can be interpreted as the probability density for finding a parton i carrying

a longitudinal fraction x of the proton momentum P (if the proton mass is small compared to the momentum transfer of the hard scattering, transversal momentum fractions are negligible). $f_k(x_1, \mu)$ is slightly scale dependent. μ is called the factorization scale. Let's brighten up this quantity a bit, since it is a bit tricky how this is treated in practice (though again at the end of the day one might not worry about this topic too much).

μ is not an observable, so (87) should be invariant under a variation of μ . This gives rise to the renormalization group equation $d\sigma_{pp}/(d\log \mu) = 0$. Thus, $\hat{\sigma}$ also has to have a scale dependence. It is hidden in its perturbative nature. Since perturbative QCD breaks down in the limit of low energies, we can't be too ambitious in making predictions for the low scale behavior of the hard scattering process. So, in other words, we have to cut off soft QCD radiation (and also collinear radiations that are undistinguishable from the unobserved hadrons that doesn't take part of the hard scattering). This cut-off should in principle correspond to the factorization scale. However, it is common in the business of QCD to push the factorization scale up to the scale of the momentum transfer \hat{s} of the hard scattering to have a reasonable hope that our calculations yield a good approximation of nature, since we are always interested (or rather restricted) to perform calculations only to the very lowest orders in α_s . Anyway, ultimately the result has to be invariant under the variation of μ in an appropriate range, thus the variation of σ_{pp} can be seen as a measure for the theoretical uncertainties. (Taking $\hat{\sigma}$ of the last section for instance we didn't consider strong coupling at all, thus there is no chance of a compensating scale dependence of $\hat{\sigma}$. In that case it is common to fix μ at \hat{s} .)

Now we want to restore the \hat{s} -dependence of $\hat{\sigma}$ in (87). Let s be the invariant mass of the protons in the pp center-of-momentum frame—which from now on we will call the laboratory frame due to obvious reasons—then in this frame the four momenta of the relativistic protons read

$$P_1 = \left(\frac{\sqrt{s}}{2}, 0, 0, \frac{\sqrt{s}}{2} \right), \quad P_2 = \left(\frac{\sqrt{s}}{2}, 0, 0, -\frac{\sqrt{s}}{2} \right). \quad (88)$$

The invariant mass of the center-of-momentum frame of the partons—which from now on we will simply call cm-frame—thus reads

$$\hat{s} = (x_1 P_1 + x_2 P_2)^2 = \frac{s}{4} \left[(x_1 + x_2)^2 - (x_1 - x_2)^2 \right] = x_1 x_2 s. \quad (89)$$

With this (87) can be written as

$$\begin{aligned} \sigma_{pp} &= \sum_{k,l} \int_0^s d\hat{s} \hat{\sigma}^{kl}(\hat{s}) \Theta(\text{mass cut}) \int_0^1 \int_0^1 dx_1 dx_2 f_k(x_1, \hat{s}) f_l(x_2, \hat{s}) \delta(\hat{s} - x_1 x_2 s) \\ &= \sum_{k,l} \int_0^s d\hat{s} \hat{\sigma}^{kl}(\hat{s}) \Theta \left(\hat{s} - \left(\sum m_{\text{final state}} \right)^2 \right) L_{kl}(\hat{s}). \end{aligned} \quad (90)$$

In the last line we (displayed the mass cut condition explicitly and) introduced the parton luminosity $L_{kl}(\hat{s})$ that contains all the information concerning the partons for a certain

hadronic channel (i, j) depending on \hat{s} . Performing one of the integrations yields

$$L_{kl}(\hat{s}) = \int_{\frac{\hat{s}}{s}}^1 \frac{dx}{xs} f_k\left(\frac{\hat{s}}{xs}, \hat{s}\right) f_l(x, \hat{s}). \quad (91)$$

What we found here is the general expression of the distribution $L_{q\bar{q}}(\hat{s})$ we mentioned

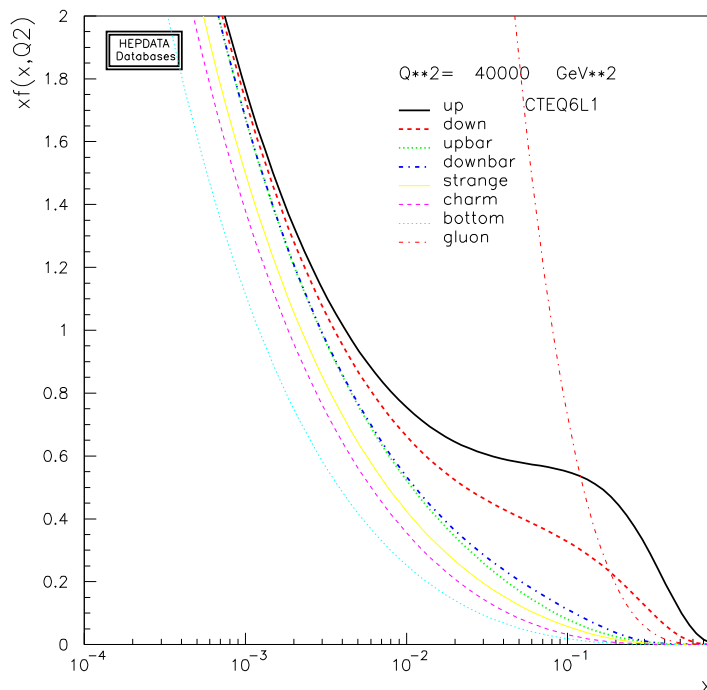


Figure 9: Parton distribution functions for the quarks and gluons in the proton, at $\mu = (200 \text{ GeV})^2$. The distributions of quarks and antiquarks has to be equal for each flavor but u and d , the valence quarks, in order to yield the right quantum numbers for the proton. Since all of these functions peak sharply at small x , it is common to display $xf_k(x, \mu)$. This plot displays the PDF set CTEQ6L1 (CTEQ collaboration), and it is taken from [68].

in the last section, discussing the challenges in stau searches at a simplified level. There we have derived the very simple expression (69) for a flat distribution in \hat{s} . Now we can see how the velocity distribution is affected when applying a realistic $L_{q\bar{q}}(\hat{s})$.

Therefore we briefly discuss the quantities of the PDFs, that enter $L_{q\bar{q}}(\hat{s})$. Figure 9 shows the PDF set CTEQ6L1 provided by the CTEQ collaboration¹⁵ [62] at a scale

¹⁵ There are further working groups providing PDF sets, for example MRST/MSTW [54], NNPDF [16] and Alekhin [5]. All the available PDF sets are in principal extracted from experimental data (often from deep inelastic scattering experiments). So they come with experimental uncertainties.

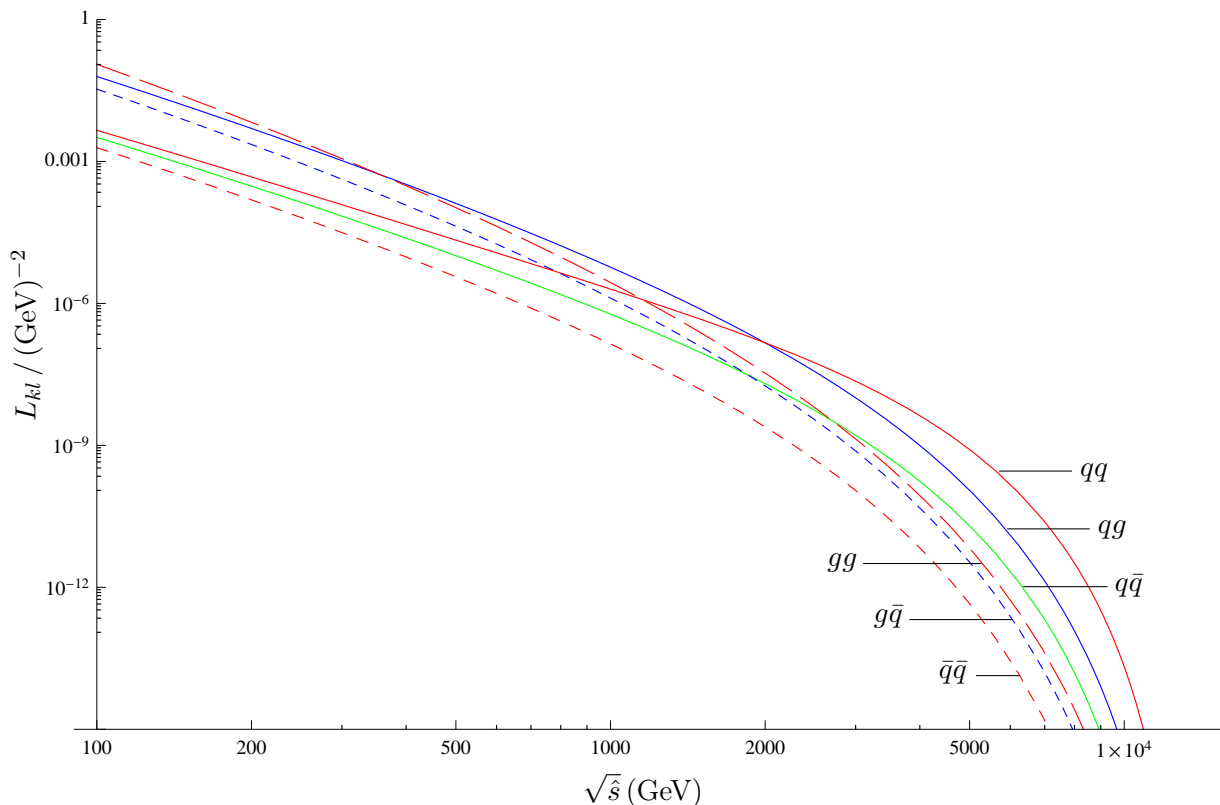


Figure 10: Parton luminosity as a function of the cm-energy $\sqrt{\hat{s}}$ for different partonic channels in a pp-collision with $\sqrt{s} = 14$ TeV. q (resp. \bar{q}) stands for the sum over d, u, s, c, b (resp. $\bar{d}, \bar{u}, \bar{s}, \bar{c}, \bar{b}$). For later discussion: The green, blue and red hadronic channels contribute to the Drell-Yan process at order α_s^0 , α_s^1 and α_s^2 , respectively.

$\mu = (200 \text{ GeV})^2$. Since the proton is composed of the valence quarks uud the u and d quarks are most likely to carry a substantial fraction of the proton momentum, whereas antiquarks tend to have small fractions. Gluons dominate over all others in the region of small x . However, all these distributions peak sharply for small x . These features can be retrieved in the parton luminosity. We have plotted $L_{q\bar{q}}(\hat{s})$ using the CTEQ6L1 PDF sets in figure 10. (We have set the factorization scale to \hat{s} in the calculation, as we already denoted in (91).) For all hadronic channels the parton luminosity decreases with increasing $\sqrt{\hat{s}}$. Up to ~ 1 TeV this decrease behaves approximately like a negative power law (at least for the hadronic channels involving one or two q). The belt that the curves of the hadronic channels span decreases as a whole by a factor of $\sim 10^{-4}$ from $\sqrt{\hat{s}} = 100$ GeV to 1 TeV. Above ~ 1 TeV the parton luminosity begins to decrease more drastically. This means that it is very unlikely to have nearly the whole beam energy available in the partonic scattering.

Now, this behavior is reflected in the velocity distribution of the staus in the cm-

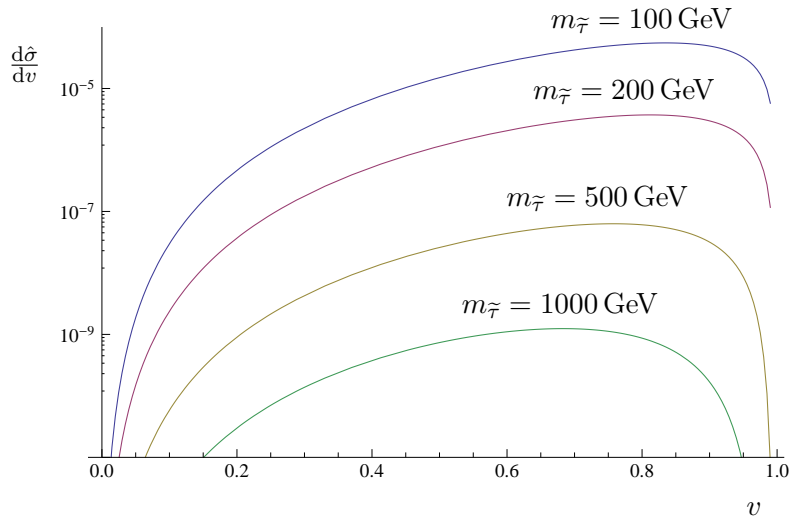


Figure 11: Velocity distribution of the staus in the cm-frame in a leading order Drell-Yan process at $\sqrt{s} = 14$ TeV. Only the relative normalization is meaningful. The curves are exact for the photon- and approximately (in the sense we have discussed concerning figure 7) for the Z -contribution. The CTEQ6L1 PDF set was used.

frame,

$$\frac{d\hat{\sigma}_{\text{pp}}}{dv} \sim L_{q\bar{q}} \left(\frac{(2m_{\tilde{\tau}})^2}{1-v^2} \right) \frac{v^4}{1-v^2}, \quad (92)$$

which is plotted in figure 11 for four different stau masses. Compared to figure 5 the divergency at $v = 1$ has gone and the mass dependence appears. The main effect by varying the mass is the change of the total cross section—the up-down-shift of the curves. The shape of the curve changes significantly only at $m_{\tilde{\tau}} = 1$ TeV, where the steep slope of $L_{q\bar{q}}(\hat{s})$ beyond a few TeV governs the higher end of the velocity distribution.

This consideration nicely illustrates the features of the velocity distribution coming from the elementary process, provided with cm-energies according to the PDFs. Nevertheless, it is not the whole story. There is another contribution coming from the boost of the cm-frame with respect to the laboratory frame. Let p_1 and p_2 be the momenta of the initial state partons. Then their total momentum is

$$q^\mu = p_1^\mu + p_2^\mu \propto \begin{pmatrix} x_1 + x_2 \\ 0 \\ 0 \\ x_1 - x_2 \end{pmatrix}. \quad (93)$$

This gives us the velocity of the cm-frame

$$\beta = \frac{q^z}{q^0} = \frac{x_1 - x_2}{x_1 + x_2}. \quad (94)$$

Therefore the distribution of the boosts according to the PDFs is

$$\begin{aligned} & \sum_{k,l} \int_0^1 \int_0^1 dx_1 dx_2 f_k(x_1) f_l(x_2) \delta\left(\frac{x_1 - x_2}{x_1 + x_2} - \beta\right) \delta(\hat{s} - x_1 x_2 s) \\ &= \sum_{k,l} f_k\left(\sqrt{\frac{\hat{s}(1+\beta)}{s(1-\beta)}}\right) f_l\left(\sqrt{\frac{\hat{s}(1-\beta)}{s(1+\beta)}}\right) \frac{\gamma_\beta^2}{s}, \end{aligned} \quad (95)$$

where γ_β is just the relativistic gamma-factor according to β and we have suppressed the scale dependence, for simplicity. We have plotted this distribution for different values of $\sqrt{\hat{s}}$ in figure 12.¹⁶

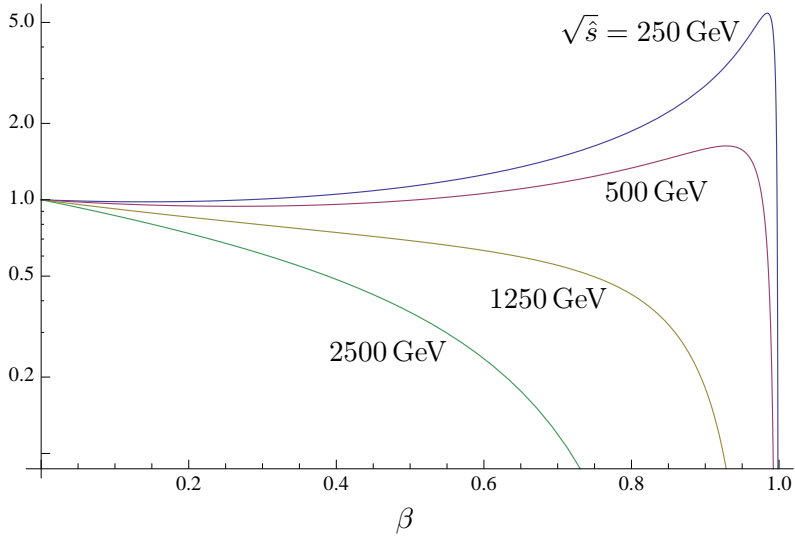


Figure 12: Distribution of the velocity (95) of the cm-frame with respect to the laboratory frame, as it is obtained from the CTEQ6L1 PDF set for the LHC at $s = 14$ TeV. The relative normalization is taken arbitrarily.

What is the impact on the stau that already comes with a velocity distribution in the cm-frame? For simplicity we consider a stau that moves in the transversal direction (i.e. has a scattering angle of around 90°) in the cm-frame. That's not a bad choice, since the angle dependency of (62) prefers this direction. Then (161) tells us (with $v'_\parallel = 0$) that the velocity in the laboratory frame is

$$v = \sqrt{v_\perp^2 + \beta^2(1 - v_\perp^2)}. \quad (96)$$

¹⁶We have chosen the numerical values $\sqrt{\hat{s}} = 250, 500, 1250, 2500$ GeV because they correspond via (68) to the cm-energy of two particles with the masses chosen in figure 11 at velocity 0.6. The latter just gives a round number.

Due to the character of the relativistic velocity transformation, if one velocity is reasonably closer to one than the other the former will prevail. So the boost of the cm-frame will cause an additional rise of the velocity distribution close to one that inherits approximately the shape of the cm-boosting curves in region near one.

To be honest, there are additional effects that come into the game when allowing more than two particles in the final state, considering higher order corrections. But we will not make efforts to discuss these effects with simple methods. In the Monte Carlo calculations we will show in the next section that these effects can be seen very clearly in the $p_{\perp}^{\tilde{+}}-p_{\perp}^{\tilde{-}}$ -plane and the $\Delta\phi$ plot ($\Delta\phi$ is the difference in the azimuth angles of the two particles). A two-to-two scattering process (with $p_{\perp} = 0$ in the initial state) will always lead to the a momentum distribution that is confined to the diagonal in the $p_{\perp}^{\tilde{+}}-p_{\perp}^{\tilde{-}}$ -plane as well as it always has $\Delta\phi = 180^{\circ}$. But before discussing higher order corrections we will provide for a formula that allows us to calculate the Drell-Yan process at leading order for the case of a differential cross section. Such a formula is not only needed for calculating the distribution of a certain observable but also when applying a certain kinematic selection, namely cuts on the cross section. Therefore we will first introduce variables that are suitable to the case of collider physics. We will partly follow the derivation given in [61], but with the explicit assumption of a non-negligible mass of the final state particles.

As mentioned above, we assume the momentum of the incoming particles of an elementary process to be parallel to the collider beam direction (longitudinal), while the momentum of the outgoing particles have longitudinal and transversal components.

Let's consider an outgoing particle and work out carefully the Lorentz transformation from it's rest frame to the laboratory frame (or any other frame which is only longitudinally boosted with respect to the laboratory frame) by first performing a transversal and then a longitudinal boost. Here ζ is the transversal while y is the longitudinal rapidity. For simplicity, we are switching to a three-component notation here, combining the 1- and 2-components to the perpendicular component. We will make use of this notation when appropriate.

$$\begin{aligned}
\begin{pmatrix} E \\ p_{\perp} \\ p_{\parallel} \end{pmatrix} &= \begin{pmatrix} \cosh y & \sinh y & 0 \\ 0 & 0 & 1 \\ \sinh y & \cosh y & 0 \end{pmatrix} \begin{pmatrix} \cosh \zeta & 0 & \sinh \zeta \\ \sinh \zeta & 0 & \cosh \zeta \\ 0 & 1 & 0 \end{pmatrix} \begin{pmatrix} m \\ 0 \\ 0 \end{pmatrix} \\
&= \begin{pmatrix} \cosh y & \sinh y & 0 \\ 0 & 0 & 1 \\ \sinh y & \cosh y & 0 \end{pmatrix} \begin{pmatrix} m \cosh \zeta \\ m \sinh \zeta \\ 0 \end{pmatrix} \\
&= \begin{pmatrix} m \cosh \zeta \cosh y \\ m \sinh \zeta \\ m \cosh \zeta \sinh y \end{pmatrix}
\end{aligned} \tag{97}$$

Note that $p_{\perp} = m \sinh \zeta$ stays unaffected by a longitudinal boost while E of course changes by the factor of $\cosh y$. Let's define

$$E_{\perp} = m \cosh \zeta \tag{98}$$

and call it the transversal energy of a particle. It's nothing else than the energy of the particle in the longitudinal comoving frame.¹⁷ It fulfills

$$E_{\perp}^2 = m^2(\sinh^2 \zeta + 1) = p_{\perp}^2 + m^2. \quad (99)$$

Now we may find an answer to the question haunting us: ‘What are the appropriate variables to describe the final state kinematics?’ One choice is to use E_{\perp} and the azimuth angle ϕ (both quantities that are not affected by a longitudinal Lorentz boost) as well as the transversal rapidity y (that is simply additive under a longitudinal Lorentz boost):

$$p^{\mu} = \begin{pmatrix} E_{\perp} \cosh y \\ p_{\perp} \sin \phi \\ p_{\perp} \cos \phi \\ E_{\perp} \sinh y \end{pmatrix} \quad (100)$$

In the final state there are two particles. But notice that p_{\perp} (and therefore through (99) E_{\perp} as well) is the same for the two particles due to momentum conservation (remember that there is no transversal momentum in the initial state). Also the azimuth angles of the two final state particles are constrained through momentum conservation. Anyway, hence we consider processes that are invariant under rotation by an angle ϕ , we don't care too much about this angle. Effectively we are left with the variables

$$y_3, y_4, E_{\perp} \quad (101)$$

to describe our final state dynamics, where y_3 and y_4 are the rapidities of the final state particles. Then we can define

$$y_{\star} = \frac{1}{2}(y_3 - y_4) \quad (102)$$

to be the rapidity of the particle 3 (resp. minus the rapidity of particle 4) in the cm-frame and

$$Y = \frac{1}{2}(y_3 + y_4) \quad (103)$$

to be the rapidity of the cm-frame with respect to the laboratory frame.

Since we have expressed the differential cross sections in the last section in terms of the Lorentz invariant Mandelstam variables, now we would like to formulate them in terms of our variables (101). We do this by just plugging in the momentum p_1, p_2 and

¹⁷One may think of $\beta_{\perp} = p_{\perp}/E_{\perp} = \tanh \zeta$ as the transversal velocity. This holds obviously only for the special case of the longitudinal comoving frame. The general expression of the transversal velocity is $\beta_{\perp} = p_{\perp}/E = \tanh \zeta / \cosh y$, which also has the right transformation properties (161) under a longitudinal boost with rapidity ξ :

$$\beta'_{\perp} = \beta_{\perp} \frac{1}{\gamma_{\xi}(1 + \beta_{\xi}\beta_{\parallel})} = \frac{\tanh \zeta}{\cosh y} \frac{1}{\cosh \xi (1 + \tanh \xi \tanh y)} = \frac{\tanh \zeta}{\cosh(y + \xi)}$$

p_3, p_4 of the initial resp. final state particles expressed in the form (100) in the cm-frame into the definition (70):

$$\hat{s} = (p_3 + p_4)^2 = \begin{pmatrix} E_\perp (\cosh y_\star + \cosh y_\star) \\ 0 \\ E_\perp (\sinh y_\star - \sinh y_\star) \end{pmatrix}^2 = 4E_\perp^2 \cosh^2 y_\star \quad (104)$$

$$\hat{t} = (p_1 - p_3)^2 = \begin{pmatrix} \sqrt{\hat{s}}/2 - E_\perp \cosh y_\star \\ p_\perp \\ \sqrt{\hat{s}}/2 - E_\perp \sinh y_\star \end{pmatrix}^2 = -2E_\perp^2 \cosh y_\star e^{-y_\star} - m^2 \quad (105)$$

$$\hat{u} = (p_1 - p_4)^2 = \begin{pmatrix} \sqrt{\hat{s}}/2 - E_\perp \cosh y_\star \\ p_\perp \\ \sqrt{\hat{s}}/2 + E_\perp \sinh y_\star \end{pmatrix}^2 = -2E_\perp^2 \cosh y_\star e^{y_\star} - m^2 \quad (106)$$

While y_\star depends only on the interaction of the subprocess, Y is only related to the momentum fractions of the incoming particles x_1, x_2 . Now, we would like to get an expression for x_1 and x_2 in terms of y_\star, Y and E_\perp . From (94) one obtains for $\tanh Y = \beta$

$$\tanh Y = \frac{e^Y - e^{-Y}}{e^Y + e^{-Y}} = \frac{x_1 - x_2}{x_1 + x_2} = \frac{\sqrt{\frac{x_1}{x_2}} - \sqrt{\frac{x_2}{x_1}}}{\sqrt{\frac{x_1}{x_2}} + \sqrt{\frac{x_2}{x_1}}}. \quad (107)$$

Thus we can pick up

$$e^Y = \sqrt{\frac{x_1}{x_2}}. \quad (108)$$

Together with (89) it yields

$$x_1 = \sqrt{\frac{\hat{s}}{s}} e^Y; \quad x_2 = \sqrt{\frac{\hat{s}}{s}} e^{-Y} \quad (109)$$

and with (104) one finally arrives at

$$x_1 = \frac{2E_\perp}{\sqrt{s}} \cosh y_\star e^Y; \quad x_2 = \frac{2E_\perp}{\sqrt{s}} \cosh y_\star e^{-Y}. \quad (110)$$

Now we can work out a differential version of (87). What we can write down immediately is

$$\frac{d^3\sigma_{pp}}{dx_1 dx_2 d\hat{t}} = \sum_{k,l} f_k(x_1, \mu) f_l(x_2, \mu) \left(\frac{d\hat{\sigma}}{d\hat{t}} \right)^{kl} \quad (111)$$

(using \hat{u} instead of \hat{t} would be equivalent). We can translate this formula to our desired final state variables y_3, y_4 and E_\perp . Therefore we compute the Jacobian

$$\frac{\partial(x_1, x_2, \hat{t})}{\partial(y_3, y_4, E_\perp)} = \frac{8E_\perp^3 \cosh^2 y_\star}{s} = \frac{2E_\perp \hat{s}}{s}, \quad (112)$$

and arrive at

$$\frac{d^3\sigma_{\text{pp}}}{dy_3 dy_4 dE_\perp} = \sum_{k,l} f_k(x_1, \mu) f_l(x_2, \mu) \frac{2E_\perp \hat{s}}{s} \left(\frac{d\hat{\sigma}}{d\hat{t}} \right)^{kl} \quad (113)$$

The expression is independent of the azimuth angle ϕ , thus you can formally substitute $2\pi E_\perp dE_\perp = d^2E_\perp$. Together with $\hat{s} = x_1 x_2 s$ (113) changes to¹⁸

$$\frac{d^4\sigma_{\text{pp}}}{dy_3 dy_4 d^2E_\perp} = \sum_{k,l} x_1 f_k(x_1, \mu) x_2 f_l(x_2, \mu) \frac{1}{\pi} \left(\frac{d\hat{\sigma}}{d\hat{t}} \right)^{kl} \quad (114)$$

Plugging in (86) in (114) gives us our master-formula for a leading-order calculation of the Drell-Yan process. k, l run over all quark-antiquark-pairs of the same flavor (the hadronic channel $q\bar{q}$). (86) stores additional lower indices i, j that specify the process.¹⁹ If one is interested in the total cross section, but with experimental cuts one has to perform the integral

$$\begin{aligned} (\sigma_{\text{pp}})_{ij}^{\text{cuts}} &= \frac{1}{\pi} \int_{-\infty}^{\infty} dy_3 dy_4 \int_{-\infty}^{\infty} d^2E_\perp \sum_{kl} x_1 f_k(x_1, \mu) x_2 f_l(x_2, \mu) \left(\frac{d\sigma}{d\hat{t}} \right)_{ij}^{kl} \\ &\times \Theta(\text{mass cut}) \Theta(\text{exp cuts}), \end{aligned} \quad (115)$$

where the expressions in the Θ -functions have to be expressed in terms of y_3, y_4, E_\perp . Within this thesis we cut on three variables.

First, the pseudo-rapidity η , that is defined as

$$\eta_i = \frac{1}{2} \log \left(\frac{|\mathbf{p}| + p_3}{|\mathbf{p}| - p_3} \right) = \frac{1}{2} \log \left(\frac{\sqrt{E_\perp^2 \cosh^2 y_i - m^2} + E_\perp \sinh y_i}{\sqrt{E_\perp^2 \cosh^2 y_i - m^2} - E_\perp \sinh y_i} \right). \quad (116)$$

For $m = 0$ the argument of the log is just e^{2y_i} , so rapidity and pseudo-rapidity agree in that case. In any case pseudo-rapidity is directly correlated to the polar angle θ by

$$\eta_i = -\log(\tan(\theta_i/2)). \quad (117)$$

We apply a η -cut on all of our calculations, since at the LHC detectors there are regions around the beam axis that are not sensitive to the data of interest. This is called the 'barrel-cut'. We use $|\eta| < 2.5$. This correspond to an angle of approximately 10° .

Second, we will apply a cut on p_\perp to reduce muon background (that sharply peaks for small p_\perp).

$$p_\perp = \sqrt{E_\perp^2 - m^2}. \quad (118)$$

¹⁸One may wonder what this last step is about. This is due to numeric computational reasons. Most often the PDF sets are provided in the form $x f(x)$ because $f(x)$ give very large numerical values at small x . If one keeps this form the numerical integration converges faster.

¹⁹Note that in the above derivation by defining E_\perp we implicitly assumed that the masses of the two particles in the final state are the same. So this formula is true for $i = j$.

Third, we will apply a velocity cut on the staus in order to discriminate them from the muons. Since, from (97),

$$v^2 = \frac{\mathbf{p}^2}{E^2} = \frac{p_{\parallel}^2 + p_{\perp}^2}{E^2} = \frac{\cosh^2 \zeta \sinh^2 y + \sinh^2 \zeta}{\cosh^2 \zeta \cosh^2 y} = 1 - \frac{1}{\cosh^2 \zeta \cosh^2 y} \quad (119)$$

with (98) we get

$$v_i = \sqrt{1 - \frac{m^2}{E_{\perp} \cosh^2 y_i}}. \quad (120)$$

Correction in order α_s

The last topic to bring up in this section concerns higher order corrections in the strong coupling α_s . We have already seen in figure 10 that at a pp-collider the hadronic channel $q\bar{q}$ is not the dominant one (unlike the situation at a $p\bar{p}$ -collider like the Tevatron). So higher order corrections in α_s could be important for sufficient accuracy, since the corresponding higher order diagrams involve additional hadronic channels whose parton luminosities are about an order of magnitude higher than $q\bar{q}$. Appendix D systematically lists all Feynman-diagrams that are accessible in the orders α^0 , α^1 and α^2 . At order α^1 just the gq ($g\bar{q}$) channel adds up while at α^2 all hadronic channels contribute.

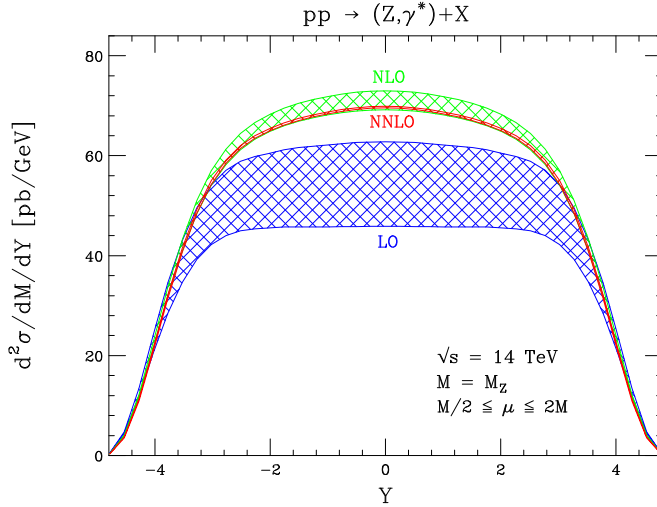


Figure 13: The rapidity distribution of the Drell-Yan process for the LHC at $\sqrt{\hat{s}} = M_Z$, calculated at leading order, NLO and NNLO. The bands indicate the variation of the renormalization and factorization scales in the range $M_Z/2$ to $2M_Z$. Taken from [15].

Figure 13 shows the cross sections of the Drell-Yan process for an on-shell Z at the LHC. It is calculated in a consistent leading order, next-to-leading order (NLO) and

next-to-next-to-leading order (NNLO) calculation, involving loop corrections and parton radiation [15]. The tree-level higher order corrections suffer infrared divergencies that had to be canceled by the (negative) divergent contributions of virtual corrections. Thus a tree level calculation in higher orders in α_s never gives a self-consistent result. As we will only work with tree-level Monte Carlo generators within this thesis, we have to deal with this shortcoming. But fortunately the shape of the observable distributions generated at tree-level are convincing.

6 Predictions for the LHC

The last two sections have equipped us with the physics for the stau search at the LHC, especially the Drell-Yan process. Let's now continue our discussion we started in the last passage of section 3 and go further into detail of the experimental issues. It already became clear that the velocity is a central observable when discriminating a heavy charged particle like the stau from muons. Unfortunately, the measurement of the velocity is not as easy as it may seem, in particular the resolution of such a measurement is much worse than e.g. the measurement of the transversal momentum. Let's consider how the velocity is measured by a detector at the LHC.

Measurement of the velocity at the LHC

There are two distinct ways to measure the velocity at the LHC detectors ATLAS and CMS, these are ionization energy loss and time-of-flight measurement.

By transversing the matter of the detector a charged particle loses energy. *Ionization energy loss* is caused by the removal of the electrons from the atoms in the detector material. The rate of ionization energy loss (or to be more precise its most probable value) is described by the Bethe-Bloch formula and depends only on the velocity of the particle. The Bethe-Bloch formula reads

$$\left\langle \frac{dE}{dx} \right\rangle = K v^{-2} + (\text{relativistic effects}) + (\text{density effects}), \quad (121)$$

where the displayed contribution in v is a good approximation in the region $0.1 < v \lesssim 0.8$ (K is a constant factor depending mainly on the detector material). At $v\gamma_v \simeq 3$ the ionization energy loss rate reaches a minimum. Above $v\gamma_v \simeq 3$ relativistic effects provide a slight raise which is again confined due to density effects so that the energy loss for ultrarelativistic particles is asymptotically constant, in particular (121) is an invertible function in the above region. At the LHC detectors the ionization energy loss is measured along the track of a particle in the tracker²⁰. A track is typically associated with ~ 15 hits. The energy deposition at one hit is statistically distributed around the most probable value in a Landau distribution which has an especially long tail on the high deposition side. If one reads out a minimum of 9 hits [2] a reasonable good approximation of the most probable value can be obtained. Thus, via the first term on the right hand side of (121) one can conclude the velocity of particles that have perceptibly higher ionization than ultrarelativistic ones.

The velocity measurement via *time-of-flight* is based on the data coming from the muon chambers located at the outermost part of the detector. The muon chambers are built up of drift tubes that are arranged off-center. Thus a typical track passes drift

²⁰The tracker is the inner part of the detector surrounding the beam pipe. At ATLAS and CMS it is about 2 m in diameter and 6 m in length. The innermost high resolution tracking layers of the tracker are built up of silicon pixel detectors surrounded by silicon stripe detectors. In the outer layers of the tracker ATLAS uses a transition radiation detector with gas straw tubes while CMS again uses silicon strip detectors [63].

tubes on both sides of the sensitive wires. The tracking system tries to reconstruct the track under the hypothesis of an ultrarelativistic muon, therefore it assigns the track to a certain bunch crossing. If a particle travels slower than speed of light, it arrives at the muon chambers with a time delay. The reconstructed hits in each drift tube will then be shifted away from the wires with respect to its real position. The result will be a zig-zag pattern instead of a straight line. From this one can conclude the velocity of the particle. Anyway, at design luminosity the distance between two bunch crossings is only 25 ns (that corresponds to 7.5 m at the speed of light), hence up to three bunch crossings are simultaneously inside the detector. Therefore there is a lowest velocity under which one cannot match the signal to the right bunch crossing anymore. This velocity is approximately $v_{\min} \simeq 0.6$ [66].

In both cases the resolution of the velocity measurement has to be evaluated from the data, especially the tails of the resolution functions—which reach in to the region where a rare discovery may wait to be made—have to be extracted from data in a robust way. This is a quite non-trivial task for experimentalists in the initial phase of LHC running. Within our further considerations we assume the resolution function to provide a 5σ -reduction of the area under its curve below $v = 0.8$ with respect to the area under the whole curve.²¹ Furthermore we take $v_{\text{cut}} = 0.8$ to be the best choice for discriminating staus from muons. This is a reasonable first approximation to the real situation [66].

Predictions from Monte Carlo generators

We have performed Monte Carlo computations via the matrix element event generator MadGraph/MadEvent [9]. The first thing we want to bring up here is to give you a rough estimate of the ratio between stau productions via cascade decays and the direct production in the Drell-Yan process as well as the decays from the production of $\tilde{\tau}_2\tilde{\nu}_\tau$ via W^\pm . If one assumes that any strongly produced sparticle decays in a prompt cascade decay into the stau NLSP the total cross section of the stau production via these cascades would dominantly be the production cross sections of the lightest squark(s) plus the gluino. We stated in section 3 that the cascade decay production of staus would dominate over the direct stau production via Drell-Yan for a large domain of parameter space. A dominant direct production indeed requires a large mass gap between the stau NLSP and the strongly coupled sparticles. For instance, in a scenario where $m_{\tilde{\tau}_1} = 150$ GeV, $m_{\tilde{\tau}_2} = m_{\tilde{\nu}_\tau} = 300$ GeV, $m_{\tilde{t}_1} = 750$ GeV and $m_{\tilde{g}} = 1200$ GeV, the production rates of all these sparticles are roughly the same—about ~ 30 fb. In this calculation we regard all contributions that contain the dominant hadronic channels $q\bar{q}$, qg and gg at the lowest possible order. Nevertheless, this estimation only concerns the total production without

²¹ In the literature other approaches can also be found. [13, 12, 47] refer to a velocity resolution of 0.03 and claim that therefore a velocity cut at 0.91 (at 3σ) would give a background rejection factor of $\sim 10^3$. Such an estimation obviously assumes a gaussian-like distribution above 0.91, but on the other hand if one avoids to shift v_{cut} further down, the only sensible reason for this could be a non-gaussian curve below 0.91. So the real parameter the choice of v_{cut} depends on is the shape of the tail (especially the transition point from the gaussian-like region of the resolution function to the wider spread region). We will come to this subject later on in this section.

applying any cuts. When applying the detection cuts on the velocity this may affect the staus from cascade decays more substantially than direct produced ones since the former are most likely to have larger velocity due to the large phase space in such decays. This would slightly attenuate the domain of parameter space that provides a dominant contribution from cascade decays. Another effect will be, that the correlation of the velocities of the two staus within one event will be smeared away by the cascade. The two staus will in general have very different velocities. The correlation effect will be even more obvious in the case of a p_{\perp} - p_{\perp} -plane plot.

Anyway, as stated in section 3 we want to claim model independent predictions. Therefore in the following we concentrate on the direct production via Drell-Yan. We have calculated the observables p_{\perp} , v , $\sqrt{\hat{s}}$, $\Delta\phi$, Y and y^* . We used MadGraph/MadEvent as a matrix element based generator and Pythia [67] to describe parton radiation. Pythia uses Markov chain techniques based on Sudakov form factors. Since MadEvent is a tree-level generator, in the case of jets in the initial state the result depends on the jet p_{\perp} -cut (and on the ΔR_{jj} -cut, the distance between two jets in the η - ϕ -plane). This is because tree-level matrix element description diverges logarithmically as jets become soft and collinear. On the other hand, the parton radiation description breaks down in the limit of hard and widely separated jets. Thus choices are to be made to adjust cutoffs in both descriptions so as to get smooth distributions in the region where they work hand in glove.

Our choices made are: To include contributions up to order α_s^2 running the MLM matching scheme [8] implemented in MadEvent; p_{\perp} -cut on jets (at MadEvent level): 15 GeV; ΔR_{jj} -cut (at MadEvent level): 0.001; xqcut (minimal k_{\perp} between partons at MadEvent level): 15 GeV; Qcut (maximal k_{\perp} between matched partons and jets at Pythia level): 30 GeV.

All the same, there remain uncertainties about the absolute normalization of the distributions since the matrix element description is only tree-level, but these uncertainties are the same for the staus and muons that we consider as the SM background since the corrections in α_s only affect the kinematics of the vector-boson and therefore the kinematics of the particles it decays into, but not their couplings.

We have used the Les Houches event output files (LHE) [10, 18] for our analysis. An LHE file stores all the generated events by listing the involved particles²², their momenta (in the laboratory frame) and the weight for each event. To extract a differential cross section from such files we have written a script²³ that analyses the data and passes it through to gnuplot. The script runs a loop over all events. For each bin of an observable it adds up the weights of those events that lie within the corresponding interval of the bin. We allow for observable-specified cuts on the events. To apply a cut on the events always means that only those events contribute to the sum whose momenta match with this cut. Applying a cut on both particles requires both momenta to fulfill the cut condition, whereas applying a cut on one particle means that the momenta of one or of the other or of both particles has to fulfill the cut condition.

²²The LHE format uses the Monte Carlo particle numbering scheme [14].

²³We have written all scripts in the programming language ruby.

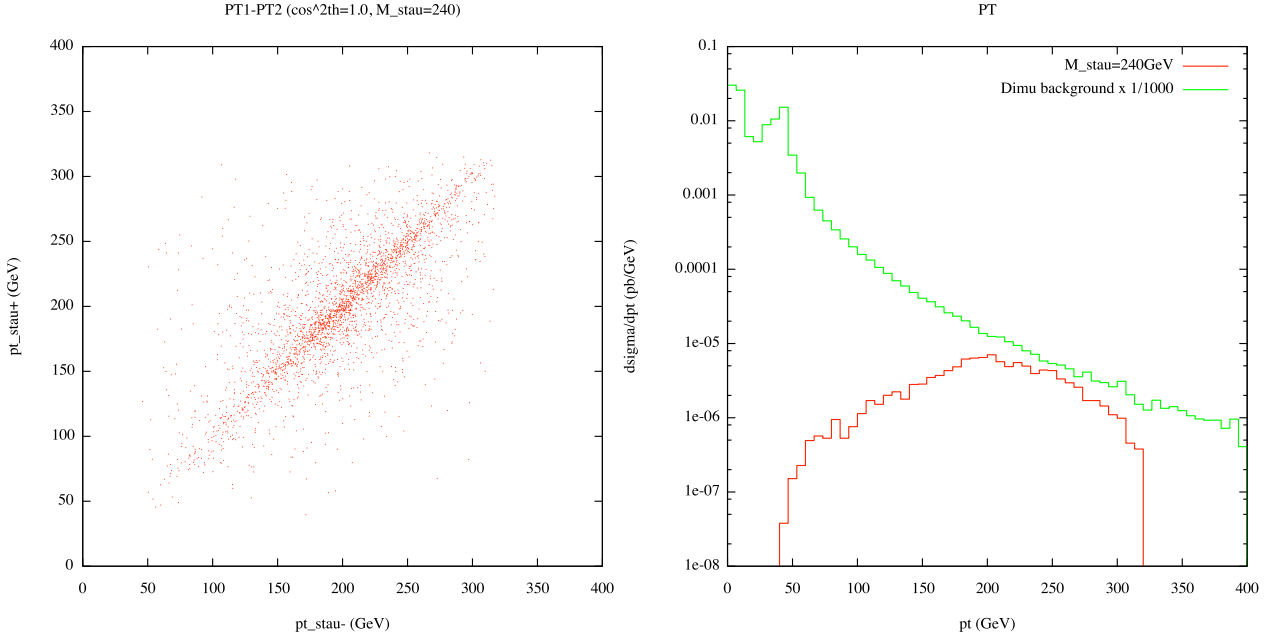


Figure 14: p_{\perp} -distribution of the staus. Left: Unweighted events as dots in the $p_{\perp}^{\tilde{\tau}_1^-}$ - $p_{\perp}^{\tilde{\tau}_1^+}$ -plane. Right: Comparison of the p_{\perp} -distribution of muons and staus. The muon distribution peaks sharply at small values. A p_{\perp} -cut at 5 GeV is already applied. On the stau distributions the velocity cut $0.6 < v < 0.8$ is applied.

The plots in figures 14, 15, 16 and 17 display the observables of $\tilde{\tau}_1$ -pairs with $\cos^2 \theta_{\tilde{\tau}} = 1$ and $m_{\tilde{\tau}_1} = 240$ GeV at the LHC with $\sqrt{s} = 14$ TeV. We have used the PDFs CTEQ6L1 [62]. As a background the Drell-Yan muon pair production is considered. In all plots the dimu cross sections are downscaled by a factor of 1000. On all distributions we apply the barrel cut $|\eta| < 2.5$ (on both particles), this takes into account that the detector is not sensitive for our signal in a certain region just around the beam axis.

Figure 14 shows the p_{\perp} -distribution. The $p_{\perp} - p_{\perp}$ -plane (left) shows that the momenta of the two particles within an event are strongly correlated. A leading order calculation would only contain events that are confined exactly to the diagonal. Through higher order corrections the events are smeared away from the exact diagonal, nevertheless they are still considerably accumulated around the diagonal. We have already applied the velocity cut $0.6 < v < 0.8$ on both staus. It is due to the upper velocity cut that there are no events above a maximum transverse momentum according to $p_{\perp}^{\max} = v_{\text{cut}} \gamma_{v_{\text{cut}}} m_{\tilde{\tau}_1}$ which gives us 320 GeV. There is also a minimum p_{\perp} that comes from lower v_{\min} combined with the η -cut, but in that region there are only a few events anyway. Of course a maximum and minimum p_{\perp} is not the only effect of the velocity cut. There are also many events within these limits that were removed by this cut. Figure 14 (right) additionally shows the p_{\perp} -

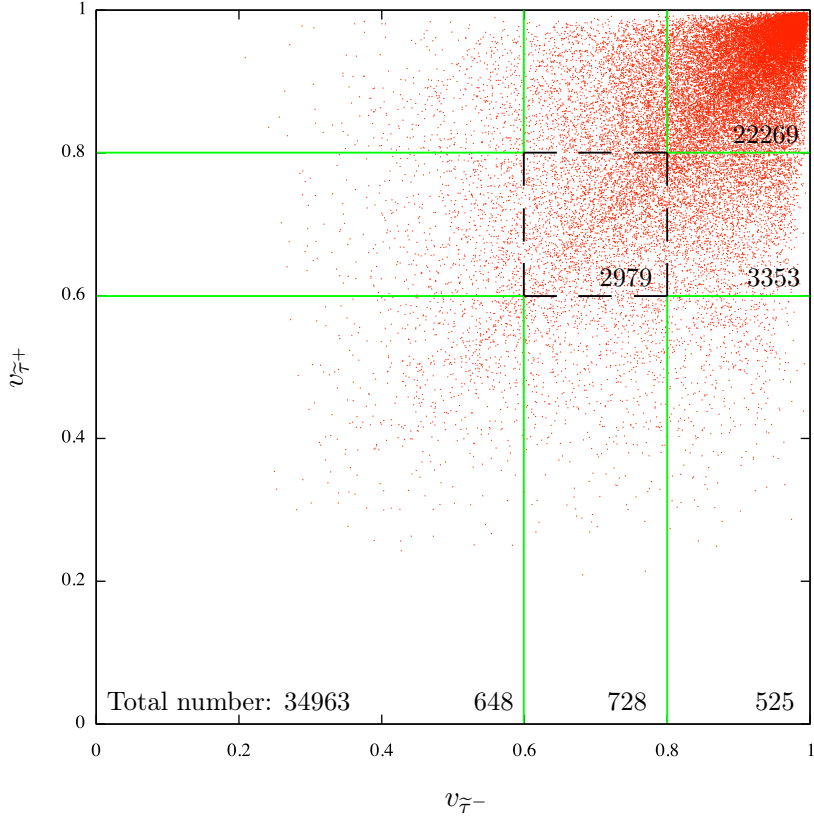


Figure 15: Unweighted events as dots in the v_{τ^-} - v_{τ^+} -plane. The numbers in the lower right corner of each region display the numbers of events in these regions. Due to the symmetry to the diagonal some numbers are omitted. The total number of events is 34963.

distribution of the muons. It peaks sharply at small²⁴ p_{\perp} with an additional enhancement around $p_{\perp} \lesssim M_Z/2$. The staus have very few events in that region. Therefore we can drastically reduce the background by applying a p_{\perp} -cut at $p_{\perp} > 50$ GeV. Such a cut is applied for the plots in figures 15, 16 and 17.

Figure 15 shows the unweighted events as dots in the v_{τ^-} - v_{τ^+} -plane. Most events ($\sim 2/3$ of the total number) lie in the region where $v > 0.8$ for both particles. The dashed box highlights the region of events that fulfill a velocity cut $0.6 < v < 0.8$ on both particles. The selection efficiency with such a cut is 8.5%. Below $v = 0.8$ there

²⁴ To gain efficiency we've already applied a p_{\perp} -cut at 5 GeV at MadEvent-level, therefore the very first bins are not reliable, the peak for $p_{\perp} \rightarrow 0$ is actually much larger.

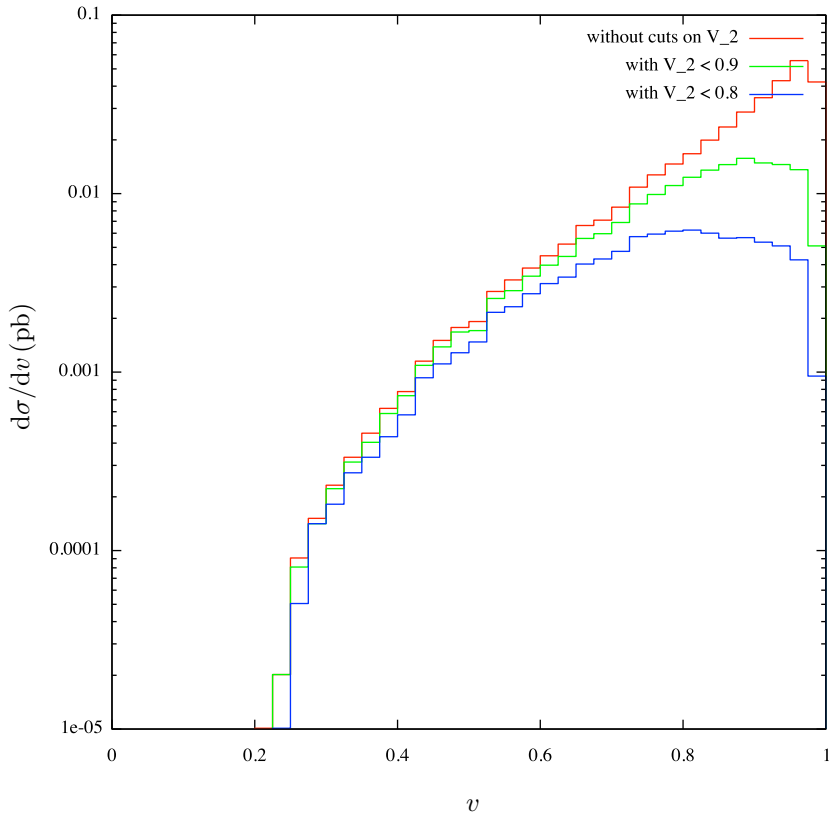


Figure 16: Velocity distribution of one stau depending on three different choices of the v -cut of the other stau in the same event.

is a slight accumulation around the diagonal, coming from events with low Y , that is a low longitudinal boost of the cm-frame. Above 0.8 there is a large contribution of events coming from large cm-frame-boosts, according to figure 12. Those events have less correlated velocities. The lower limit of the velocity measurement v_{\min} has only a small effect on the efficiency. In the region ‘both particles below 0.6’ we find less than 2% of the events and in the whole region ‘at least one particle below 0.6’ there are approximately 9% of the events.

Figure 16 shows the velocity distribution of one particle, when cutting on the other particle (that is one removes an event in which the other particle lies above v_{cut}). Not surprisingly, one loses events mainly in the region where the plotted particle also has high velocity. We’ve applied a velocity cut $0.6 < v < 0.8$ on both staus in all distributions of figure 17.

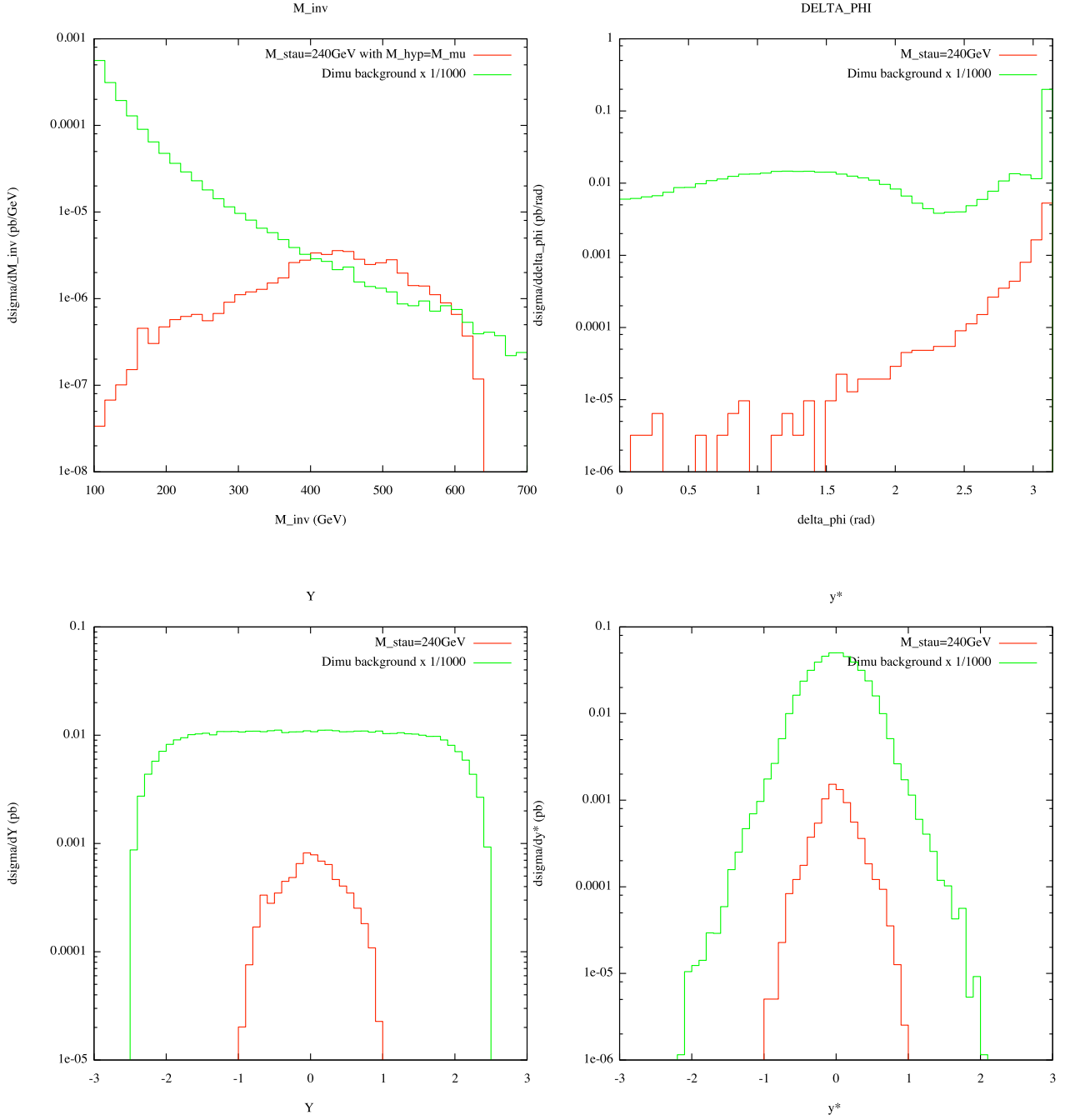


Figure 17: Top left: Invariant mass distribution of the staus applying the hypothetical mass of muons (therefore we take only the spatial momenta from the generated events and substitute the energy with the muon-mass energy-momentum relation). Top right: Distribution of the distance in the angle ϕ of the two staus, $\Delta\phi$. Bottom: Distribution of $Y = \frac{1}{2}(y_{\tilde{\tau}^-} + y_{\tilde{\tau}^+})$ (left) and $y_* = \frac{1}{2}(y_{\tilde{\tau}^-} - y_{\tilde{\tau}^+})$ (right). In all these plots the velocity cut $0.6 < v < 0.8$ is applied.

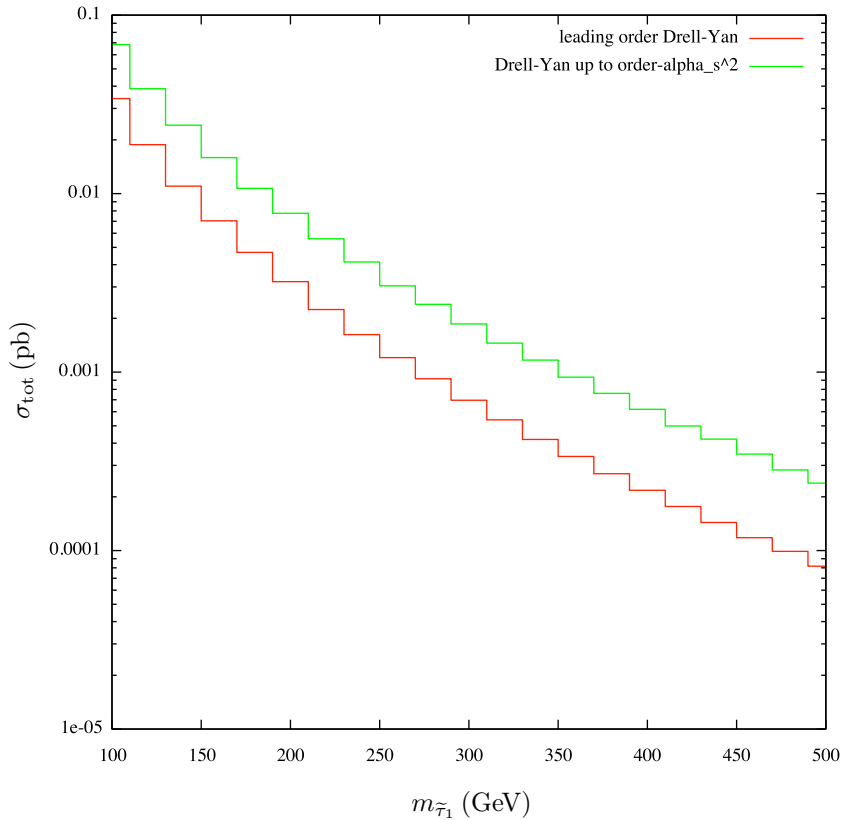


Figure 18: Inclusive cross section for stau-pair production via Drell-Yan as a function of $m_{\tilde{\tau}_1}$ with $\cos^2 \theta_{\tilde{\tau}} = 1$, at leading order (red) and order- α_s^2 (green) at the LHC. The barrel-cut $|\eta| < 2.5$ and p_{\perp} -cut $p_{\perp} > 50$ GeV is applied to both staus. Weighted events were used. The number of events per process before cuts were 6000-8000. The mash of the calculation is $\Delta m = 20$ GeV, the height of a step represents the value of its middle-position in $m_{\tilde{\tau}_1}$.

Figure 17 shows several observables. In the top left plot the invariant mass $\sqrt{\hat{s}}$ of the stau and muon is plotted. In the experiment such a distribution is obtained from the momentum measurement under a certain mass hypothesis. We have plotted the stau invariant mass under a hypothesis of a muon mass. Again the plot shows a maximum value of $\sqrt{\hat{s}}$ which is due to the velocity cut according to (68), but shifted downwards here due to the ‘wrong’ mass hypothesis. The $\Delta\phi$ -distribution makes the higher order corrections obvious. At leading order this would be a delta-function located at π . Y describes the longitudinal boost of the cm-frame (of the staus or muons). The

Y -distribution of the muons is relatively broad according to the large cm-frame boost a muon with negligible mass gives rise to (according to figure 12). Y is simply limited through the barrel cut since in the massless case one has $\eta_i = y_i$ and furthermore, applying (103), $y_i \leq y_{\max}$ means $Y \leq y_{\max}$. Similarly, the Y -distribution of the staus is narrowed due to their high mass. According to figure 12 a mass of 240 GeV will already drive the PDFs in a region where the required $\sqrt{\hat{s}}$ doesn't favor a large asymmetry since one of the x would have to be very close to 1 in that case. And in those regions the PDFs decrease sharply. y_* describes the longitudinal boost of the particles in the cm-frame, so it is related to the angle dependency in the cm-frame. According to the different angle dependencies of the stau (62) and the muon (64) the former is a narrower distribution than the latter.

We have also calculated the total cross section depending on the mass of the produced staus. Therefore, we have written a script that runs a loop over the mass steps executing MadEvent for each choice of mass. So, there is one LHE file for each mass step. We have written another script that reads out all the generated LHE files and passes the results through to gnuplot. Similarly to the above case we allow for kinematic cuts. We have implemented the barrel-cut $|\eta| < 2.5$ and the p_{\perp} -cut $p_{\perp} > 50$ GeV on both particles. We have performed the calculation for leading order Drell-Yan process and Drell-Yan including all tree-level QCD corrections up to order α_s^2 . Figure 18 shows the result. The ratio between order α_s^2 and leading order is approximately 2 at 100 GeV and 3 at 500 GeV. Let's compare this to the ratio of NNLO (involving loops) and leading order calculations in figure 13. There the ratio (in the central Y -region) at $\sqrt{\hat{s}}$ is ~ 1.3 . So, although the calculations for the stau cross section involve much higher $\sqrt{\hat{s}}$ the order α_s^2 MadEvent prediction may be a bit overestimated. However, we are pretty sure that a precise calculation would give a value somewhere in between the two curves in figure 18.

The discovery potential of the LHC

Now we would like to give an answer to the question: Up to which stau mass could we expect to discover the gravitino-stau scenario at 5σ -level at the LHC? For simplicity we'll perform this procedure for the case of (at least) one stau. A consideration of two staus may lead to a better signal-to-background ratio. Anyway, we have to keep in mind that an exhausting estimation of the discovery potential can only be obtained by a full detector simulation. And this would be beyond the scope of this thesis.

Figure 19 shows the cross section for the inclusive cross section of (at least) one stau in the initial state. All the same we only apply cuts on one of the staus.²⁵ Such a

²⁵There's one subtlety about such a choice for the case in which one considers the velocity distribution. If both particles of an event survive the cuts, one has to choose which one to plot. This situation has its counterpart in the experiment. If there are more than one 'slow muon' one has to choose which one to pass through to the analysis. One might be tempted to take the slowest one. But this choice would alter the resolution function to give larger contributions at low velocities because of selection effects. Depending on the exact shape this might be overcompensated by a similar reweighting of the stau velocity distribution. Anyway, we will not get involved in this business. Instead we'll make the (seemingly strange) choice of simply taking one arbitrarily chosen stau (or 'slow muon') that survives the cuts.

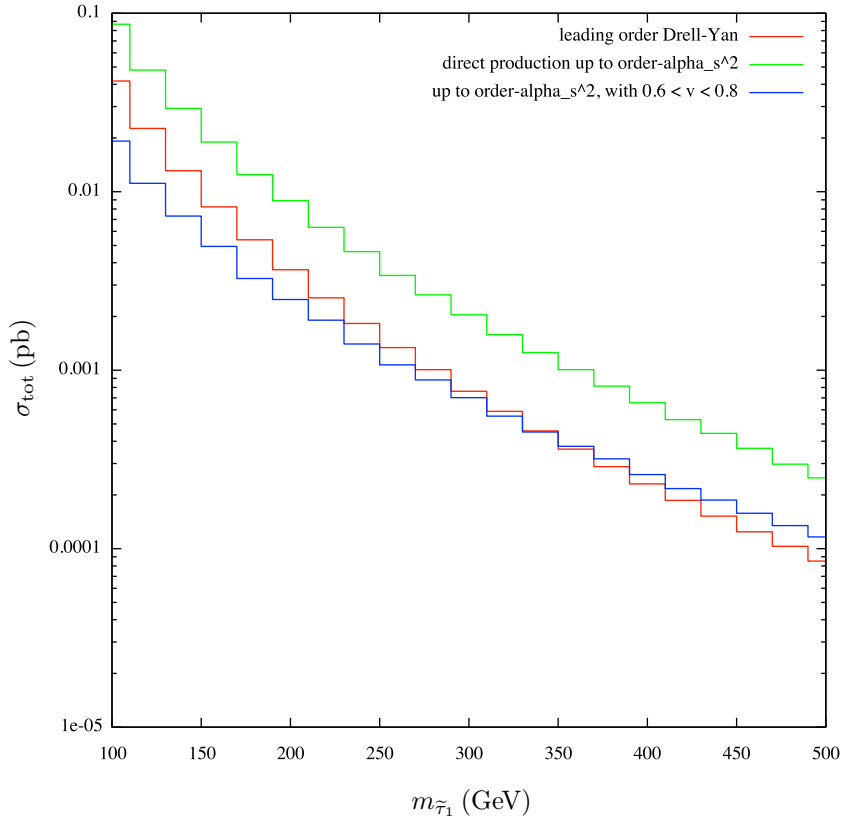


Figure 19: Inclusive cross section for single stau production via Drell-Yan as a function of $m_{\tilde{\tau}_1}$ with $\cos^2 \theta_{\tilde{\tau}} = 1$ to leading order (red) and order α_s^2 (green) at the LHC. The barrel-cut $|\eta| < 2.5$ and p_{\perp} -cut $p_{\perp} > 50$ GeV is applied on one stau. For the blue curve the velocity cut $0.6 < v < 0.8$ is applied additionally. Weighted events were used. The number of events per process before cuts have been 6000-8000. The mash of the calculation is $\Delta m = 20$ GeV, the height of a step represents the value of its middle-position in $m_{\tilde{\tau}_1}$.

velocity-cut selects the events that lie within the green rendered cross in figure 15. By considering (at least) one stau the cross section increases by a factor of ~ 4 with respect to the case of requiring two staus within the cuts. This is the approximate enhancement you get from adding up the appropriate numbers in figure 15 since the cuts on p_{\perp} and η have only a small effect on the stau events (at least for the higher end of the considered stau masses). The blue curve in 19 shows the respective cross section with a cut on p_{\perp} , η and v .

The inclusive cross section for single muon production with $p_{\perp} > 50$ GeV and $|\eta| < 2.5$ is $\sigma_{\mu}^{\text{tot}} \simeq 1.1$ nb. The dominant contribution comes from the decay of W^+ and W^- that were produced either directly in the hard scattering or within the decay of the heavy quarks t , b and c [34]. (Due to the fact that the LHC is a pp-collider, the cross section for direct W^- -production is appreciably smaller than W^+ -production—it is more likely to have a $u\bar{d}$ initial state than a $d\bar{u}$. Hence, there should be a slight asymmetry in the single muon events favoring positive charged muons.)

Now, the number of stau events we expect at a certain (integrated) luminosity \mathcal{L} is

$$\mathcal{L} \int_{v_{\text{min}}}^{v_{\text{cut}}} dv \frac{d\sigma_{\tilde{\tau}}}{dv}(v) \quad (122)$$

where we display the velocity cut explicitly and assume that the others are already applied in $\sigma_{\tilde{\tau}}$. From a statistical point of view $(d\sigma/dv)(v)$ is the theoretical distribution that is assumed to be traced by the experimental data according to the discrete nature of events. Similarly, one can think of the resolution function $R(v, 1)$ times the total cross section of the muons

$$\sigma_{\mu}^{\text{tot}} \int dv' \delta(v' - 1) R(v, v') = \sigma_{\mu}^{\text{tot}} R(v, 1) \quad (123)$$

as a distribution that will also be complied by the events of the experiment. Now, we take the latter distribution to be the background of the former one²⁶ and express the significance of our signal through the formula

$$n_{\sigma} = \frac{S}{\sqrt{S+B}} = \frac{\sqrt{\mathcal{L}} \int_{v_{\text{min}}}^{v_{\text{cut}}} dv \frac{d\sigma_{\tilde{\tau}}}{dv}(v)}{\sqrt{\int_{v_{\text{min}}}^{v_{\text{cut}}} dv \frac{d\sigma_{\tilde{\tau}}}{dv}(v) + \sigma_{\mu}^{\text{tot}} \int_{v_{\text{min}}}^{v_{\text{cut}}} dv R(v, 1)}}, \quad (124)$$

where S and B stand for signal and background, respectively.²⁷ (124) can be seen rather as a function of \mathcal{L} , $m_{\tilde{\tau}_1}$ or even v_{cut} . We adopt the feature

$$\int_{0.6}^{0.8} dv R(v, 1) \simeq \frac{1}{1.7 \times 10^6} \quad (125)$$

²⁶ A justified question on the subject of this treatment would be, how we accommodate the uncertainties of the stau measurement. Ok, we aren't doing this, but let us explain. Our approach is truly a simplified treatment, but it is the best we can do without knowing the explicit form of the resolution function. The accurate treatment of this problem would be to smear the velocity distribution of the staus with the resolution function

$$\int dv' \frac{d\sigma_{\tilde{\tau}}}{dv'}(v') R(v, v')$$

as well. Therefore we additionally need to now the shape of $R(v, v')$ below $v' = 1$. Anyway, looking at the velocity distribution of the staus in figure 16 the curve is still rising at v_{cut} . So, if the shape of $R(v, v')$ doesn't alter in the region $v' > 0.8$ to $v' < 0.8$ in a completely unexpected way (for instance that it is very sharp above and very wide below 0.8) we would gain more events that were smeared from above 0.8 to below 0.8 than we would lose through the opposite effect. (The 0.6-limit would be less dominant.) So we claim that the simplified approach is a conservative estimation.

²⁷This formula holds for the limit of $S, B \gg 1$. Especially, if there are only a few signals and effectively no background at all, this formula considerably underestimates the significance. The appropriate treatment then is to argue with the null hypothesis.

for the resolution function given in the discussion in the first passage of this section and take

$$\int_{0.6}^{0.8} dv \frac{d\sigma_{\tilde{\tau}}}{dv}(m_{\tilde{\tau}_1}) \quad (126)$$

from the blue curve in figure 19. Therewith we have plotted (124) as a function of $m_{\tilde{\tau}_1}$ for four different luminosities. The result is shown in figure 20. The intersection point of each curve with the 5σ -significance-line shows up the maximum stau mass that would be accessible to a 5σ -discovery at the respective luminosity.

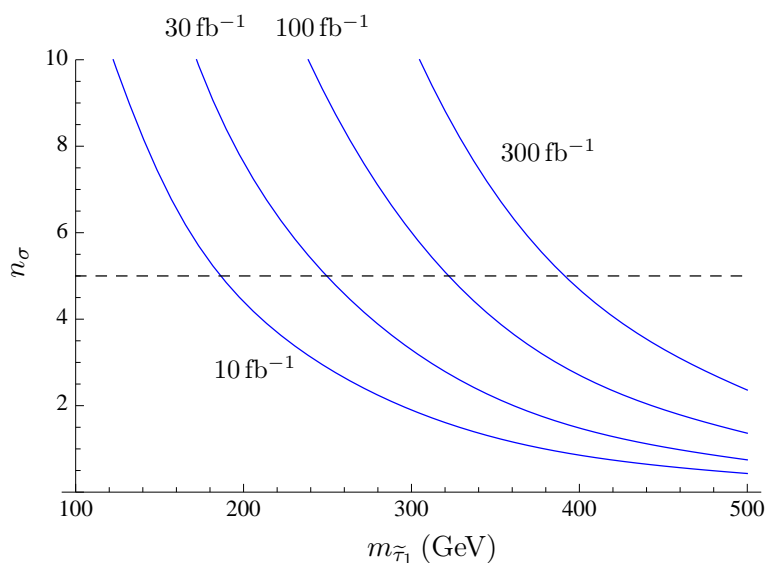


Figure 20: Significance of the inclusive one-stau signal, as a function of the stau mass $m_{\tilde{\tau}_1}$ for four different luminosities. The intersection points with the dashed 5σ are at the masses 186, 249, 322, 391 in GeV.

We want to emphasize that these results are very rough and should be used with caution. On the one hand we were very conservative in our estimation of the stau production. We only considered the Drell-Yan contribution that is just one production channel under many others that might be rather dominating. So this result is to be seen as a lower bound for the discovery potential. But since it is fully model independent we can claim that if the considered gravitino-stau scenario is chosen by nature than we can expect to see it at the LHC according to the above results in any case. On the other hand—just to continue our ‘disclaimer’—the errors of the resolution of the velocity measurement are not very well known. This is a quantity that has to be developed

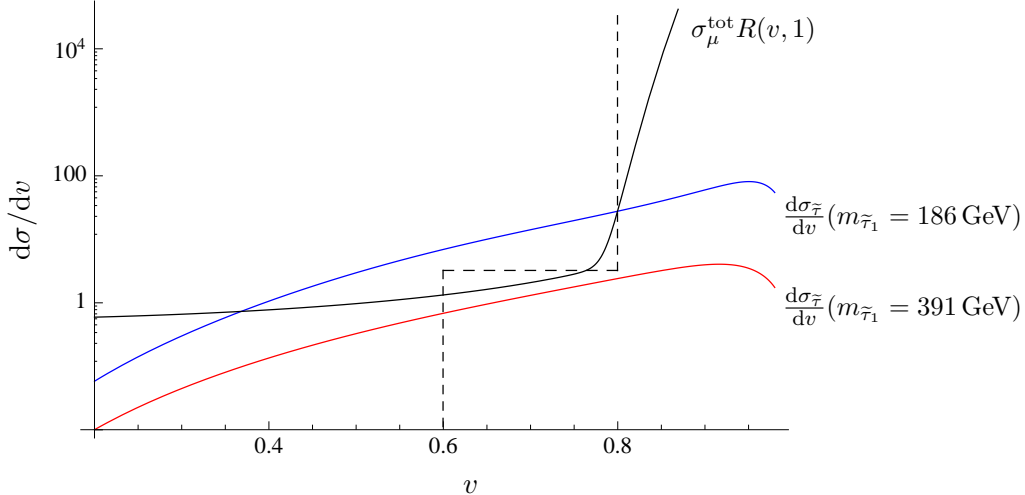


Figure 21: Velocity distributions of the muons and staus. The black curve shows a resolution function (times σ_μ^{tot} that fulfills the condition (125) and the condition that $v_{\text{cut}} = 0.8$ provides the highest significance for a stau mass of 249 GeV. The blue and red curves are the velocity distributions for a stau mass of 186 and 391 GeV respectively. Only the relative normalization is meaningful. The dashed black line shows the trivial distribution that fulfills the above condition for any stau mass.

from data. Thus our assumption that a velocity cut at $v = 0.8$ leads to a background-suppression at 5σ -level is a very rough estimation. Ultimately a sufficiently accurate signal-background calculation is the subject of a full detector simulation.

Nevertheless, one can make a few general statements about choosing the right velocity cut for a certain discovery. The resolution function is presumably not Gaussian. (Otherwise we can always reduce v_{cut} to a point under which the signal-to-background ratio is abundant, due to the steep slope of the Gaussian distributions, in comparison to the one of the velocity distribution of the staus. Ok, if this point is below 0.6 then this is untrue but then there would be no chance to discover the particle anyway.) Typically, such resolution functions are Gaussian-like but with an additional long tail that gives a perceptible contribution down to the lower end of the considered velocity frame. We model such a curve by combining a Gaussian and a Lorentzian distribution. However, we take just one curve that reconstructs the simplified situation from above for one choice of stau mass: The integral over the interval $0.6 < v < 0.8$ is suppression at 5σ -level against the total integral (125) and $v_{\text{cut}} = 0.8$ provides the best significance for this specific stau mass. We have taken $m_{\tilde{\tau}_1}$ from the intersection point of the 30 fb^{-1} -curve with the

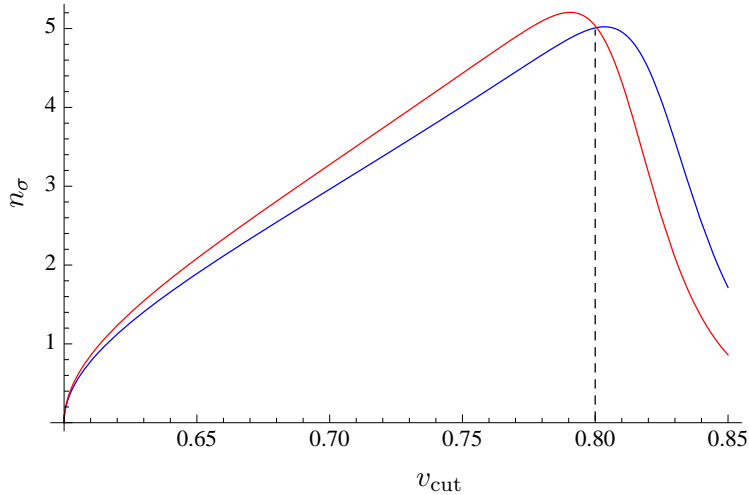


Figure 22: Significance as a function of v_{cut} for two stau masses. The blue ($m_{\tilde{\tau}_1} = 186$ GeV) and red ($m_{\tilde{\tau}_1} = 391$ GeV) curve correspond to the first and last intersection point mass from figure 20, respectively.

5σ -line in figure 20 (249 GeV). This curve is shown in figure 21 as the solid black line.

Now, we have taken two velocity distributions of staus for masses that correspond to the 10fb^{-1} - and 300fb^{-1} -intersection point in figure 20. It is plotted as the blue and red curve in figure 21, respectively. (For this purpose we use a fit on the MadEvent-computed data, the fit is optimized for the region 0.6-0.9.) With this we evaluated equation (124) as a function of v_{cut} . This is shown in figure 22. Of course both curves intersect with each other at $v = 0.8$ and $n_\sigma = 5$, that's how they are chosen. But this point is no longer the maximum. Anyway, in this example (we just took the usual suspects for the distribution and tried it out) the effect is unspectacular. But we may see a tendency here. Searching for heavy particles at high luminosities might favor smaller values of v_{cut} than searching for lighter particles with less data.

This procedure can be seen as a procedure for finding the ‘right’ v_{cut} in order to maximize the significance when the resolution function of the velocity measurement $R(v, v')$ is known from experiment.

7 Conclusion and Outlook

In models of gauge-mediation, gaugino-mediation and in a certain domain of parameter space of gravity-mediation a gravitino LSP is provided and is naturally accompanied by a stau NLSP. The stau plays a key role in this scenario since its decay into the gravitino is suppressed by $1/\langle F \rangle^2$. For $\langle F \rangle \gtrsim (10^5 \text{ GeV})^2$ the stau will be long-lived in a collider experiment.

Our discussion has shown that there are different production channels of long-lived staus that provide for different signatures. The staus coming from cascades of strongly interacting particles will typically have very large velocities and the correlation of the momenta of the initially produced squarks or gluinos will be smeared away in the course of the cascade decays.

The electroweak direct production via the Drell-Yan process always provides stau events with two staus of opposite charge and with strongly correlated momenta. Its production rate depends only on the two supersymmetry parameters $m_{\tilde{\tau}_1}$ and $\theta_{\tilde{\tau}}$. The $\theta_{\tilde{\tau}}$ -dependence of the cross section is independent of the kinematical variables \hat{t} , \hat{u} and at first approximation independent of \hat{s} (as long as \hat{s} is larger than a few times M_Z^2), thus $\theta_{\tilde{\tau}}$ only causes a shift of the total cross section. We have seen that there is a universal velocity distribution in the cm-frame that holds for all sfermion-pairs in the s-channel production. And we have made further investigations to understand how such a distribution is affected by boosts of the cm-frame. The conclusion is, that even at high stau masses around 500 GeV the maximum of the velocity distribution lies near 1 and the largest domain of events lies in the region 0.8-1. This characteristic feature doesn't change before the cm-energy comes close to the beam-cm-energy, this takes place at above $m_{\tilde{\tau}_1} \sim 1 \text{ TeV}$. Below $m_{\tilde{\tau}_1} \sim 500 \text{ GeV}$ the total cross section of the staus decreases roughly by an order of magnitude when doubling the mass. Above 500 GeV the decrease is larger due to the change of the character of the slope of the parton luminosity above $\sim 1 \text{ TeV}$.

Our discussion has also touched some experimental issues. The determination of the resolution function of the velocity measurement is a quantity to be extracted from data at the LHC. The knowledge of such a resolution function is crucial for a precise estimation of the muon-background, since mis-identified muons are the only background to heavy charged (s)particles. We have shown how the choice of a velocity cut in principle affects the significance of a discovery.

In a model-independent, conservative estimation (and with a first estimation for the velocity measurement resolution function) we stated that if the gravitino-stau scenario is chosen by nature we can expect to discover it at the LHC at least up to a stau mass of $m_{\tilde{\tau}_1} \sim 400 \text{ GeV}$ (with 300 fb^{-1}).

The LHC also resembles the appropriate environment to measure the mass of the staus, once they are discovered. Due to the (relatively) precise momentum measurement a combination of the velocities and transverse momenta of the stau pairs will give a relatively easy access to the stau mass. To some extent also the measurement of the mixing angle is possible. This is especially true when considering other contributions

to stau production that are sensitive to the mixing angle (like H -resonance or decays from heavier sleptons that were produced via W^\pm). Another interesting outlook is to determine the properties of the gravitino by considering stau decays. This could be done by analyzing data from staus that are stopped inside or near the detector and decay afterwards into the gravitino and the τ . If the origin of such a stau can be reconstructed from the data it is in principle possible to conclude the gravitino mass via the lifetime of the stau and $m_{\tilde{\tau}_1}$.

A Conventions

Throughout this thesis we work in Heaviside-Lorentz units, that is

$$\hbar = c = 1, \quad (127)$$

and

$$\alpha = \frac{e^2}{4\pi}. \quad (128)$$

Whenever cross sections are computed we need to translate the result from GeV^{-2} to the SI-related unit barn. So, we have to restore the appropriate powers in \hbar and c . Thus, a factor of

$$(\hbar c)^2 \simeq 0.39 \text{ mbarn GeV}^2 \quad (129)$$

has to be multiplied. (The precise numerical value can be found at [14].)

The kinetic terms of the Lagrangians contain two quantities we want to fix here. First, a sign depending on the choice of the Minkowski metric. We have chosen

$$\eta = \text{diag}(-1, +1, +1, +1). \quad (130)$$

Second, σ^μ and $\bar{\sigma}^\mu$, which is defined as

$$\begin{aligned} \sigma^0 = \bar{\sigma}^0 &= \begin{pmatrix} 1 & 0 \\ 0 & 1 \end{pmatrix}, & \sigma^1 = -\bar{\sigma}^1 &= \begin{pmatrix} 0 & 1 \\ 1 & 0 \end{pmatrix}, \\ \sigma^2 = -\bar{\sigma}^2 &= \begin{pmatrix} 0 & -i \\ i & 0 \end{pmatrix}, & \sigma^3 = -\bar{\sigma}^3 &= \begin{pmatrix} 1 & 0 \\ 0 & -1 \end{pmatrix}. \end{aligned} \quad (131)$$

With this we can write down the gamma matrices as

$$\gamma^\mu = \begin{pmatrix} 0 & \sigma^\mu \\ \bar{\sigma}^\mu & 0 \end{pmatrix}, \quad \gamma_5 = \begin{pmatrix} -1 & 0 \\ 0 & 1 \end{pmatrix}, \quad (132)$$

where we adopt a 2×2 block notation.

A comprehensive treatment of translating between two-component Weyl spinors and four component Dirac spinors can be found in [33].

B Supersymmetry interactions

In this section we would like to give an overview of the allowed interactions the supersymmetry Lagrangian and the soft breaking terms give rise to. We start with the terms induced by (16).

Terms from $W^{ij}\psi_i\psi_j$

The fermion mass terms:

$$M^{ij}\psi_i\psi_j \longrightarrow \longrightarrow \times \longleftarrow \longleftarrow \quad (133)$$

$$M_{ij}^*\psi^{\dagger i}\psi^{\dagger j} \longrightarrow \longleftarrow \times \longrightarrow \longrightarrow \quad (134)$$

The Yukawa couplings:

$$y^{ijk}\phi_i\psi_j\psi_k \longrightarrow \text{---} \longrightarrow \begin{array}{l} \nearrow \\ \searrow \end{array} \quad (135)$$

$$y_{ijk}^*\phi^{*i}\psi^{\dagger j}\psi^{\dagger k} \longrightarrow \text{---} \longleftarrow \begin{array}{l} \nearrow \\ \searrow \end{array} \quad (136)$$

Note that in the case of the R -parity preserving MSSM (that is with a superpotential of the form (20)) in (135) and (136) there is always exactly one of the fields belonging to the Higgs supermultiplets. So in other words the entries of y^{ijk} have to be zero except for the case when i, j or k denotes a Higgs supermultiplet (this is due to the symmetry of y^{ijk}). Similarly, M^{ij} is restricted to vanish except for the H_u - H_d and H_d - H_u component. This fact also restricts the (scalar)³-interactions.

Terms from $|W^i|^2$

The scalar mass term:

$$M_{ik}^*M^{kj}\phi^{*i}\phi_j \longrightarrow \text{---} \longrightarrow \times \longrightarrow \text{---} \quad (137)$$

The (scalar)³-couplings:

$$M_{in}^*y^{jkn}\phi^{*i}\phi_j\phi_k \longrightarrow \text{---} \longleftarrow \begin{array}{l} \nearrow \\ \searrow \end{array} \quad (138)$$

$$M^{in} y_{jkn}^* \phi_i \phi^{*j} \phi^{*k} \longrightarrow \text{---} \rightarrow \text{---} \begin{array}{l} \nearrow \\ \searrow \end{array} \quad (139)$$

The (scalar)⁴-coupling:

$$y^{ijn} y_{klm}^* \phi_i \phi_j \phi^{*k} \phi^{*l} \longrightarrow \begin{array}{c} \nearrow \quad \searrow \\ \times \\ \swarrow \quad \nwarrow \end{array} \quad (140)$$

Terms from $F_{\mu\nu}^a F^{\mu\nu a}$

The (vector)³-coupling:

$$g f^{abc} A^{\mu b} A^{\nu c} (\partial_\mu A_\nu^a - \partial_\nu A_\mu^a) \longrightarrow \text{---} \begin{array}{l} \nearrow \\ \searrow \end{array} \quad (141)$$

The (vector)⁴-coupling:

$$g^2 f^{abc} f^{ade} A_\mu^b a_\nu^c A^{\mu d} A^{\nu e} \longrightarrow \begin{array}{c} \nearrow \\ \times \\ \searrow \end{array} \quad (142)$$

These are just SM couplings. g and f^{abc} are the gauge couplings and the totally antisymmetric structure constants (fulfilling $[T^a, T^b] = i f^{abc} T^c$) of the gauge groups, respectively. To reduce clutter, we won't display the gauge group index here, of course these interactions only exist in the non-abelian case of $SU(2)_L$ and $SU(3)_C$ ($a = 1, \dots, 3$ for $SU(2)_L$ and $a = 1, \dots, 8$ for $SU(3)_C$).

Gauge couplings from the covariant derivatives

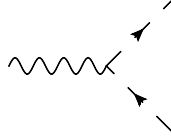
The fermion gauge coupling:

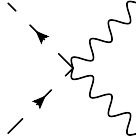
$$g A_\mu^a \psi^\dagger \bar{\sigma}^\mu (T^a \psi)_i \psi_i \longrightarrow \text{---} \begin{array}{l} \nearrow \\ \searrow \end{array} \quad (143)$$

The gaugino gauge coupling:

$$g f^{abc} A_\mu^b \lambda^\dagger \bar{\sigma}^\mu \lambda^a \longrightarrow \text{---} \begin{array}{l} \nearrow \\ \times \\ \searrow \end{array} \quad (144)$$

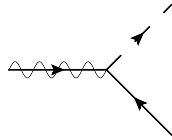
The scalar gauge couplings:

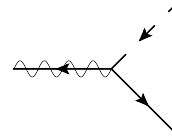
$$g(\partial_\mu \phi^{*i}) A_\mu^a (T^a \phi)_i \longrightarrow \text{Diagram (145)}$$

(145)

$$g^2 A_\mu^a A^{\mu a} (T^a \phi)_i (\phi^* T^a)^i \longrightarrow \text{Diagram (146)}$$

(146)

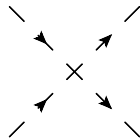
Other interactions including gauge couplings

The gaugino coupling to a scalar-fermion chiral multiplet pair:

$$g(\phi^{*i} T^a \psi_i) \lambda^a \longrightarrow \text{Diagram (147)}$$

(147)

$$g\lambda^{\dagger a} (\psi^{\dagger i} T^a \phi_i) \longrightarrow \text{Diagram (148)}$$

(148)

Another contribution to the (scalar)⁴ coupling:

$$g_a^2 (\phi^{*i} T^a \phi_i)^2 \longrightarrow \text{Diagram (149)}$$

(149)

This (scalar)⁴ coupling gives the (Higgs)⁴-contribution to the Higgs potential and therefore allows electroweak symmetry breaking. Such a contribution cannot be obtained from (140), since at most two of the fields can be Higgs fields there.

As a consequence of R -parity conservation you can take each SM three leg diagram and turn an even number of legs (that are simply two legs) into its superpartner legs to obtain a corresponding supersymmetry diagram, characterized by the same couplings. The (scalar)³-, (scalar)⁴- and the (scalar)²(vector)²-couplings cannot be obtained by this procedure. As well as that there is no corresponding diagram for the (vector)⁴-interaction.

Next, we will display the additional diagrams that come with soft supersymmetry breaking, written down in (22).

Soft supersymmetry breaking terms

The non-analytic scalar squared mass terms (bilinear terms):

$$(m^2)^i_j \phi_i^* \phi^j \longrightarrow \text{---} \rightarrow \times \rightarrow \text{---} \quad (150)$$

The analytic scalar squared mass terms:

$$b^{ij} \phi_i \phi_j \longrightarrow \text{---} \rightarrow \times \leftarrow \text{---} \quad (151)$$

$$b_{ij}^* \phi^{*i} \phi^{*j} \longrightarrow \text{---} \leftarrow \times \rightarrow \text{---} \quad (152)$$

The trilinear terms:

$$a^{ijk} \phi_i \phi_j \phi_k \longrightarrow \text{---} \rightarrow \begin{array}{l} \diagup \\ \diagdown \end{array} \quad (153)$$

$$a_{ijk}^* \phi^{*i} \phi^{*j} \phi^{*k} \longrightarrow \text{---} \leftarrow \begin{array}{l} \diagup \\ \diagdown \end{array} \quad (154)$$

The gaugino mass terms:

$$M_a \lambda^a \lambda^a \longrightarrow \text{---} \times \text{---} \quad (155)$$

As you can see in equation (22), only the Higgs fields appear in the analytic scalar mass terms, while in the non-analytic scalar mass terms there are only the sfermions.

The Goldstino/gravitino couplings to the MSSM multiplets

The Goldstino-scalar-fermion term:

$$(\partial_\mu \tilde{G}^\alpha) (\sigma^\nu \bar{\sigma}^\mu \psi_i)_\alpha \partial_\nu \phi^{*i} \longrightarrow \text{---} \begin{array}{l} \diagup \\ \diagdown \end{array} \quad (156)$$

The Goldstino-gaugino-(gauge boson) term:

$$(\partial_\mu \tilde{G}^\alpha) (\sigma^\mu \bar{\sigma}^\nu \sigma^\rho \lambda^\dagger)_\alpha (\partial_\mu A_\nu^a - \partial_\nu A_\mu^a) \longrightarrow \text{---} \begin{array}{l} \diagup \\ \diagdown \end{array} \quad (157)$$

The Goldstino-gaugino-(gauge boson)² term:

$$g f^{abc} (\partial_\mu \tilde{G}^\alpha) (\sigma^\mu \bar{\sigma}^\nu \sigma^\rho \lambda^\dagger)_\alpha A_\mu^b A_\nu^c \longrightarrow \text{---} \begin{array}{l} \diagup \\ \diagdown \end{array} \quad (158)$$

C Transformation of velocities and angles

In the case the cm-frame is boosted along the z -axis, the velocities as well as the angles transform in a non trivial way. This is what we want to show here.

Let's see how to perform the Lorentz-boost with velocity β along the z -axis. Let's consider an arbitrary vector \mathbf{x}' defined in the cm-frame. We can write it as $\mathbf{x}' = x'_{\parallel} \hat{e}_{\parallel} + x'_{\perp} \hat{e}_{\perp}$ splitting up the vector in its projection parallel and orthogonal to the beam, the direction of the boost. The Lorentz boost is

$$\begin{pmatrix} t \\ x_{\perp} \\ x_{\parallel} \end{pmatrix} = \begin{pmatrix} \gamma & \beta\gamma & 0 \\ 0 & 0 & 1 \\ \beta\gamma & \gamma & 0 \end{pmatrix} \begin{pmatrix} t' \\ x'_{\perp} \\ x'_{\parallel} \end{pmatrix} = \begin{pmatrix} \gamma(t' + \beta x'_{\parallel}) \\ x'_{\perp} \\ \gamma(\beta t' + x'_{\parallel}) \end{pmatrix}. \quad (159)$$

Thus we find

$$v_{\parallel} = \frac{dx_{\parallel}}{dt} = \frac{\gamma d(\beta t' + x'_{\parallel})}{\gamma d(t' + \beta x'_{\parallel})} = \left(\frac{dt' + \beta dx'_{\parallel}}{\beta dt'} \right)^{-1} + \left(\frac{dt' + \beta dx'_{\parallel}}{dx'_{\parallel}} \right)^{-1} = \frac{\beta + v'_{\parallel}}{1 + \beta v'_{\parallel}} \quad (160)$$

and

$$v_{\perp} = \frac{dx_{\perp}}{dt} = \frac{x'_{\perp}}{\gamma d(t' + \beta x'_{\parallel})} = \left(\frac{\gamma dt' + \gamma \beta dx'_{\parallel}}{dx'_{\perp}} \right)^{-1} = \frac{v'_{\perp}}{\gamma(1 + \beta v'_{\parallel})}. \quad (161)$$

We always measure the angle θ from the beam-axis, so that (same for primed quantities)

$$\begin{aligned} v_{\perp} &= v \sin \theta \\ v_{\parallel} &= v \cos \theta. \end{aligned} \quad (162)$$

Thus for the angle in the laboratory frame one obtains

$$\tan \theta = \frac{\sin \theta'}{\gamma(\beta/v' + \cos \theta')}. \quad (163)$$

This transformation law has inverse functions that can only be defined by sections.

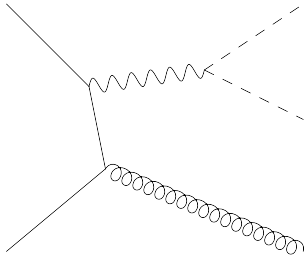
D The corrections to the Drell-Yan process in α_s

To get an overview over the possible diagrams that contribute to the Drell-Yan corrections up to order α_s^2 we have listed all these contributions.

Please note that in figures 23-26 we use a shortened notation: All (s)fermion lines come without arrows and so all possible combinations of arrow directions are meant by one diagram. As a consequence we suppress the bar on the q s in the titles. But of course only in the two diagrams in the first line of figure 26 ' qq ' (in the accurate notation) is possible, since the two initial state (anti-)quarks are part of distinct fermion-lines.

In the titles we only display the strong interacting initial and final states.

$qq \rightarrow g$:



$gq \rightarrow q$:

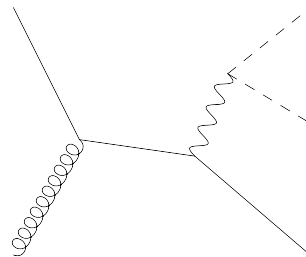
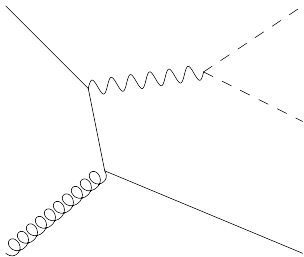


Figure 23: Order- α_s^1 -contributions to the inclusive $pp \rightarrow \tilde{\tau}^- \tilde{\tau}^+$ tree-level process.

$gq \rightarrow gq$:

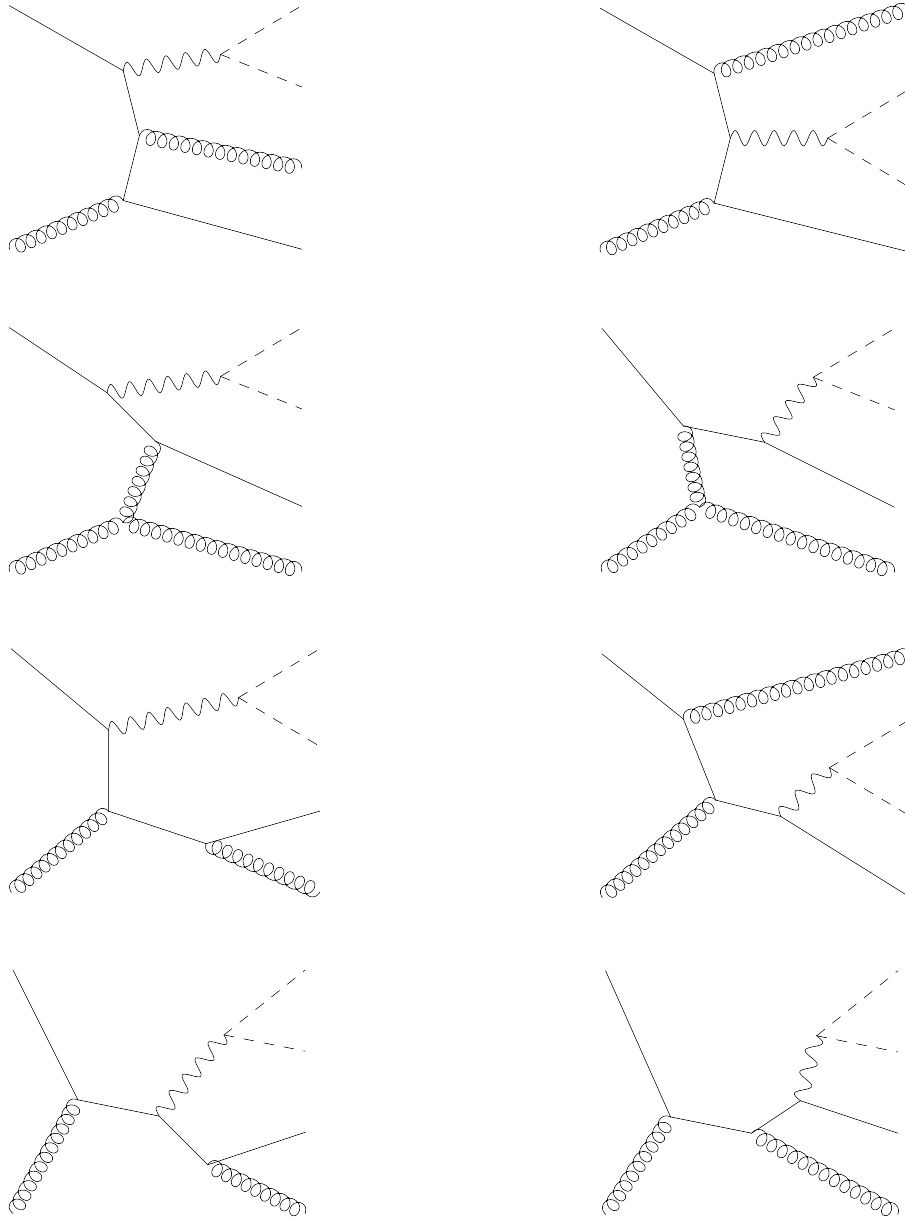
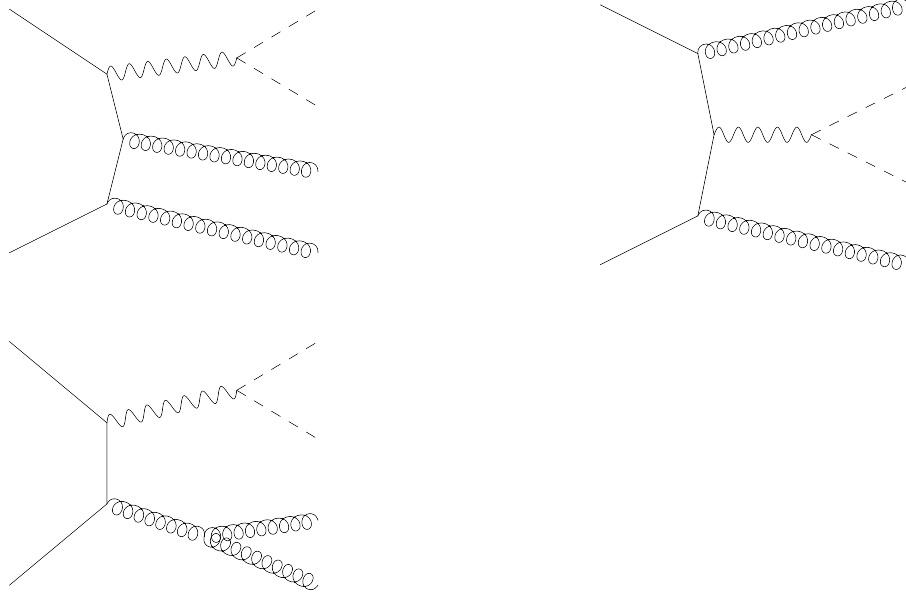


Figure 24: Order- α_s^2 -contributions to the inclusive $pp \rightarrow \tilde{\tau}^- \tilde{\tau}^+$ tree-level process.

$qq \rightarrow gg$:



$gg \rightarrow qq$:

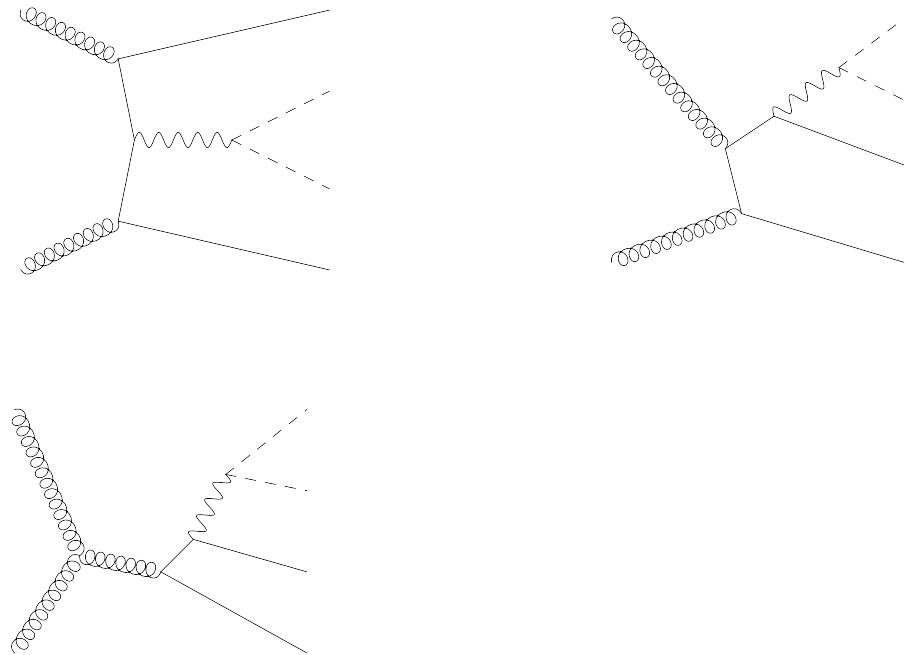


Figure 25: Order- α_s^2 -contributions to the inclusive $pp \rightarrow \tilde{\tau}^- \tilde{\tau}^+$ tree-level process.

$qq \rightarrow qq$:

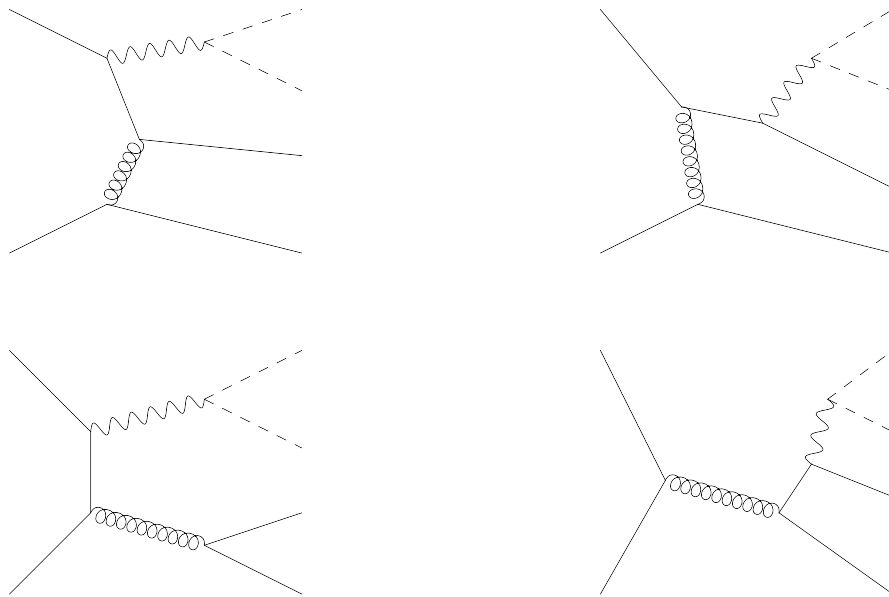


Figure 26: Order- α_s^2 -contributions to the inclusive $pp \rightarrow \tilde{\tau}^- \tilde{\tau}^+$ tree-level process. The two diagrams in the first row are the only ones that allow two distinct quarks in the initial state and thus interfere with the initial state qq (and here it is meant explicitly without a bar on one of the quarks).

References

- [1] *ATLAS detector and physics performance: Technical Design Report, 1*. Technical Design Report ATLAS. CERN, Geneva, 1999. Electronic version not available.
- [2] Search for heavy stable charged particles with 100 inverse picobarns and 1 inverse femtobarn in the cms experiment. Feb 2009.
- [3] D. Acosta, Michel Della Negra, L. Foa, A. Herve, and Achille Petrelli. *CMS physics: Technical Design Report*. Technical Design Report CMS. CERN, Geneva, 2006. There is an error on cover due to a technical problem for some items.
- [4] Ian J. R. Aitchison. *Supersymmetry and the mssm: An elementary introduction*, 2005.
- [5] S. Alekhin. Parton distribution functions from the precise nnlo qcd fit. *PISMA ZH.EKSP.TEOR.FIZ.*, 82:710, 2005.
- [6] B. C. Allanach. SOFTSUSY: A C++ program for calculating supersymmetric spectra. *Comput. Phys. Commun.*, 143:305–331, 2002.
- [7] B. C. Allanach et al. The Snowmass points and slopes: Benchmarks for SUSY searches. *Eur. Phys. J.*, C25:113–123, 2002.
- [8] J. Alwall, S. Hoeche, F. Krauss, N. Lavesson, L. Lonnblad, F. Maltoni, M. L. Mangano, M. Moretti, C. G. Papadopoulos, F. Piccinini, S. Schumann, M. Trecani, J. Winter, and M. Worek. Comparative study of various algorithms for the merging of parton showers and matrix elements in hadronic collisions. *European Physical Journal C*, 53:473, 2008.
- [9] Johan Alwall, Pavel Demin, Simon de Visscher, Rikkert Frederix, Michel Herquet, Fabio Maltoni, Tilman Plehn, David L. Rainwater, and Tim Stelzer. Madgraph/madevent v4: The new web generation, 2007.
- [10] Johan Alwall et al. A standard format for Les Houches event files. *Comput. Phys. Commun.*, 176:300–304, 2007.
- [11] Ugo Amaldi, Wim de Boer, and Hermann Fuerstenau. Comparison of grand unified theories with electroweak and strong coupling constants measured at lep. *Physics Letters B*, 260(3-4):447 – 455, 1991.
- [12] S. Ambrosanio et al. SUSY long-lived massive particles: Detection and physics at the LHC. 2000.
- [13] S. Ambrosanio, B. Mele, S. Petrarca, G. Polesello, and A. Rimoldi. Measuring the SUSY breaking scale at the LHC in the slepton NLSP scenario of GMSB models. *JHEP*, 01:014, 2001.

- [14] C. Amsler et al. Review of particle physics. *Phys. Lett.*, B667:1, 2008.
- [15] Charalampos Anastasiou, Lance Dixon, Kirill Melnikov, and Frank Petriello. High-precision qcd at hadron colliders: Electroweak gauge boson rapidity distributions at next-to-next-to leading order. *Phys. Rev. D*, 69(9):094008, May 2004.
- [16] Richard D. Ball et al. A first unbiased global NLO determination of parton distributions and their uncertainties. 2010.
- [17] R. Barbier, C. Berat, M. Besancon, M. Chemtob, A. Deandrea, E. Dudas, P. Fayet, S. Lavignac, G. Moreau, E. Perez, and Y. Sirois. R-parity violating supersymmetry, 2004.
- [18] E. Boos et al. Generic user process interface for event generators. 2001.
- [19] Wilfried Buchmuller, Koichi Hamaguchi, and Joern Kersten. The gravitino in gaugino mediation. *Phys. Lett.*, B632:366–370, 2006.
- [20] D. G. Cerdeno and C. Munoz. An introduction to supergravity. Prepared for 6th Hellenic School and Workshop on Elementary Particle Physics:, Corfu, Greece, 6-26 Sep 1998.
- [21] Z. Chacko, Markus A. Luty, Ann E. Nelson, and Eduardo Ponton. Gaugino mediated supersymmetry breaking. *JHEP*, 01:003, 2000.
- [22] A. H. Chamseddine, R. Arnowitt, and Pran Nath. Locally supersymmetric grand unification. *Phys. Rev. Lett.*, 49(14):970–974, Oct 1982.
- [23] John C. Collins and Davison E. Soper. The Theorems of Perturbative QCD. *Ann. Rev. Nucl. Part. Sci.*, 37:383–409, 1987.
- [24] John C. Collins, Davison E. Soper, and George Sterman. Factorization of hard processes in qcd, 1988.
- [25] E. Cremmer, S. Ferrara, L. Girardello, and A. Van Proeyen. Yang-mills theories with local supersymmetry: Lagrangian, transformation laws and super-higgs effect. *Nuclear Physics B*, 212(3):413 – 442, 1983.
- [26] S. Deser and B. Zumino. Broken supersymmetry and supergravity. *Phys. Rev. Lett.*, 38(25):1433–1436, Jun 1977.
- [27] Michael Dine and Ann E. Nelson. Dynamical supersymmetry breaking at low-energies. *Phys. Rev.*, D48:1277–1287, 1993.
- [28] Michael Dine, Ann E. Nelson, Yosef Nir, and Yuri Shirman. New tools for low energy dynamical supersymmetry breaking. *Phys. Rev. D*, 53(5):2658–2669, Mar 1996.
- [29] Michael Dine, Ann E. Nelson, and Yuri Shirman. Low-energy dynamical supersymmetry breaking simplified. *Phys. Rev.*, D51:1362–1370, 1995.

- [30] Manuel Drees. An Introduction to supersymmetry. 1996.
- [31] Manuel Drees, Rohini M Godbole, and Probir Roy. *Theory and phenomenology of Sparticles: an account of four-dimensional N=1 supersymmetry in high-energy physics*. World Scientific, Singapore, 2004.
- [32] Herbert K. Dreiner. An introduction to explicit R-parity violation. 1997.
- [33] Herbi K. Dreiner, Howard E. Haber, and Stephen P. Martin. Two-component spinor techniques and feynman rules for quantum field theory and supersymmetry, 2008.
- [34] Paule Anna Mari Eerola. The inclusive muon cross-section in atlas 222. Technical Report ATL-MUON-98-222. ATL-M-PN-222, CERN, Geneva, Feb 1998.
- [35] John R. Ellis, Are R. Raklev, and Ola K. Oye. Gravitino dark matter scenarios with massive metastable charged sparticles at the LHC. *JHEP*, 10:061, 2006.
- [36] M. Fairbairn et al. Stable massive particles at colliders. *Phys. Rept.*, 438:1–63, 2007.
- [37] Glennys R. Farrar and Pierre Fayet. Phenomenology of the production, decay, and detection of new hadronic states associated with supersymmetry. *Physics Letters B*, 76(5):575 – 579, 1978.
- [38] P. Fayet. Scattering cross sections of the photino and the goldstino (gravitino) on matter. *Physics Letters B*, 86(3-4):272 – 278, 1979.
- [39] Jonathan L. Feng, Shufang Su, and Fumihiro Takayama. Supergravity with a gravitino LSP. *Phys. Rev.*, D70:075019, 2004.
- [40] G. F. Giudice and R. Rattazzi. Theories with gauge-mediated supersymmetry breaking. *Physics Reports*, 322(6):419 – 499, 1999.
- [41] Gian F. Giudice, Markus A. Luty, Hitoshi Murayama, and Riccardo Rattazzi. Gaugino Mass without Singlets. *JHEP*, 12:027, 1998.
- [42] Yu. A. Gol’fand and E. P. Likhtman. Extension of the algebra of poincare group generators and violation of p invariance. *JTPLA*, 13(8):323 – 326, 1971.
- [43] Rudolf Haag, Jan T. Lopuszanski, and Martin Sohnius. All possible generators of supersymmetries of the s-matrix. *Nuclear Physics B*, 88(2):257 – 274, 1975.
- [44] H. Haber and G. L. Kane. The search for supersymmetry: Probing physics beyond the standard model. *Physics Reports*, 117(2-4):75–263, January 1985.
- [45] Howard E. Haber. Low-energy supersymmetry and its phenomenology. *Nucl. Phys. Proc. Suppl.*, 101:217–236, 2001.
- [46] Lawrence Hall, Joe Lykken, and Steven Weinberg. Supergravity as the messenger of supersymmetry breaking. *Phys. Rev. D*, 27(10):2359–2378, May 1983.

- [47] Jonathan J. Heckman, Jing Shao, and Cumrun Vafa. F-theory and the LHC: Stau Search. 2010.
- [48] Dan Hooper and Tilman Plehn. Supersymmetric dark matter: How light can the LSP be? *Phys. Lett.*, B562:18–27, 2003.
- [49] Takumi Ito, Ryuichiro Kitano, and Takeo Moroi. Measurement of the Superparticle Mass Spectrum in the Long-Lived Stau Scenario at the LHC. *JHEP*, 04:017, 2010.
- [50] D. Elazzar Kaplan, Graham D. Kribs, and Martin Schmaltz. Supersymmetry breaking through transparent extra dimensions. *Phys. Rev. D*, 62(3):035010, Jul 2000.
- [51] Christopher F. Kolda. Gauge-mediated supersymmetry breaking: Introduction, review and update. *Nucl. Phys. Proc. Suppl.*, 62:266–275, 1998.
- [52] A. B. Lahanas and D. V. Nanopoulos. The road to no-scale supergravity. *Physics Reports*, 145(1-2):1 – 139, 1987.
- [53] Taekoon Lee and Guo-Hong Wu. Interactions of a single Goldstino. *Phys. Lett.*, B447:83–88, 1999.
- [54] A. D. Martin, W. J. Stirling, R. S. Thorne, and G. Watt. Uncertainties on α_s in global pdf analyses and implications for predicted hadronic cross sections. *European Physical Journal C*, 64:653, 2009.
- [55] Stephen P. Martin. A supersymmetry primer, Jun 2006.
- [56] Gudrid Moortgat-Pick. Lectures on collider physics, 2010.
- [57] Takeo Moroi. Effects of the gravitino on the inflationary universe, 1995.
- [58] A. Neveu and J. H. Schwarz. Factorizable dual model of pions. *Nuclear Physics B*, 31(1):86 – 112, 1971.
- [59] H. P. Nilles. Supersymmetry, supergravity and particle physics. *Physics Reports*, 110(1-2):1 – 162, 1984.
- [60] Keith A. Olive. Introduction to supersymmetry: Astrophysical and phenomenological constraints. 1999.
- [61] Michael E. Peskin and Daniel V. Schroeder. *An introduction to quantum field theory*. Addison-Wesley Pub. Co., October 1995.
- [62] J. Pumplin et al. New generation of parton distributions with uncertainties from global QCD analysis. *JHEP*, 07:012, 2002.
- [63] F Ragusa and L Rolandi. Tracking at lhc. *New Journal of Physics*, 9(9):336, 2007.
- [64] Are R. Raklev. Massive Metastable Charged (S)Particles at the LHC. 2009.

- [65] Lisa Randall and Raman Sundrum. Out of this world supersymmetry breaking. *Nucl. Phys.*, B557:79–118, 1999.
- [66] Peter Schleper. Personal communication, May 2010.
- [67] Torbjorn Sjostrand, Stephen Mrenna, and Peter Skands. Pythia 6.4 physics and manual. *JHEP*, 0605:026, 2006.
- [68] Durham University. On-line plotting and calculation, <http://durpdg.dur.ac.uk/hepdata/pdf3.html>, 2010.
- [69] J. Wess and B. Zumino. Supergauge transformations in four dimensions. *Nuclear Physics B*, 70(1):39 – 50, 1974.